UNIVERSITY OF SOUTHAMPTON

FACULTY OF ENGINEERING, SCIENCE AND MATHEMATICS

SCHOOL OF ENGINEERING SCIENCES

A GUIDANCE-CONTROL APPROACH APPLIED TO AN AUTONOMOUS UNDERWATER VEHICLE

PAKPONG JANTAPREMJIT

THESIS FOR THE DEGREE OF DOCTOR OF PHILOSOPHY

JUNE 2008

To my parents, brother and beloved wife,

for their encouragement, patience and love

UNIVERSITY OF SOUTHAMPTON

ABSTRACT

FACULTY OF ENGINEERING, SCIENCE AND MATHEMATICS
SCHOOL OF ENGINEERING SCIENCES

Doctor of Philosophy

A GUIDANCE-CONTROL APPROACH APPLIED TO AN AUTONOMOUS UNDERWATER VEHICLE

by Pakpong Jantapremjit

This thesis is concerned with the guidance and control problem for autonomous homing and docking tasks using an autonomous underwater vehicle. The tasks will play a key rôle in long-term underwater applications in the future. Current technology allows most vehicles capable of short-term operation. Because of limitations of energy storage and sensor capability, underwater vehicles considered in large networks are unable to operate continuously in completing a large task assignment for extended periods of time. To extend a large scope of the missions, autonomous homing and docking tasks are therefore required allowing a vehicle to automatically return to the docking station and then recharge its own battery and exchange data before continuing the operations.

The thesis describes work towards guidance and control systems to enable a nonholonomic torpedo shaped underwater vehicle to perform automatic homing and docking preparation tasks. The artificial potential field and the vector field path generation methods construct the predefined trajectory by extracting position information from surrounding sensor nodes. Thus, the predefined path leads an AUV relatively close to the docking station with obstacle avoidance. With an enhanced model, the switching weighted vector field technique applies a set of varying weights. This technique shapes a trajectory which a docking preparation manoeuvre can improve. The Line-of-Sight

guidance law with the control system then forces the vehicle to follow its predefined path to the desired destination with the proper orientation at the dock. The sliding mode controller is designed for both heading and depth control. A subsystem using sliding mode is applied to obtain a robust controller for handling nonlinear system behaviours. Due to a problem of chattering effects caused by the standard sliding mode control, the high-order sliding mode control solves it with success whilst its main characteristic is maintained. To improve performance of the controllers, the optimal control technique via state-dependent Riccati equation is explored. Finally, a novel method integrates the guidance and control laws with optimal waypoint guidance algorithm for smooth commanded transitions. Based on the Lyapunov stability theorem, the guidance-control system guarantees stability of tracking. The feasibility of this approach is analytically formulated and the simulation is numerically demonstrated using an autonomous underwater vehicle.

Contents

List of Tables

List of Figures

Acknowledgements

Firstly I express deep gratitude to my supervisor Professor Philip A. Wilson for his vision, patience and encouragement, the tremendous opportunities, and personal guidance which he provided to me during the PhD study at Southampton. Without him this research would not have been possible.

My sincere thanks are due to the official examiners: Dr. Yvan R. Petillot from Heriot-Watt University, and Professor Sandor M. Veres from Electromechanical Engineering Research Group, University of Southampton, for their detailed reviews, constructive criticism and excellent comments throughout the final viva.

I also would like to recognise the support for my PhD scholarship funded by the royal Thai government.

Many thanks to all friends in the Fluid-Structure Interaction Research Group and many Thai friends at whose friendship I always enjoy.

Finally, and most importantly, I would like to thank my parents and family who have always been there for me providing love, care and support throughout my life. Lastly, I especially want to express my heartfelt gratitude to my wife Pareecha for her understanding, love over the years of my school life and good meals for long nights.

Nomenclature

Symbols

$\boldsymbol{A}$	State transition matrix in the state space
$\boldsymbol{B}$	Control input matrix in the state space
$\boldsymbol{C}(\boldsymbol{\nu})$	Coriolis and centripetal matrix
$\boldsymbol{D}(\boldsymbol{\nu})$	Hydrodynamic damping and lift matrix
$\boldsymbol{e}$	Error matrix
$\boldsymbol{f}(\boldsymbol{x})$	Nonlinear function representing disturbance and unmodelled dynamics
$\boldsymbol{g}(\boldsymbol{\eta})$	Gravitational and buoyancy forces and moments matrix
$\boldsymbol{h}$	Right eigenvector of $(\boldsymbol{A} - \boldsymbol{B}\boldsymbol{k}^{\mathsf{T}})^{\mathsf{T}}$
I_{xx}, I_{yy}, I_{zz}	Moment of inertia about X_o, Y_o, Z_o axes
$\boldsymbol{I}_o$	Inertia matrix referring to the body-fixed frame with origin O
J_0	Performance index
$\boldsymbol{J}(\boldsymbol{\Theta})$	Transformation matrix in equation of motion
$\boldsymbol{M}$	Inertia and added inertia matrix in equation of motion
$\boldsymbol{k}$	Feedback gain matrix
K_σ	Tunable parameter in the sliding mode control law
$[K, M, N]$	Moment of external forces about origin in the body-fixed frame
$[p, q, r]$	Angular velocity about origin in the body-fixed frame
$\boldsymbol{P}(\boldsymbol{x})$	Positive definite matrix

$\boldsymbol{Q}_u$	State-dependent control weight matrix
$\boldsymbol{Q}_x$	State-dependent weight matrix
$\boldsymbol{R}(\boldsymbol{\Theta})$	Linear rotation matrix
$\mathbb{R}^n$	The set of all real $n \times 1$ vectors
$\mathbb{R}^{n \times m}$	The set of all real $n \times m$ matrices
$\text{sat}(\cdot)$	Saturation function
$\text{sign}(\cdot)$	Signum function
$\boldsymbol{S}(\cdot)$	Skew-symmetric matrix
$\mathcal{S}$	Sliding manifold
$\boldsymbol{T}(\boldsymbol{\Theta})$	Angular rotational matrix
$[u, v, w]$	Translation motion along X_o, Y_o, Z_o axes
u_o	Constant forward speed of a vehicle
$\boldsymbol{u}$	Control input in the state space
$U(\cdot)$	Potential function
$V(\cdot)$	Candidate Lyapunov function
$[x, y, z]$	Position of a vehicle in the inertial frame
$[x_b, y_b, z_b]$	Position of the centre of buoyancy
$[x_g, y_g, z_g]$	Position of the centre of gravity
$\boldsymbol{x}$	State variable
$\boldsymbol{x}_d$	Desired value of the state variable $\boldsymbol{x}$
$\tilde{\boldsymbol{x}}$	Tracking error from its desired value
$[X, Y, Z]$	External forces about origin in the body-fixed frame

Greek Symbols

$\boldsymbol{\eta}$	Position and attitude matrix
$\boldsymbol{\nu}$	Linear and angular velocity matrix

τ	Control input matrix
σ	Scalar parameter representing the sliding surface
Φ	Thickness of the sliding surface boundary layer
$\nabla U(\cdot)$	Vector field of an artificial force
δ_r	Rudder deflection
δ_s	Sternplane deflection
θ_d	Desired value for the pitch angle
ψ_d	Desired value for the yaw angle
$[\phi, \theta, \psi]$	Attitude of the vehicle in the inertial frame

Abbreviations

AUV	Autonomous Underwater Vehicle
DOF	Degree of Freedom
GNC	Guidance, Navigation and Control
HOSMC	High-order Sliding Mode Control
LOS	Line-of-Sight
PID	Proportional, Derivative and Integral
SDRE	State-Dependent Riccati Equation
SDRE-HOSMC	Integration of State-Dependent Riccati Equation and High-order Sliding Mode Control
SMC	Sliding Mode Control
RMS	Root Mean Square
ROV	Remotely Operated Vehicle

Chapter 1

Introduction

This thesis considers the problem of homing and docking tasks for long-term applications, hence a guidance-control framework using an autonomous underwater vehicle is proposed. In this chapter, the motivation for this work is introduced, and followed by the requirement for long-term application and the general guidance-navigation-control concept. Building upon the general framework, the research objectives are stated and the proposed approach is described. Finally an outline of the thesis is described, and publications for this work are summarised.

1.1 Motivation

The oceans embody extraordinarily dynamic and complex environments. Immense biological and mineral resources from the oceans are largely unexplored and unknown. Underwater exploration and surveying are needed thus they can be managed to allow both use and protection of ocean resources. Some operations in the underwater environment, for instance, deep sea and under-iceberg can be deeply unfriendly to humans. Underwater tools and robots are desirable for these missions. The robotics

community has currently played attention to a field of unmanned underwater vehicles which encompasses a wide range of research topics. One of the largest focus areas is the development of robotic vehicles and the investigations into their possible applications.

The requirement for autonomy in vehicle design and for automatic control technology, is however increasing at a big rate and it is a prevalent issue in many situations and various environments. The communication between the operator and vehicle is a main factor to classify whether it is a Remotely Operated Vehicle (ROV) or an Autonomous Underwater Vehicle (AUV). For example, an automatic control is required as opposed to a remote control in underwater environments where communication with a unmanned or manned vehicle is possible. Although ROVs have been the dominant robotic field of interest with researchers for many years and they are useful for many underwater operations such as collecting biological and mineral resources, there are some limitations for those vehicles during long-term operations in hostile environments. It is well known that ROVs are linked to the support ship by an umbilical cable and remotely operated by a human pilot, whereas AUVs do not have this inhibition and are therefore playing a vital rôle in underwater exploration allowing humans to explore great depths in various new underwater worlds. AUVs are self-contained and are able to have predefined solutions built into their architecture and to take control actions more accurately and reliably without human intervention. Thus, an AUV is an alternative in complex underwater operations. Examples of such operations are seabed mapping and surveying, studying underwater environment and disasters, underwater inspections and constructions, and under-ice explorations [51]. However, the development of AUVs have been relatively slow due to their high level of complexity in technology and at a high operational cost [87]. In addition there are three main ongoing areas for AUV technology, namely scientific research, commercial sector and military. In summary, table 1.1 shows examples of current development

of the AUV technology and their applications. This exemplifies why AUVs have various potential applications and great advantages in terms of operational ranges and reliable operations [160].

Table 1.1: Examples of current development of the AUVs

Reference	Vehicle name	Year	Range (km)	Depth (m)	Purpose
MBARI [104]	Dorado	2008	55-85	6,000	Seafloor mapping
IFREMER [110]	ASTER	2008	100	3,000	Environmental survey
Kongsberg [75]	HUGIN-3000	2006	440	3,000	Environmental monitoring
Hydroid [56]	REMUS-6000	2006	420	6,000	Environmental survey
MARIDAN [8]	MARIDAN-600	2001	100	1,500	Offshore industry and military
AQUA Ex-2 [73]	AQUA Explorer 2	2001	420	2,000	Environmental survey
JAMSTEC [65]	URASHIMA	1998	300	3,500	Bottom surveying
Griffiths [52]	Autosub-1	1995	220	750	Environmental monitoring

1.2 Requirements for Long-Term Application

Studies have been made of AUVs over the past thirty years [160], still AUV technology limitations remain. In long-term operations, energy and data storages are critical factors [51]. In long-term experimentation, a vehicle should operate continuously to complete a large scope of a mission for extended periods of time. Therefore most underwater vehicles are typically capable of short-term operation. To continue the mission, a vehicle requires both software and hardware to be turned off before its batteries can be manually recharged or replaced whilst operators manually download data from each mission. It can be seen that current state of technology for power capability and data storage capacity is not fully supported in such operations.

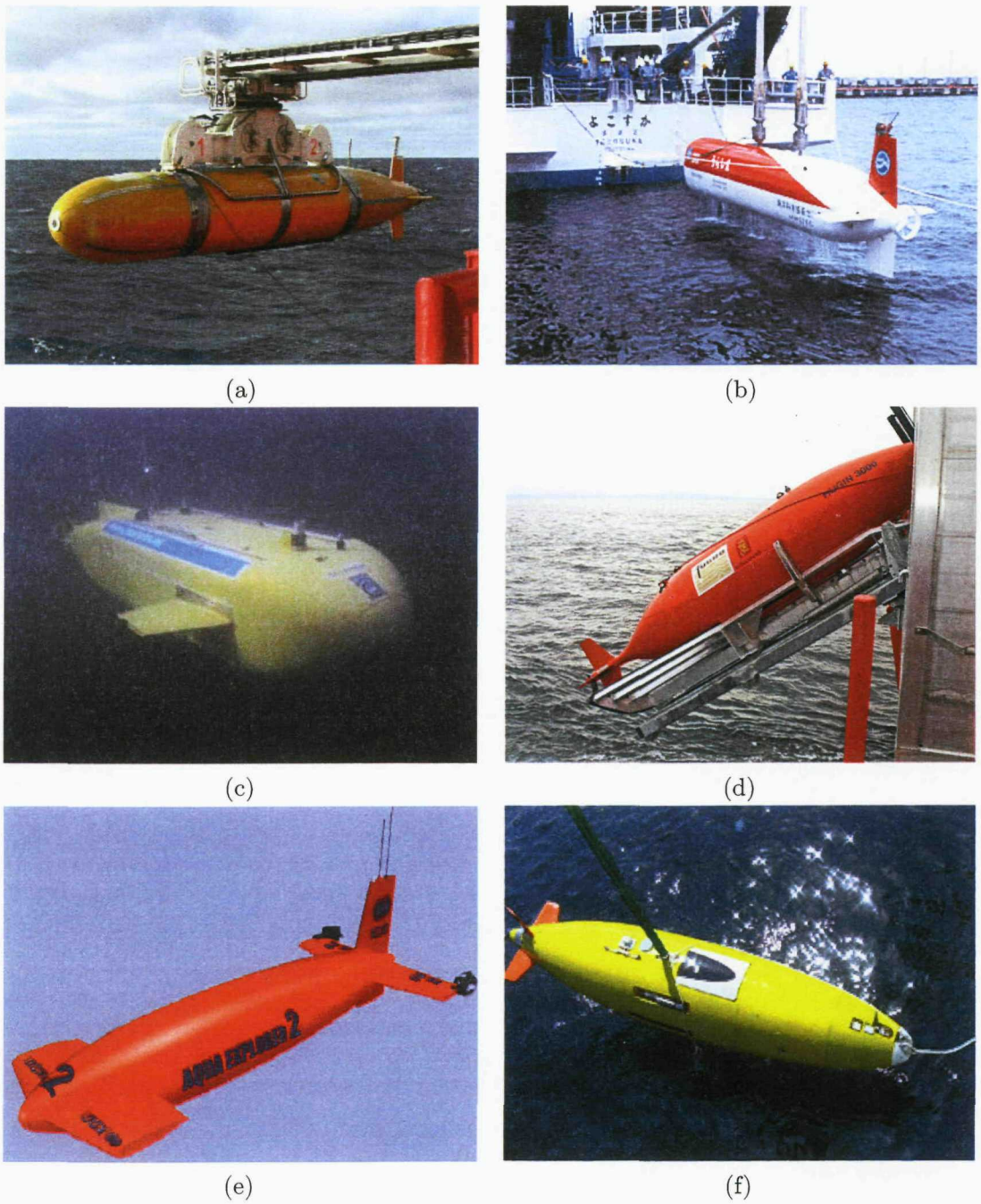

(a) (b) (c) (d) (e) (f)

Figure 1.1: Various designs of AUVs: (a) AutoSub 2 [52], (b) Urashima [157], (c) Maridan [8], (d) Hugin 3000 [61], (e) Aqua Explorer 2 [73], (f) REMUS-6000 [56].

Table 1.2: Current development of power source for various AUVs

Reference	Vehicle Name	Displacement (tonne)	Power Source	Mission Endurance
Kongsberg [75]	HUGIN-3000	14	Semi-fuel Cell, 45kWh	50-60 hours
McPhail [100]	Autosub-1	1	MN-alkaline	50 hours
JAMSTEC [65]	URASHIMA	10	Fuel Cell 4kW-120V	43 hours
Hydroid [56]	REMUS-6000	8.6	Li-ion, 11kWh	22 hours
MARIDAN [8]	SeaOtter-MkI	15	NiMH battery	15 hours
AQUA Ex-2 [73]	AQUA Explorer 2	2.6	Rechargeable Lithium	10 hours

Table 1.2 shows various types of power source and operation time for current AUVs technology. Its short operational periods limit the scopes of each undersea exploration. For future development, AUVs do require high-efficiency power source and high-volume storages thus they have the ability to widely explore in large unknown environments, especially for long-term missions. Figure 1.1 shows various AUVs that could be potentially used for undersea long-term tasks. In addition, modern AUVs technology can be realised on large undersea networks in long-term applications. Ocean networks will provide the data necessary to widely explore underwater environments. Small sized AUVs can be applicable for complex and wider missions. However as mentioned previously, current technology for unlimited battery power and larger data storage is unavailable. To overcome the limitations of onboard battery capacity, data storage and sensor ranges, floating docking platforms are required to provide a large area of potential missions. By focusing on homing and docking operations, this allows a vehicle to return in the midst of the mission to the docking platform and then to recharge its own battery. This also allows an exchange information between the ship and the AUV before continuing its normal operations. To be able to perform its docking mission accurately, the guidance, navigation and control

system must be reliable. Path planning and tracking for homing and docking are also required in the task. The field of autonomous system for homing and docking for underwater exploration is still open and have been extensively studied in the research and development communities.

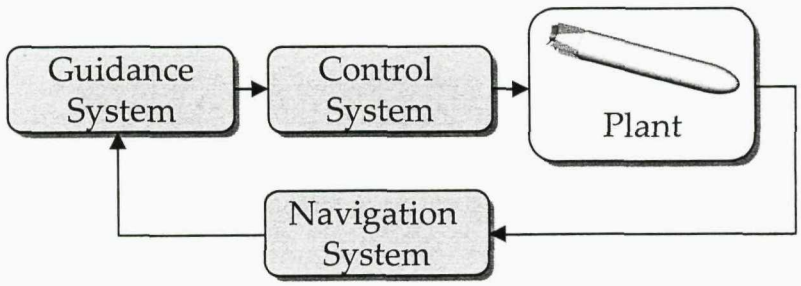

Figure 1.2: Illustration of the basic block diagram of Guidance, Navigation and Control system for marine applications.

1.3 Guidance, Navigation and Control

As reported in [39], a control system for a robotic system or a marine vehicle is constructed as three building blocks denoted as the Guidance, Navigation and Control (GNC), shown in figure 1.2. Simply, GNC can be described by three fundamental questions:

- **Where am I going ?** Firstly, the guidance can be defined as the process of determining the desired position, velocity and acceleration of the vehicle that will achieve target conditions despite changes in the vehicle's motion and its environment, to be used by the control system. If the vehicle states and environmental conditions are exactly known and do not change, the guidance will be a relatively simple enough, requiring only an open-loop control system.

- **Where am I ?** Secondly, the navigation problem is to find the vehicle kinematic states (position, velocity and acceleration). Its information is managed by a device known as the inertial measurement unit (IMU), which is essentially an arrangement of accelerometers and rate gyros. More complex devices includes the Inertial Navigation System (INS) and the Kalman filter techniques applied to doppler velocity logs and acoustic doppler. These devices continuously track the position, orientation and velocity of a vehicle without the need for external references.

- **How should I go there ?** Finally, the control is the action to maintain the vehicle states commanded by the guidance system. Design of the vehicle control must satisfy objectives, for instance, feedback control laws, path following, trajectory tracking and energy minimising. The vehicle stability is the primary and most difficult criterion to satisfy. Its requirements are often contradictory to the speed of response of the control algorithms and the actions. This would be an interesting question to be answered.

1.4 Approach

There are many ways to solve the problem of automated homing and guidance of an AUV to a stationary docking platform, for example, an AUV is able to detect when the batteries need recharging or when information needs transferring. A reason for docking criterion is either the voltage has reduced, or the storage capacity is saturated. By determining a factor, an AUV is able to predict how long it should be for a safe return to the platform. In the homing and docking tasks, an AUV must be placed relatively close to the docking station. With a navigation system, an AUV is able to determine positional information with existing sensor technology such as underwater acoustic devices. Two stages for returning and docking preparation are developed. In the guidance system, the potential and vector field technique generate a

predefined trajectory with a desired position and orientation for an AUV in those two stages. In the tracking control problem, the sliding mode is generally used to obtain a robust controller for nonlinear system behaviour. The path following technique with available control actions forces an AUV to follow its trajectory with the speed profile from any given starting position in the workspace, to a desired destination location with proper orientation at the dock. The entire system guarantees stability of tracking positions and orientation whilst following the predefined path until reaching the docking platform.

1.5 Objectives

The three principal objectives of the research are summarised,

- To give an analytical robust control algorithm as a tool ensuring system stability that may be disturbed by uncertainties and disturbance caused by ocean currents and waves.
- To propose a novel path planning concept for generating a predefined trajectory which converges closer to the destination (docking point).
- To develop a new approach for guidance and control for homing and docking tasks using an AUV. The objective of this task is that an AUV is to follow and track the predefined trajectory, whilst a control design can guarantee a stability for both position and orientation.

1.6 Scopes, Assumptions and Limitations

In this thesis, the following are considered:

- The concept of a homing and docking manoeuvre; guidance based path following with control efforts are considered.

- The underwater vehicle which is considered in a set of simulation studies, is not a fully actuated system. The nonholonomic torpedo shaped underwater vehicle is considered and used to demonstrate the case studied for homing and docking tasks.

- This study only deals with time-continuous plants. Studies and analyses for discrete plants are not included here.

- Parameters includes dimensions and hydrodynamic model used in the simulation studies [54]. All plant models considered are of known structure. Some parameters of the models, however, may or may not be known.

- A navigation system is not covered in this work. It is therefore assumed that an underwater vehicle equipped with sensors is able to track position and orientation from the sensor networks, for example responder-transponder arrays. Output feedback designs and controller/observer designs are not considered.

1.7 Brief of Sensor Networks

The field of navigation covers a very wide range of interesting areas and techniques employed by ROVs/AUVs. Underwater vehicles can get information from outside (environments). Sensors are therefore very necessary information providers and are heavily used in ROVs/AUVs application. However, as mentioned previously, the navigation system is not considered in this work. Such that only a brief review of navigational sensor for vehicles is given in this section. Future works would allow the complete system for an autonomous underwater vehicle.

Sensor network system is considered as an array of the acoustic equipment which give the range and the bearing from a vehicle based transceiver to seafloor transponders and floating station or surface ship's transceivers. Acoustic navigation systems

work best in open water. The vehicle sends out an acoustic signal which is then returned by each transponders as it is received. The measurements can be represented in the spherical coordinates, as such the position relative to the surface ship, the vehicle and each array node can be calculated. Figure 1.3 shows one example diagram of the acoustic systems. Following details are collected from reference [76].

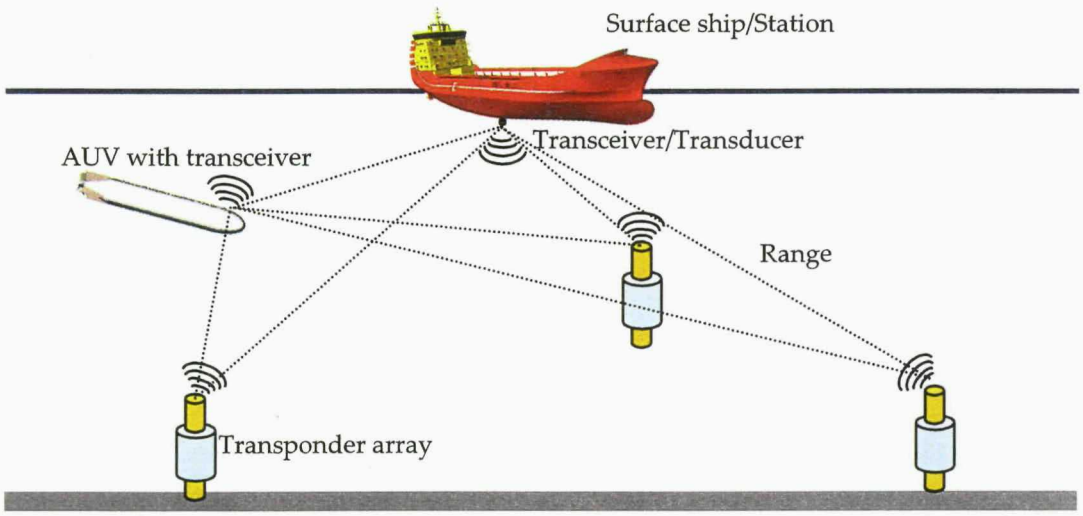

Figure 1.3: Illustration of the Long baseline acoustic positioning system diagram.

Ultra Short Baseline System (USBL)

Ultra short baseline system consists of a transceiver, which is mounted underneath a surface ship, and a transponder/responder on the seafloor, and/or on an underwater vehicle. The range and bearing are derived from a USBL system with respect to the transceiver mounted to the vehicle. An acoustic pulse is converted into range whilst a phase-differencing within transducer array is used to calculate the bearing to the subset transponder. The advantage of USBL system is that it has single transducer assembly on the surface vessel to locate the transponder on the ROVs/AUVs.

Short Baseline System (SBL)

A short baseline system derives a bearing to a beacon from multiple surface mounted transceivers. This bearing is derived as a ping passes each of the transceivers and the relative time of arrival is detected. A time of flight interrogation technique will provide a range to the beacon. The position will be with respect to the transceivers.

Long Baseline System (LBL)

A long baseline system derives a position with respect to a seafloor deployed array of transponders in combination with a hydrophone on the surface vessel to locate ROVs/AUVs. The position is generated from using three or more time of flight ranges to/from the seafloor platforms. This system gives the position in absolute or relative seafloor coordinates and does not require additional sensors. The main advantage of the LBL positioning system is excellent and constant accuracy whatever the movements and the position of the vehicles being tracked over the area. The accuracy is independent of depth if environmental parameters are properly compensated. This type of acoustic equipments would suit for the sensor networks providing the positions for the large scope of applications.

1.8 Main Contributions and Outline of the Thesis

The main thesis contributions are summarised below:

- **Optimal sliding mode control scheme**
  An optimal sliding mode controller is introduced. The model is proposed so it solves the problem of convergence and stability of a nonlinear system by considering the Lyapunov theorem. Firstly, the traditional sliding mode is described. By enhancing the design, the high-order sliding mode is capable of tracking the error whilst eliminating the chattering effects for the common decoupled depth

and heading subsystems of an AUV. Secondly, an optimal control input is determined by solving algebraic Riccati equation. The integration of two control schemes is then proposed to ensure stabilisation and effective means of designing the AUV subsystems in the presence of small input additional disturbances [63]. To illustrate the control law developed in this work, only computer simulation results are presented in the thesis.

- **Predefined path for homing and docking preparation strategy**

  Two strategies, namely homing and docking path generation are proposed so that they provide a predefined trajectory for an AUV to a close neighborhood of a target position with desired orientation. Firstly, a homing strategy is achieved by generating a virtual path using an artificial potential field method. This virtual path is obstacle free whilst converging to an area for docking preparation stage. Secondly, the conventional method is modified to the so-called vector field method for a docking strategy. This is to ensure a predefined trajectory for an AUV to be able to follow the path with a final desired orientation. Constant and switching weight set are further studied for a better model of predefined path closer to the target. Simulation results using MATLAB® software are demonstrated in a later chapter [62].

- **Guidance-control approach**

  Trajectory tracking and path following of an underwater vehicle to a target with desired orientation is achieved by means of the proposed method. A novel guidance-control approach is proposed. Line-of-Sight guidance algorithm is used to solve path following whilst a robust sliding mode control is derived that yields the convergence of the predefined path. A proposed optimal waypoint gives a smooth command transition. Simulations results are presented in 2D and 3D to illustrate the behaviour of the proposed control scheme. The model shows statistic results of convergence and stabilisation of the system to an arbitrarily

small errors in position and orientation.

The outline is shown in figure 1.4, and detailed as following:

- Chapter 2 explores a literature review on the development of control algorithm designed for marine vehicles by the researcher and academic communities. The aim is to provide advantages and disadvantages of the different control schemes developed in the field of marine applications, and to comment on which methods that seem most promising from a practical viewpoint. This is followed by a brief mathematical model for kinematics and dynamics of marine vehicle. A fully coupled six degrees of freedom of an underwater vehicle is considered. State space representations using Euler angles are presented.

- Chapter 3 presents the design of a sliding mode controllers for an underwater vehicle. Common decoupled subsystems, namely depth and heading subsystem of sliding mode controllers are presented. The controller is a general controller which utilises sliding surfaces based in time. A discussion on how this general controller can be used for tracking errors of desired states is given. Then, a focus is dedicated to an optimal high-order sliding mode control via state-dependent Riccati equation for decoupled systems. The proposed controller not only keeps the advantage of the standard sliding mode, but also eliminates the chattering effects. Another issue in the designed approximate method is to select an appropriate sliding surface. The work determines an optimal sliding surface by involving a state-dependent Riccati equation technique. Simulation results are shown that the sliding mode controller is able to keep steady state error small due to disturbances and give an enhancement of the controller performances.

- Chapter 4 introduces a trajectory planning for a homing and docking problem. The vector field based on an conventional artificial potential field method gives a desired trajectory using existing information from ocean network sensors. In

the homing stage, the conventional artificial potential field provides an obstacle avoidance. In the docking stage, the vector field provides a guidance for a virtual AUV to follow the path to a required position with final desired orientation. A weighted vector field is a better model to enhance performance in achieving desired target. Furthermore, in order to improve a docking manoeuvre, a switched weighted technique is proposed for controlling a vehicle's path and final stage docking. Simulation results illustrated in this chapter compare trajectory planning using constant and switched weight sets.

- Chapter 5 gives literature concerning trajectory tracking, and path following for various applications are detailed. A novel guidance-control approach is constructed. To provide an accurate motion control for an AUV in the docking task, a robust control methods is needed, which the vehicle is able to steer along a reference curve and follow the desired path. The Line-of-Sight guidance algorithm is used for path following. In addition, the sliding mode controller design is a proposed control strategy that guarantees global stability to track the path. Optimal waypoint guidance is introduced. Simulations results in 2D and 3D are demonstrated showing the performance of the proposed system.

- Chapter 6 draws conclusions from the development and implementation of the proposed approach and identifies continuing research themes that have arisen out of this work.

1.9 Publications

The following is a list of the author's publications written during his study. This includes both accepted and published papers and posters.

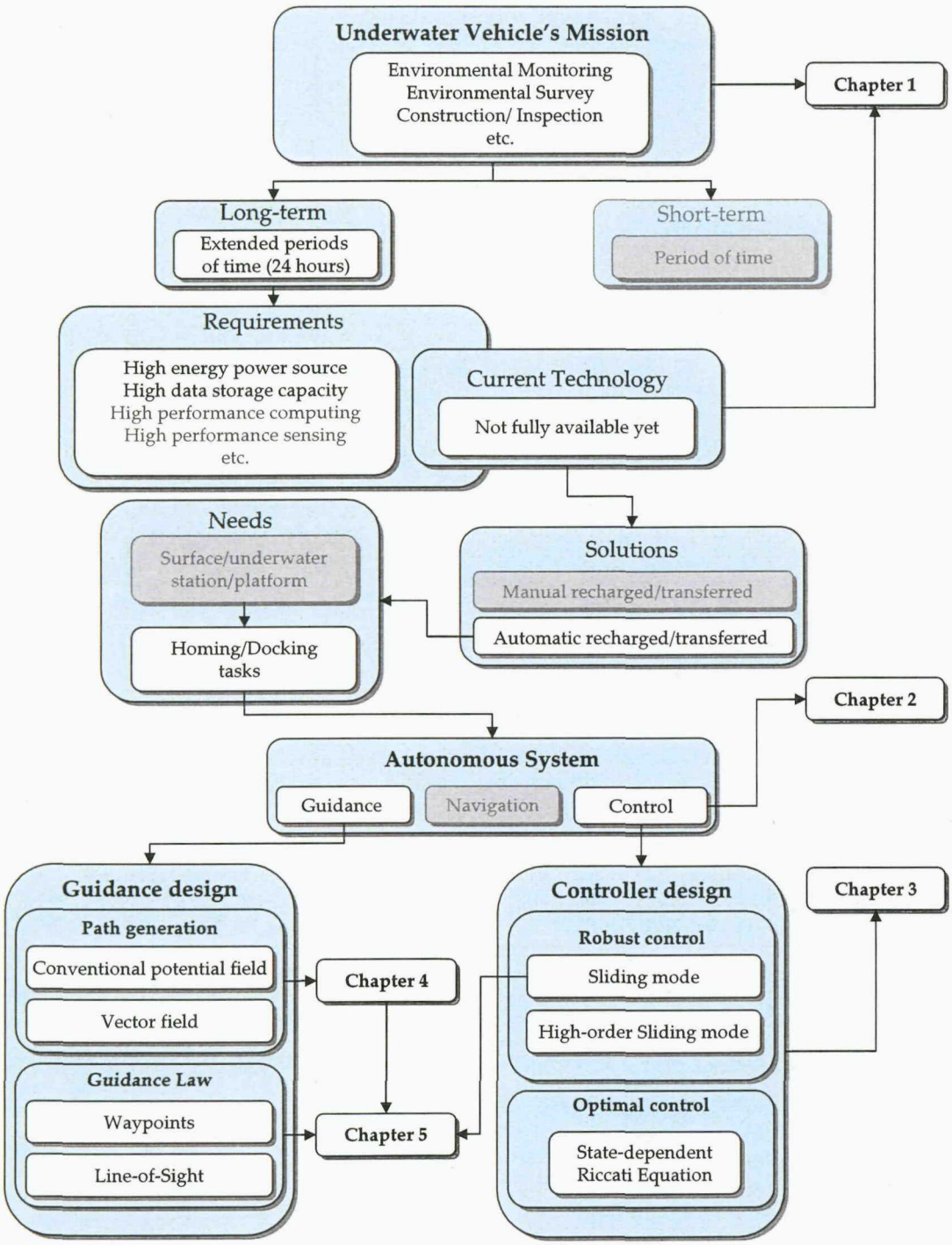

Figure 1.4: Illustration of thesis outline diagram.

Journal Paper

- P. Jantapremjit and P.A. Wilson. Control and guidance for homing and docking tasks using autonomous underwater vehicle, *The International Journal of Maritime Engineering*, (In press).

Conference Paper

- P. Jantapremjit and P.A. Wilson. Guidance-control based path following for homing and docking using an autonomous underwater vehicle, *The Oceans'08 MTS/IEEE Kobe-Techno-Ocean'08*, Kobe, Japan, 6 pp., 2008.
- P. Jantapremjit and P.A. Wilson. Control and guidance for homing and docking tasks using an autonomous underwater vehicle, *The 2007 IEEE/RSJ International Conference on Intelligent Robots and Systems (IROS)*, San Diego, USA, pp. 3672-3677, 2007.
- P. Jantapremjit and P.A. Wilson. Optimal control and guidance for homing and docking tasks using an autonomous underwater vehicle, *The 2007 IEEE International Conference on Mechatronics and Automation (ICMA)*, Harbin, China, pp. 243-248, 2007.
- P. Jantapremjit, P.A. Wilson and A.J. Murphy. A study of autonomous docking with an AUV using intelligent control, *International Conference on Underwater System Technology: Theory and Applications*, Penang, Malaysia, pp. 12-16, 2006.

Posters

- P. Jantapremjit. Guidance-control approach for homing and docking using an autonomous underwater vehicle, *FSI Away Day*, University of Southampton, January 2008.

- P. Jantapremjit. Homing and docking for autonomous underwater vehicle, *FSI Away Day*, University of Southampton, January 2007.
- P. Jantapremjit. Autonomous underwater vehicles: Autonomous servicing - rendezvous and docking, *FSI Away Day*, University of Southampton, January 2006.

1.10 Summary

This chapter outlines the basis of the thesis. It provides an overview of homing and docking tasks for long-term application. A fundamental of Guidance-Navigation-Control is explained. Aims of the research have been stated and the proposed methodology has been briefly described. This has been followed by discussion of the research scope, main contributions and summary of each chapter. Based on these, it is now ready to proceed to detailed descriptions of the thesis research.

Chapter 2

Review of Control Techniques for Marine Vessels

2.1 Overview of Chapter

In the previous chapter, the topics of underwater vehicles were introduced. Motivation and objective were given. Before continuing, it is appropriate to explore the different controllers that have been implemented on AUVs by the research community. As such, this chapter focuses at the problems of controlling AUVs and control techniques available for autonomous vehicles, especially underwater vehicles. Section 2.2 discusses an overview of the problem in marine vessels. Section 2.3 explains various control techniques; classical control, adaptive control, intelligent control, optimal control and robust control. A brief of the marine control system is given in section 2.4, following by a summary in section 2.5.

2.2 Problem and Requirement

It is a challenge to control underwater vehicles since there are particular difficulties due to the existence of several complex and nonlinear forces acting upon the vehicle. Hydrodynamics is the main source of nonlinearity term in the dynamics of underwater vehicles. Precisely measuring the hydrodynamic terms by carrying out the experimental facilities and Planar Motion Mechanism (PMM) tests is expensive and time consuming [151]. Compared with other environments, underwater vehicles are probably the most difficult to determine with an accurate dynamic model. For example, the AUV's dynamic model is changed when its thruster is lost. Furthermore in the real world environment a number of uncertainties such as disturbance and sensor noise are presented and have to be extensively considered in the model. If only those hydrodynamic terms are available, a robust and reliable model of the guidance, navigation and control for an AUV is required. It is to avoid failures that may occur during operational envelope. These failures can result in damage to hardware or even loss of the vehicle in unknown environments.

In any control problem in underwater applications there will typically be differences between the actual plant and the mathematical model developed for the controller design. The variation may be due to unmodelled dynamics in the system parameters or the approximation of the complex system. It is therefore required that the resulting controller has the ability to produce the desired performance levels in the practices. This has led to an intense interest in the development of robust control methods which seek to solve this problem. The main control structure should be characterised by a suite of feedback control laws. The design should have the ability to combine useful properties of each subsystem where each subsystem has a fixed control configuration. The closed loop response should be totally insensitive to a particular class of uncertainty. The intuitive concepts of controller design should be formulated in a general form of single-input single-output to multi-input multi-output systems.

2.3 Control Techniques

With intensive studies and developments of AUV technology and the increase in a number of vehicles worldwide, there has been a great push towards research in the design and implementation of controllers to determine an accurate vehicle model and to improve dynamic response. There are a number of researchers that study control for nonholonomic systems. Many researchers have considered nonholonomic systems [1]. Generally, the nonholonomic system can be described by a set of parameters subject to differential constraints. The constraints restrict and reduce some dimensions of the motions in the physical space [74]. Nonholonomic AUVs have a smaller dimension than that of the configuration space [155], and theses are considered in this thesis. In general, control methodologies for systems fall into two major areas: open loop and closed loop. The open loop controller relies on the knowledge of input commands whilst the closed loop controller utilises feedback from the output providing more robustness against system errors. Thus, a system with closed loop control is able to compensate for the error induced due to external disturbance of the system. Motion control for AUVs has been studied in the community for many decades [43], [158], there are still many areas of fruitful research.

In this section, a number of current studies in control techniques for marine applications are explored, ranging from classical controls such as proportional-derivative (PD), proportional-integral-derivative (PID) to modern controls such as adaptive control, fuzzy logic, neural networks, genetic algorithms, optimal control and sliding mode control, detailed in the following sections. Table 2.1, 2.2 and 2.3 show summaries of developed controllers using in various kinds of underwater vehicles (shown in figure 2.1). Table 2.4 shows advantages and disadvantages of control techniques.

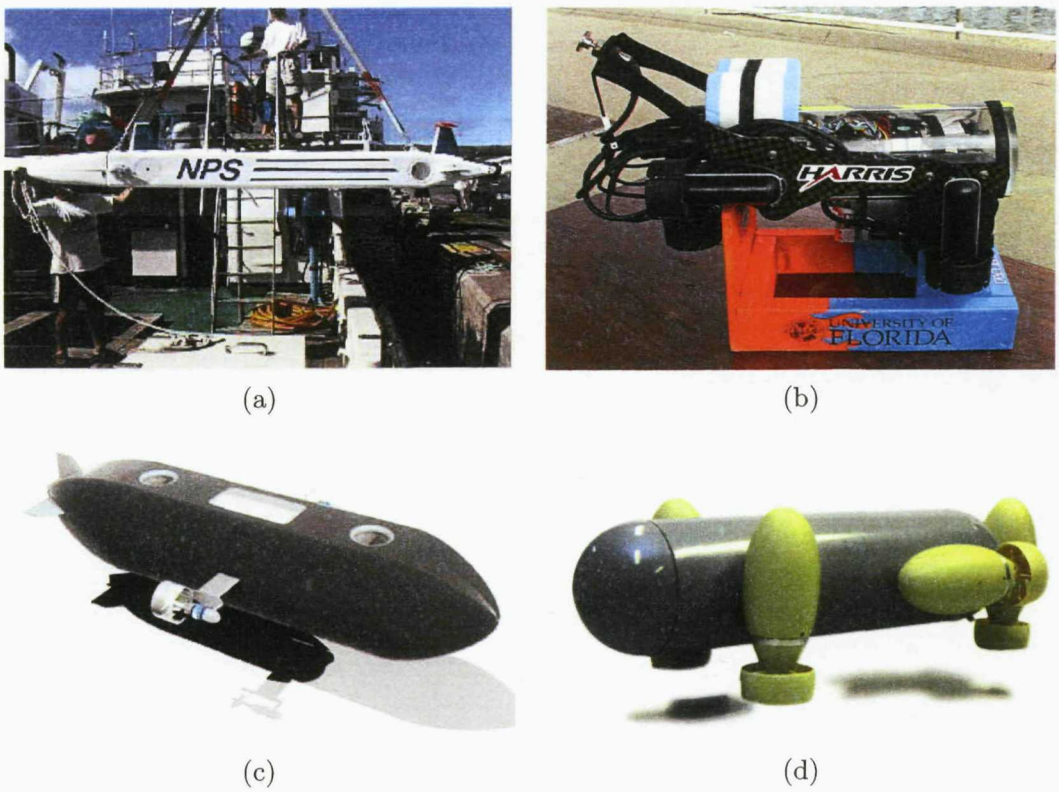

(a) (b)

(c) (d)

Figure 2.1: Various examples of AUVs design: (a) ARIES of Naval Postgraduate School [54], (b) Subjugator of University of Florida [149], (c) SotonAUV of University of Southampton [4], (d) Serafina of Australian National University [163].

2.3.1 Classical Control

Classical control is based on a linearised model. A technique of PD/PID control is commonly used in various applications. It is easily understood and provided reasonable robustness and performance. However, it is inadequate when uncertainties such as disturbance and sensor noise are presented in the real world environment [51]. There are a number of controllers used for the marine motion control, such as PID controls detailed in controller model analysis [31], PID tracking controller [129], linear controller design [136].

The most common algorithm for PID control is to correct the output u by using the formulation,

$$u = k_P e + k_D \frac{de}{dt} + k_I \int e dt$$

where e is defined as error, k_P, k_D and k_I, are proportional, derivative and integral gain, respectively. Egeland and Gravdahl [31] provide starting points for electromechanical element modelling and simulation of dynamic systems in the PID controller design for automatic control systems. Smallwood and Whitcomb [136] have shown experimental comparative studies between PD and model based control approaches for dynamic positioning of ROVs. It shows that the model-based controller has outperformed the PD controller in nonlinear tracking problems, however it relies on accuracy of sensor equipments and unmodelled dynamics. Jalving [61] has used a PID control for NDRE-AUV sea tests which were satisfactorily successful. However it is expected to give unsatisfactory responses due to nonlinear model of actuators which causes oscillation of the rudder and sternplane. Silpa-Anan *et al.* [129] have proposed a nonlinear PI controller for *Kambara* thrusters. Lea [87] has successfully presented experiments of speed, depth and heading controls for *Subzero II* by using conventional PID combining with fuzzy sliding mode controller.

The classical PID control is parameterised in term of the reference error feedback. The PID gain is tuned using the single parameter on account of the gain analysis.

In the underwater application, the large differences arising in the control of an AUV. Because an AUV is in the slow control and measurement frequency with significant measurement corruptions and severe thruster saturation. This is quite difficult to tune the PID controller gains properly.

2.3.2 Adaptive Control

One way to use PID in nonlinear systems is to utilise a technique known as gain scheduling [90]. In a conventional manner, gains of the controller are chosen as a function of some variables in an attempt to compensate for the changes in the operating state of a system. In other words, gain scheduling is the process of modifying the gain parameters of P, I and D depending on the desired state of the system. This method works well for systems that have predictable changes in dynamics, so that predetermined gains can be calculated and applied. Gain scheduling provides the ability to control a process with nonlinearities by dividing it up into processes which are approximately linearised. Each process can then be tuned to several sets of operating points that optimally control the system.

Silvestre *et al.* [131] have described a methodology for the design of gain scheduling for the Infante AUV tracking trajectory. The method builds on three key issues: (i) trajectories of autonomous vehicles are parameterized by the vehicles linear speed, yaw rate, and flight path angle; (ii) tracking of a trajectory is driving error to zero; (iii) the linearisation of the generalized error dynamics about any trimming trajectory is time-invariant. The simulation studies without the presence of external disturbances and noise studies show considerable promising results.

Goheen and Jefferys [49] describe multivariable self-tuning autopilots control for autonomous and remotely operated underwater vehicles leading to a satisfaction for model uncertainties. Fossen and Sagatun [43] have proposed two approaches, namely

an adaptive passivity based control and a hybrid control to overcome the model uncertainties of the nonlinear thruster models in a 6-DOFs AUV. Fossen and Fjellstad [40] compared the performance of two adaptive control laws, namely Adaptive Control Law of Slotine and Benedetto and Adaptive Control Law of Sadegh and Horowithz in the context of measurement noise. Nakamura and Savant [109] have considered the use of nonholonomic nature without the dynamic of the 4-DOFs AUV to overcome the problem in stability of the nonlinear tracking control.

2.3.3 Fuzzy Logic

Most of real physical systems are nonlinear systems, however conventional design approaches use different approximation methods to handle nonlinearity. Some typical control method are based on linear, and lookup table approximations to trade off factors of complexity, cost, and system performance. An alternative solution to nonlinear control because it is close to the real world is Fuzzy Logic. It is an intelligent controller which can deal with uncertainty. It is able to construct a complex control system. Unlike classical control, a fuzzy logic controller is developed in a linguistic information manner without the use of analytical models. The operations in fuzzy logic can be described in three sequences called fuzzification, fuzzy inference and defuzzification. Fuzzification converts input data into linguistic variables that may be viewed as labels of fuzzy sets. The fuzzy set is defined as,

$$A = \{(x, \mu_A(x) | x \in X\},$$

where $\mu_A(x)$ is called the membership function of the fuzzy variables.
A list of rules, which is normally expresses in the i^{th} IF-THEN format is given,

$$Rule^i : \texttt{IF } x_1 \text{ is } A_1^i \texttt{ AND/OR } x_2 \text{ is } A_2^i \ \ldots \ x_n \text{ is } A_n^i \texttt{ THEN } y_i \text{ is } B^i.$$

where x_i, y_i are linguistic variables and A_n^i, B^i are fuzzy sets. Inference engine evaluates IF-THEN rules expression, whilst a defuzzification converts fuzzy values into result outputs.

Fuzzy logic control is a successful branch of automation and control theory, which is developed based on fuzzy set theory. Furthermore, fuzzy logic control is generally applicable to systems that are mathematically ill-modelled. Fuzzy logic controller is particularly suitable for those systems with uncertain or complex dynamics. On the contrary, fuzzy logic requires qualitative knowledge from experienced operators to be able to design a good system. The controller is difficult to understand and analyse. It also needs a use of rules and membership functions to approximate any continuous function. Another drawback of using fuzzy logic in this application is the use of computational resources to select and calibrate the control rules. The fuzzy logic model is built on look-up tables and rules which the selection may/may not lead to a robustness and stability of the system.

There are numbers of research in using this technique. Lea [87] has shown the fuzzy control is sensitive to noises which appears to be less robust when compared to PID and sliding mode controls. Song *et al.* [139] designed a controller with a use fuzzy logic in designing sliding mode surface. It is more flexible in the controller design of OEX-AUV. This paper reports that the method provides a good result in pitch and heading controls. Kanakakis *et al.*[67] have presented model based fuzzy logic controllers. Good results from simulations of NPS Phoenix were shown in the paper.

2.3.4 Neural Networks

Neural networks as shown in figure 2.2 are used as a learning algorithm for controlling a system by using a knowledge of input and output data. A neural network controller does not require a formal dynamic model. Its feature provides parallel structures with distributed storage and processing of large amounts of data. The learning process is given by tuning the network interconnection weights and biases based on learning

algorithms [53]. The neuron output $\boldsymbol{u}$ can be written as,

$$\boldsymbol{u} = \boldsymbol{f}(\boldsymbol{W}\boldsymbol{p} + \boldsymbol{b}).$$

where $\boldsymbol{W}$ and $\boldsymbol{b}$ are weight and bias matrices, respectively.

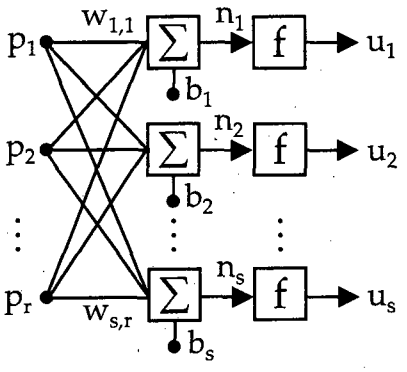

Figure 2.2: Schematic of multi-layer neural networks.

The key idea of neural networks is their nonlinear nature which is able to make them particularly well suited for solving complex control problems with unmodelled dynamics. However, the drawback to this method is that it is enormous computation overhead, and is time consuming due to the learning procedures for completing hypotheses. Thus, robustness and stability in the controller design are not ensured. It would not be suitable for realtime control in underwater application, especially in the docking task. Borovic *et al.* [14] have proposed an adaptive neural network controller for positioning control of the AUV's manoeuvres. The control model is simple as it is added to the conventional vehicle dynamics. Gaskett *et al.* [47] and Wettergreen *et al.* [152] have discussed an autonomous guidance and control architecture of a 6-DOFs AUV with reinforcement learning and without dynamic modelling.

2.3.5 Genetic Algorithm

Holland *et al.* [50], [154] at the University of Michigan developed the Genetic Algorithms (GAs). GAs are search algorithms based on the mechanism of nature selection and genes. The key idea of the algorithms is that they are used as a tool for solving search and optimisation problems over a period of generations. By giving the limits of sets and an initial population of the string, the method generates randomly strings for each of the limits. Then, the representation of the membership function is formed and calculated the merit of solutions that achieve the desired optimisation goal as known as a fitness function. If it is not the case, the *reproduction* operator generates many new strings with highest fitness. The next step which is called the *crossover* operator randomly exchanges components to generate new offsprings which are reserved some characteristics from the parents. The *mutation* operator is finally applied to produce a close identical copy with some altered components of the strings. The loop continues by creating successive new generations and ends when some thresholds (e.g. maximum fitness, average fitness or number of generations) are achieved. In the control problem, GAs are used to design and tune controllers. The tool can provide an effective way to evaluate the merit of each solution. A near-optimal controller can be achieved, this allows a reduction of control output workload. However, the main disadvantage is that it is problem dependent to be able to form a general, robust learning tool.

In marine applications of genetic algorithms, McGookin *et al.* [97], [98], [99] have combined genetic algorithm and sliding mode control for diving and heading control. A given result of manual tuning and GA shows that it provides a faster design of controller than conventional design. Naeem *et al.* [106] have presented a new approaches in autopilot design using a genetic algorithm based model predictive control for a low cost AUV. GAs for the model predictive controller provides minimised cost function and process model both linear and nonlinear terms. It claims that the

design is online optimisation which reports a good result of simulations.

2.3.6 Optimal Control

Optimality also plays an important rôle in the field of motion controls where many researchers have carried out work in optimality principles in marine applications. It appears that they want a system to perform better over a long time duration. Consider a dynamical system with state variable $\boldsymbol{x} \in \mathbb{R}^m$ and control signal $\boldsymbol{u} \in \mathbb{R}^n$,

$$\dot{\boldsymbol{x}} = f(\boldsymbol{x}, \boldsymbol{u}, \boldsymbol{t}), \quad \boldsymbol{x}(0) = \boldsymbol{x}_0,$$

and the performance criterion is expressed as,

$$J_0 = \int_0^T L(\boldsymbol{x}(t), \boldsymbol{u}(t)), \boldsymbol{t}) dt$$

The aim of the optimal control problem is to determine an admissible control $\boldsymbol{u}^*(t)$ that drives the system to follow a trajectory $\boldsymbol{x}^*(t)$ such that the cost function is minimised. Linear differential equations and the cost which are commonly described by a quadratic function is potentially considered for a controller design for marine vessels. The Lyapunov stability condition shows that the system $\dot{\boldsymbol{x}}(t) = \boldsymbol{A}\boldsymbol{x}(t)$ is stable if and only if there exists a positive definite matrix $\boldsymbol{P}$ such that $\boldsymbol{A}^\mathsf{T}\boldsymbol{P} + \boldsymbol{P}\boldsymbol{A} = 0$. In the context of nonlinear problem, one of the design methodologies is the state-dependent Riccati equation approach [21], [140]. The system $\dot{\boldsymbol{x}} = \boldsymbol{A}(\boldsymbol{x})\boldsymbol{x} + \boldsymbol{B}(\boldsymbol{x})\boldsymbol{u}$, such that the state-dependent Riccati equation can be solved as $\boldsymbol{A}^\mathsf{T}(\boldsymbol{x})\boldsymbol{P}(\boldsymbol{x}) + \boldsymbol{P}(\boldsymbol{x})\boldsymbol{A}(\boldsymbol{x}) - \boldsymbol{P}(\boldsymbol{x})\boldsymbol{B}(\boldsymbol{x})\boldsymbol{R}^{-1}(\boldsymbol{x})\boldsymbol{B}^\mathsf{T}(\boldsymbol{x})\ \boldsymbol{P}(\boldsymbol{x}) + \boldsymbol{Q}(\boldsymbol{x}) = 0$, where $\boldsymbol{P}(\boldsymbol{x}) > 0$. Recently, work on a depth control based on solving the algebraic Riccati equation [108] for an AUV has been developed.

Another popular optimal control method is Model Predictive Control (MPC). MPC is an open-loop control sequence calculation for future behaviour of a process plant over a prescribed period. The main idea behind MPC is to determine future

values of the control inputs by optimising a cost function which expresses the control objectives. MPC can be found in a wide area of applications such as chemical process industries, automotive engineering. The main characteristics of the controller are: (i) explicit use of a nonlinear model to predict the process output at future time instants; (ii) calculation of a control sequence minimising an open-loop objective function and; (iii) receding horizon strategy so that at each instant the horizon is displaced towards the future, which involves the application of the first control signal of the sequence calculated at each step. Naeem *et al.* [105], [107] have studied MPC for AUV's heading control. Optimum design of the cost function is done by using the genetic algorithm. The optimisation of the GA controller can be implemented online however it is computational time consuming. The MPC is quite suitable for the real implementation because it needs only finite future command signals. However, it would be difficult in the infinite time optimal tracking problem since it need the command signals known for the infinite time previously. The MPC can be a proper control design method for an AUV with system's uncertainties and disturbance which are added at arbitrary time and only finite horizon command signals is known.

2.3.7 Backstepping

Backstepping is an important nonlinear control design technique with numerous applications [77]. The backstepping technique employs Lyapunov synthesis to recursively determine controllers for systems satisfying a particular cascaded structure [156]. Furthermore, it can accommodate, by explicitly accounting for, large nonlinearities and uncertainties in the system's model whilst ignoring dynamics, input and measurement disturbances. However, standard backstepping techniques produce highly aggressive controllers that require unbounded inputs. This is unsuitable for real systems due to actuator saturation and the possibility of hard bounds on the physical system states [112].

Basically, the backstepping technique is a mathematically model-based for exam-

ining the system, introducing new variables into it in a form depending upon the state variables, controlling parameters, and stabilising functions. The task of a stabilising function, the so called Control Lyapunov Function (CLF) is to compensate for nonlinearities recorded in the system and affecting the stability of its operation. The use of linearisation methods in feedback-based systems aims at eliminating nonlinearities existing in the system. The backstepping method is then recursively used to create, in an arbitrary way, additional nonlinearities [44] and introduce them into the control process to eliminate undesirable nonlinearities from the system.

In the marine application, ship control systems which are studied in [39], [44] require information on accurate models of all existing nonlinearities, which are unavailable in most practices. The backstepping method permits global stability to be obtained in the cases when the feedback linearisation method only secures local stability. In [26], [27] the backstepping methods are used in controlling ship's steering on its course to secure course stabilisation. Other uses of the backstepping technique can be found in chapter 5.

2.3.8 Sliding Mode Control

Sliding Mode Control also known as variable structure system is able to provide robustness against disturbances and parameter variations. Sliding mode control has been in existence since the 1960s in the Soviet Union and primarily proposed by Utkin [146]. The basic idea of sliding mode control is to reduce the difficult problem of a high order nonlinear system with uncertainty to a simpler problem of a first order system. In order to illustrate this, consider a Single Input/Single Output (SISO) system. The goal of the controller is to drive the state space error of the system e to zero. In general, a system with degree n can use a sliding mode of the form,

$$\sigma = \frac{d^{n-1}}{dt^{n-1}}e + \sum_{i=0}^{n-2} \frac{d^i}{dt^i}\lambda_i e.$$

where the λ_i values are chosen so that the dynamics defined by $\sigma = 0$ are stable. Work from Utkin [146] present the state feedback equivalent control which guarantees the robustness by using Lyapunov functions. SISO and Multi-Input/Multi-Output (MIMO) method are formally stated in the book published by Slotine and Li [135]. Yoerger and Slotine [158] used a robust sliding mode control, where a nonlinear control system design was applied to underwater vehicles' trajectory control at low speed. Fossen and Foss [42] improved the performance of a sliding mode control of a nonlinear system by using MIMO mode which is illustrated by the simulation of a polymerization reactor using in the process control. Healey and Lienard [54] used a multivariable sliding mode control for underwater vehicles and combine its equations of motion for three separate autopilot modes of speed, steering and diving control. Sliding mode control has been successfully implemented and tested for underwater vehicles. It is shown in these articles that the sliding mode controller is robust to uncertainties in the system. It can compensate for the deficiencies caused by unmodelled dynamics and external disturbances. It also can be extended to an adaptive control to compensate for changes in environment and vehicle configuration.

2.4 Overview of Marine Control System

To study marine control systems, Fossen [39] has standardised the notation for marine vessel models. The mathematical modellings are briefly presented in this section, whilst a more detailed description is found in appendix A, B.

Modelling

A marine vessel has six degrees of freedom as a rigid body. The generalised position, velocity and force-moment vectors are,

$$\begin{aligned} \boldsymbol{\eta} &= [x, y, z, \phi, \theta, \psi]^{\mathsf{T}} \\ \boldsymbol{\nu} &= [u, v, w, p, q, r]^{\mathsf{T}} \\ \boldsymbol{\tau} &= [X, Y, Z, K, M, N]^{\mathsf{T}} \end{aligned}$$

where $[\bullet]^{\mathsf{T}}$ is the transpose of a matrix. The generalised position $\boldsymbol{\eta}$ and velocity $\boldsymbol{\nu}$ are expressed with respect to a earth-fixed frame and body-fixed frame as following,

$$\dot{\boldsymbol{\eta}} = \boldsymbol{J}(\boldsymbol{\Theta})\boldsymbol{\nu}$$

The transformation matrix is,

$$\boldsymbol{J}(\boldsymbol{\Theta}) = \begin{bmatrix} \boldsymbol{R}(\boldsymbol{\Theta}) & \mathbf{0} \\ \mathbf{0} & \boldsymbol{T}(\boldsymbol{\Theta}) \end{bmatrix}$$

where $\boldsymbol{\Theta} = [\phi, \theta, \psi]^{\mathsf{T}}$, $\boldsymbol{R}(\boldsymbol{\Theta})$, $\boldsymbol{T}(\boldsymbol{\Theta})$ are a linear and angular velocity transformation respectively.

Now consider the rigid-body equation of motion,

$$\boldsymbol{M}_{RB}\dot{\boldsymbol{\nu}} + \boldsymbol{C}_{RB}(\boldsymbol{\nu})\boldsymbol{\nu} = \boldsymbol{\tau}_{RB}$$

The generalised hydrodynamic force $\boldsymbol{\tau}_H$ can be expressed,

$$\boldsymbol{\tau}_H = -\boldsymbol{M}_A\dot{\boldsymbol{\nu}} - \boldsymbol{C}_A(\boldsymbol{\nu})\boldsymbol{\nu} - \boldsymbol{D}(\boldsymbol{\nu})\boldsymbol{\nu} - \boldsymbol{g}(\boldsymbol{\nu})$$

The forces and moments can defined,

$$\boldsymbol{\tau}_H = \boldsymbol{\tau} + \boldsymbol{\tau}_{env}$$

where $\boldsymbol{\tau}$ is the control forces and moments, $\boldsymbol{\tau}_{env}$ is the forces and moments due to wind, waves and currents.

The system inertia and Coriolis/Centripetal matrices (see appendix B) are determined,

$$\boldsymbol{M} = \boldsymbol{M}_{RB} + \boldsymbol{M}_{A}$$

and,

$$\boldsymbol{C} = \boldsymbol{C}_{RB} + \boldsymbol{C}_{A}$$

Hence, the generalised equation of motion for a marine vessel is,

$$\boldsymbol{M}\dot{\boldsymbol{\nu}} + \boldsymbol{C}(\boldsymbol{\nu})\boldsymbol{\nu} + \boldsymbol{D}(\boldsymbol{\nu})\boldsymbol{\nu} + \boldsymbol{g}(\boldsymbol{\eta}) = \boldsymbol{\tau} + \boldsymbol{\tau}_{env}$$

2.5 Summary

Various kinds of controller designed for underwater vehicle have been described and summarised in this chapter. Advantages and disadvantages of the control techniques are given. In the underwater environment, there are hydrodynamics affects and uncertainties such as disturbance and sensor noise which influence the vehicle and thruster dynamics. These are nonlinear terms which make controlling AUVs challenging. To deal with this control problem, a robust sliding mode control is researched because it is well-established in other engineering communities, and more importantly it is able to provide robustness against unmodelled uncertainty and external disturbances. The sliding mode control is a mature discipline and formulated in a mathematically model-based form. The sliding mode design consists of two general components. The first involves the design of a switching function so that the sliding motion satisfies the design criteria. The second is considered with the selection of a control law which will make the switching function attractive to the system state. These makes the method an appropriate candidate for a robust control. Further study is detailed in chapter 3

Table 2.1: Summary of controls for underwater vehicles

Reference	Vehicle	Country	Year	Control Technique	Result
Healey [54]	NPS	USA	1993	Sliding mode control	Simulation
Logan [95]	Sea Squirt	USA	1994	$\mathcal{H}_\infty$, Sliding mode control	Simulation
Jalving [61], [59]	NDRE-AUV	Norway	1994	PID	Experiment
Liceaga-Castro [94]	Submarine	UK	1995	$\mathcal{H}_\infty$	Experiment
McGookin [98], [97]	Submarine	UK	1996	Sliding mode control, GAs	Simulation
McPhail [101]	Autosub-1	UK	1997	PID	Simulation & Experiment
Silvestre [130], [131]	SIREN	Portugal	1998	Sliding mode control, Gain scheduling	Simulation & Experiment
Lea [87]	Subzero II	UK	1999	PID, Sliding mode control, Fuzzy logic	Simulation & Experiment
Yuh [161]	ODIN	USA	1999	Adaptive control	Simulation
Innocenti [58]	AUV-model	Italy	1999	Sliding mode control, $\mathcal{H}_\infty$	Simulation

Table 2.2: Summary of controls for underwater vehicles (continued)

Reference	Vehicle	Country	Year	Control Technique	Result
Silpa-Anan [129]	Kambara	Australia	2001	PID, Visual servo	Simulation
Song [139]	OEX	USA	2002	Sliding mode control, Fuzzy logic	Simulation & Experiment
Kim [71]	AUV-model	Korea	2002	Sliding mode observer, Kalman	Simulation
Walchko [149]	Subjugator	USA	2003	Sliding mode control, Kalman	Experiment
Salgado-Jimenez [123]	Taipan	France	2003	PD, Sliding mode control	Experiment
Jalving [60]	HUGIN AUV	Norway	2003	Kalman	Simulation & Experiment
Sun [141]	ODIN	Singapore	2003	Adaptive set-point PD	Simulation
Kim [72]	AUV-SNUUV I	Korea	2004	sliding mode control, Kalman	Simulation & Experiment
Kanakakis [67]	NPS Pheonix	Greece	2004	Fuzzy logic	Simulation
Naeem [106]	REMUS	UK	2005	GAs, Model predictive control	Simulation & Experiment

Table 2.3: Summary of controls for underwater robotic vehicles

Reference	Vehicle	Year	Control Techniques	Vehicle-Arm DOF (n)	Result
Schjølberg [127]	ROV	1994	Linearisation	6+n	–
Dunnigan [30], [29]	ODIN	1998	PI, Sliding mode control	6+3	Simulation
Antonelli [7], [6]	UVMS	1998	Sliding mode control	6+n	Simulation
Lee [88]	ROV	2000	Neural networks	6+2	Simulation
Sarkar [126]	UVMS	2001	PI	6+n	Simulation
Ryn [122]	ROV	2001	Disturbance observer	3+2	Simulation
Lapierre [81]	ODIN	2003	PID	3+2	Simulation & Experiment
Kim [70]	ODIN	2003	Linearisation	6+n	–
Vossoughi [147]	ROV	2004	Sliding mode control, Kalman	6+n	Simulation
Do [26]	ROV	2004	Output-feedback	3+0	–

Table 2.4: Summary of advantages and disadvantages of control techniques for marine applications

Control Techniques	Problem	Solution	Robustness against uncertainty	Stability	Required dynamic model	Control level	Computational Time
Classical PID	Linear	General/ Analytical	No	Yes	Accurate	Low	Less
Adaptive control	Linear/ Nonlinear	General/ Analytical	Yes	Yes	Accurate	Low	Medium
Fuzzy logic	Linear/ Nonlinear	Linguistic	No/Yes	No/Yes	ill-modelled	High	Medium-Costly
Neural networks	Linear/ Nonlinear	Learning method	No/Yes	No/Yes	ill-modelled	High	Costly
GAs	Linear/ Nonlinear	Searching algorithm	No/Yes	No/Yes	ill-modelled	High	Costly
Optimal control	Linear/ Nonlinear	General/ Analytical	No/Yes	Yes	Accurate	Low	Medium-Costly
Backstepping	Linear/ Nonlinear	Complex recursive analytical	Yes	Yes	Accurate	Low	Medium
Sliding mode	Linear/ Nonlinear	General/ Analytical	Yes	Yes	Accurate	Low	Less

Chapter 3

Controller Design

3.1 Overview of Chapter

As pointed out in the previous chapter, a robust control plays a fundamental rôle in marine applications. However, a conventional PID controller is insufficient in non-linear problems. For example, an AUV is in the slow control and measurement frequency with significant measurement corruptions and severe thruster saturation. This is quite difficult to tune the PID controller gains properly. In this chapter the interest therefore focuses on designing a robust controller based on the sliding mode control and an optimal control based on state-dependent Riccati equation approach. One of the advantages of the sliding mode is that the closed loop response becomes totally insensitive to a particular class of uncertainty. In addition, a closed loop system solved by using the state-dependent Riccati equation method provides a selection of an optimal sliding surface producing optimal control inputs for the system. An introduction to sliding mode control concept is given in section 3.2. In section 3.3 the decoupled models of an AUV is developed. Section 3.4 illustrates simulation results of this conventional sliding mode controller for each subsystem. Section 3.5 presents

a high-order sliding mode controller. This is followed by an optimal control using the state-dependent Riccati equation method in section 3.6. The simulations of comparative studies are demonstrated in section 3.7. Finally section 3.8 gives a chapter summary.

3.2 Sliding Mode Control

Many studies have been undertaken in order to correct errors in attitude and depth control [15], [144] for nonlinear control system. Most stability schemes are formulated based on the Lyapunov method. The method is a power tool for stability analysis which can be used for the design of the nonlinear controllers. One of the most common nonlinear feedback controller designs based on the Lyapunov analysis is sliding mode control (SMC). It is categorised as a variable structure control system [146] which has been studied in the Soviet Union for many years. The SMC has been used for AUV control because of excellent stability, robustness and disturbance rejection characteristics [54], [135]. Fundamentally, the sliding mode controller is composed of two main parts, namely nominal part and discontinuous terms dealing with uncertainties. The controller with the typical sliding mode is to drive the system state error trajectory onto the sliding surface and maintain that trajectory onto the surface for all times. Thus, the sliding mode becomes insensitive to system disturbances whilst on the sliding surface. Figure 3.1 illustrates the basic block diagram of the sliding mode controller for heading and depth subsystem. Furthermore the significant characteristics of the sliding mode are order reduction and robust stability [54], [146].

3.2.1 Fundamental

To derive the steady state error to converge to zero, a global asymptotical convergence of system trajectory to a stable equilibrium on the sliding surface should be ensured.

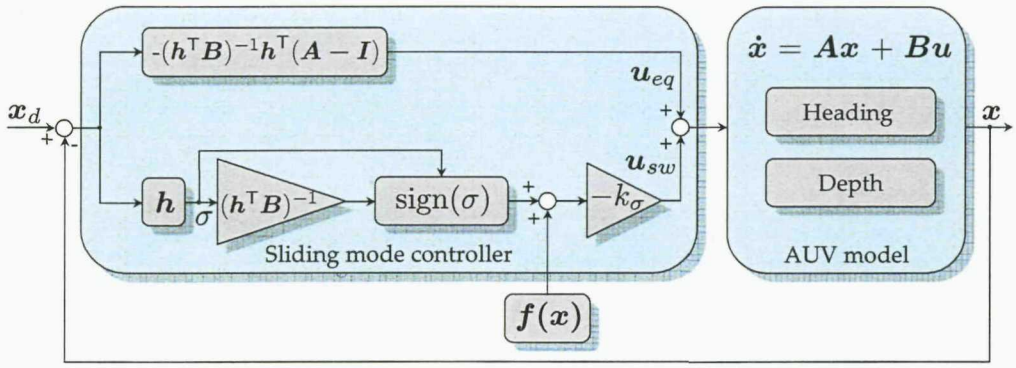

Figure 3.1: Block diagram of a sliding mode controller.

A candidate Lyapunov function $V(\sigma)$ is suitably selected such that the Lyapunov stability theorem (see details in appendix C) is satisfied [135].

3.2.2 Sliding Surface

In the system described by nonlinear differential equations,

$$x = f(x, u, t) \tag{3.1}$$

where $x \in \mathbb{R}^n$, $f \in \mathbb{R}^n$, $u \in \mathbb{R}^m$ and t denotes the time.

The control is chosen as a discontinuous function to force system state trajectories to some nonlinear surfaces $\sigma_i = 0$,

$$u_i = \begin{cases} u_i^+(x,t), & \text{if } \sigma_i(x) > 0, \quad (i = 1, \ldots, m); \\ u_i^-(x,t), & \text{if } \sigma_i(x) < 0, \quad (i = 1, \ldots, m); \end{cases}$$

where $u_i^+(x,t)$ and $u_i^-(x,t)$ are continuous state function with $u_i^+(x,t) \neq u_i^-(x,t)$ and the $\sigma_i(x)$ are continuous state functions.

The sliding manifold on which the system state in the intersection of the $m-$dimensional sliding surface,

$$\mathcal{S} = \{(x,t) \in \mathbb{R}^n \times \mathbb{R} \quad | \quad \sigma(x,t) = 0\} \tag{3.2}$$

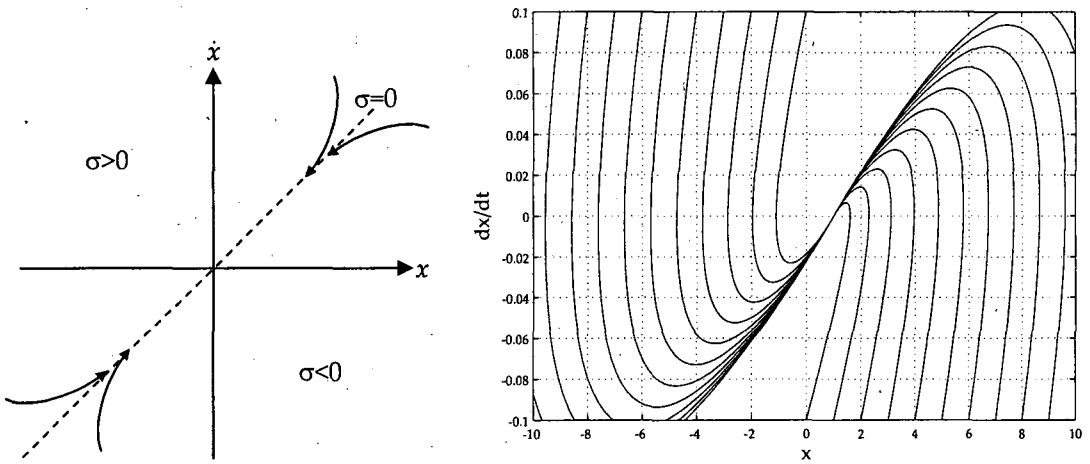

(a) (b)

Figure 3.2: Sliding surface: (a) Phase portrait, (b) Computer simulation of solution trajectory converged to sliding surface.

where $\sigma(x,t) = [\sigma_1(x,t), \ldots, \sigma_m(x,t)]^{\mathsf{T}} = 0$.

Generally the state space of a nonlinear system [54] is described by,

$$\dot{\boldsymbol{x}} = \boldsymbol{A}\boldsymbol{x} + \boldsymbol{B}\boldsymbol{u} + \boldsymbol{f}(\boldsymbol{x}). \tag{3.3}$$

where $\boldsymbol{x}$ is the state vector, $\boldsymbol{A}$ is the system matrix, $\boldsymbol{B}$ is the input matrix, $\boldsymbol{u}$ is the input of the system and $\boldsymbol{f}(\boldsymbol{x})$ is the unknown function representing the model uncertainty that would cause the system deviate from its equilibrium point. Define the tracking error,

$$\tilde{\boldsymbol{x}} = \boldsymbol{x} - \boldsymbol{x}_d, \tag{3.4}$$

where $\boldsymbol{x}_d$ is desired state trajectory. The problem of tracking defined as $\boldsymbol{x} \equiv \boldsymbol{x}_d$ is equivalent to that of remaining on the surface ($\sigma = \sigma(x,t)$) for all time $t > 0$.

Next, a time-varying sliding surface σ suggested in [39], [98] can be defined as,

$$\sigma = \boldsymbol{h}^{\mathsf{T}}\tilde{\boldsymbol{x}} = \boldsymbol{h}^{\mathsf{T}}(\boldsymbol{x} - \boldsymbol{x}_d), \tag{3.5}$$

where $\boldsymbol{h}$ is a chosen design vector such that $\sigma(\tilde{\boldsymbol{x}})$ converges to zero. The sliding surface is designed so that the trajectories of a dynamical system tend to and converge to

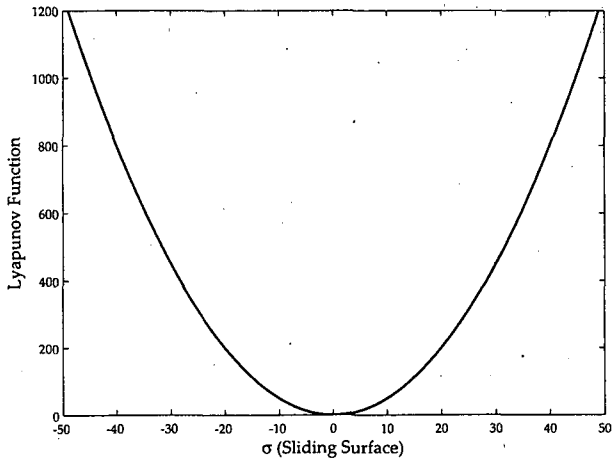

Figure 3.3: A sample plot of Lyapunov function against sliding surface.

the sliding surface (see figure 3.2 (a)) when it satisfies the Lyapunov stability [135]. An example of computer simulation shows the state trajectories for a dynamic system using the design sliding mode control (shown in figure 3.2 (b)).

The candidate Lyapunov function is expressed as follows,

$$V(\sigma) = \frac{1}{2}\sigma^2, \tag{3.6}$$

Figure 3.3 shows a plot of candidate Lyapunov function in equation (3.6), and then its derivative must satisfy,

$$\dot{V}(\sigma) = \frac{\partial V(\sigma)}{dt} = \frac{\partial V(\sigma)}{\partial \sigma}\frac{\partial \sigma}{dt} = \frac{\partial(\frac{1}{2}\sigma^2)}{\partial \sigma}\frac{\partial \sigma}{dt} = \sigma\frac{d\sigma}{dt} = \sigma\dot{\sigma} \leq 0 \tag{3.7}$$

The condition when the sliding surface $\sigma = 0$ and $\dot{\sigma} = 0$ is reached in a finite time if,

$$\begin{aligned} \dot{\sigma}\sigma &\leq -k_\sigma|\sigma|, \\ \dot{\sigma} &\leq -k_\sigma \operatorname{sign}(\sigma), \end{aligned} \tag{3.8}$$

and sign(σ) is a signum function which is defined as,

$$\text{sign}(\sigma) = \begin{cases} -1, & \text{if } \sigma < 0; \\ 0, & \text{if } \sigma = 0; \\ 1, & \text{if } \sigma > 0. \end{cases}$$

Differentiating equation (3.5) with respect to time,

$$\dot{\sigma} = \boldsymbol{h}^{\mathsf{T}}(\boldsymbol{A}\boldsymbol{x} + \boldsymbol{B}\boldsymbol{u} + \boldsymbol{f}(\boldsymbol{x}) - \dot{\boldsymbol{x}}_d), \tag{3.9}$$

and substituting with equation (3.3) and (3.8), gives,

$$\boldsymbol{h}^{\mathsf{T}}(\boldsymbol{A}\boldsymbol{x} + \boldsymbol{B}\boldsymbol{u} + \boldsymbol{f}(\boldsymbol{x}) - \dot{\boldsymbol{x}}_d) = -k_\sigma \,\text{sign}(\sigma). \tag{3.10}$$

These control inputs can be regarded as that for the nominal plant (equivalent control) and discontinuous term (switching function) for the uncertainty,

$$\boldsymbol{u} = \boldsymbol{u}_{eq} + \boldsymbol{u}_{sw}. \tag{3.11}$$

Therefore equation (3.10) can be rearranged in the following feedback control law,

$$\boldsymbol{u} = \frac{1}{\boldsymbol{h}^{\mathsf{T}}\boldsymbol{B}}(-\boldsymbol{h}^{\mathsf{T}}\boldsymbol{A}\boldsymbol{x}) + \frac{1}{\boldsymbol{h}^{\mathsf{T}}\boldsymbol{B}}(\boldsymbol{h}^{\mathsf{T}}\dot{\boldsymbol{x}}_d - \boldsymbol{h}^{\mathsf{T}}\boldsymbol{f}(\boldsymbol{x}) - k_\sigma \,\text{sign}(\sigma)). \tag{3.12}$$

This simplifies equation (3.12) when $\dot{\boldsymbol{x}}_d$ and $\boldsymbol{f}(\boldsymbol{x}) = 0$ leads to the following,

$$\boldsymbol{u} = -\boldsymbol{k}^{\mathsf{T}}\boldsymbol{x} - K_\sigma \,\text{sign}(\sigma). \tag{3.13}$$

Substituting equation (3.13) into equation (3.9). Consider only the first term, the equation is now written,

$$\boldsymbol{k}^{\mathsf{T}} = (\boldsymbol{h}^{\mathsf{T}}\boldsymbol{B})^{-1}\boldsymbol{h}^{\mathsf{T}}\boldsymbol{A}$$

such that,

$$\boldsymbol{h}^{\mathsf{T}}(\boldsymbol{A} - \boldsymbol{B}\boldsymbol{k}^{\mathsf{T}}) = 0 \quad \text{and} \quad \boldsymbol{A}_c = \boldsymbol{A} - \boldsymbol{B}\boldsymbol{k}^{\mathsf{T}}.$$

Hence, $\boldsymbol{h}$ is a right eigenvector of $\boldsymbol{A}_c^{\mathsf{T}}$ where $\boldsymbol{k}$ is the state feedback gain vector (see appendix C) obtained from pole placement or by solving linear quadratic regulation problem and K_σ is a constant, corresponding to the maximum value of the controller input.

3.2.3 Chattering

A switching action known as chattering which is caused by a signum function, thus the switching action may cause the system response to oscillate about the zero sliding surface in high frequency mode. It can thus cause wear on the actuators. To reduce the effect of chattering, a thin boundary layer of thickness around the switching surface is proposed in [135],

$$\boldsymbol{u} = -\boldsymbol{k}^{\mathsf{T}}\boldsymbol{x} - K_\sigma \,\mathrm{sat}(\frac{\sigma}{\Phi}) \tag{3.14}$$

where the constant Φ defines the thickness of the boundary layer and $\mathrm{sat}(\frac{\sigma}{\Phi})$ is a saturation function that is defined as,

$$\mathrm{sat}(\frac{\sigma}{\Phi}) = \begin{cases} \frac{\sigma}{\Phi}, & \text{if } |\frac{\sigma}{\Phi}| \leq 1; \\ \mathrm{sign}(\frac{\sigma}{\Phi}), & \text{otherwise.} \end{cases}$$

Furthermore an improvement to this behaviour is found by using a hyperbolic tangent function to replace the signum, to give a smooth control activity near sliding surface [148], so,

$$\boldsymbol{u} = -\boldsymbol{k}^{\mathsf{T}}\boldsymbol{x} - K_\sigma \tanh(\frac{\sigma}{\Phi}) \tag{3.15}$$

Three types of switching function previously defined are illustrated for the single case in figure 3.4. The rôle of the sliding mode controller is to drive the system towards the sliding surface and keep it on the sliding surface. The sliding mode control is therefore able to improve a capability to track the desired state of the AUV modelling. Decoupled models of an AUV is discussed in the following section. The rôle of the sliding mode controller is to drive the system towards the sliding surface and keep it on the sliding surface. The sliding mode is a robust control design therefore it is able to improve a capability to track the desired state of the AUV modelling. Decoupled models of an AUV are discussed in the following section.

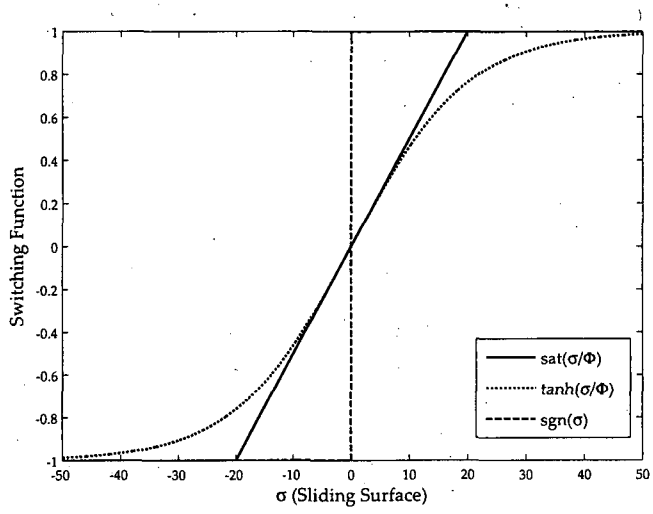

Figure 3.4: Plots of three switching functions VS sliding surface

3.3 Common Decoupled Subsystems of an AUV

The control of all six degrees of freedom AUV may be important for the operation, particularly in the motion transition. It is however not the primary focus in this research due to its complexity. The general six degrees of freedom AUV can divided into lightly interacting or non-interacting subsystems. Thus the computational time in determining each single control element will be relatively short. A controller that is decoupled into two subsystems of heading and depth (see figure 3.5) is commonly found in [39], [54]. In the following sections, two subsystems based on the sliding mode are detailed. Based on the parameters defined in appendix D.

Generally, the kinematics and dynamics of 6-DOFs AUV can be represented as,

$$\begin{aligned} \dot{\boldsymbol{\eta}} &= \boldsymbol{J}(\Theta)\boldsymbol{\nu} \\ \boldsymbol{M}\dot{\boldsymbol{\nu}} + \boldsymbol{C}(\boldsymbol{\nu})\boldsymbol{\nu} + \boldsymbol{D}(\boldsymbol{\nu})\boldsymbol{\nu} + \boldsymbol{g}(\boldsymbol{\eta}) &= \boldsymbol{\tau} \end{aligned}$$

thus, it can be written in the following form,

$$\dot{\boldsymbol{\nu}} = \boldsymbol{A}\boldsymbol{\nu} + \boldsymbol{B}\boldsymbol{\tau} + \boldsymbol{f}(\boldsymbol{\nu}, \boldsymbol{\eta}), \tag{3.16}$$

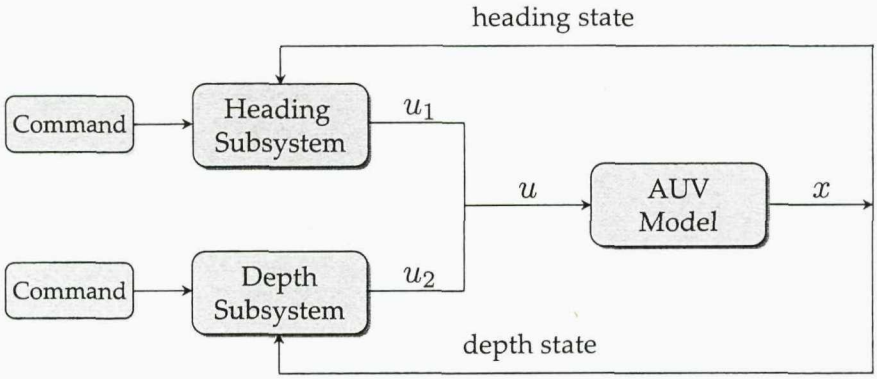

Figure 3.5: Simple block diagram of heading and depth subsystem.

from section 3.2,

$$\dot{\boldsymbol{\nu}}_1 = \boldsymbol{A}_1\boldsymbol{\nu}_1 + \boldsymbol{B}_1\boldsymbol{\tau}_1 + \boldsymbol{f}(\boldsymbol{\nu}_1, \boldsymbol{\eta}_1), \tag{3.17}$$

$$\dot{\boldsymbol{\nu}}_2 = \boldsymbol{A}_2\boldsymbol{\nu}_2 + \boldsymbol{B}_2\boldsymbol{\tau}_2 + \boldsymbol{f}(\boldsymbol{\nu}_2, \boldsymbol{\eta}_2), \tag{3.18}$$

Controller design using the sliding mode control in equation (3.17) and (3.18) are then proceeded in the following section. However, some modifications are made that allows the vehicle to be able to track a time-varying and surge velocity references.

Controller Design for a Torpedo Shaped AUV

The controller design is concerned in this section. The heading subsystem comprises the sway velocity v, the yaw rate r and the heading angle ψ. The depth subsystem comprised the surge velocity u, the heave velocity w, the pitch velocity q and the pitch angle θ.

Let us define,

$$\boldsymbol{\nu}_1 = [v, r]^\mathsf{T} \tag{3.19}$$

$$\boldsymbol{\nu}_2 = [u, w, q]^\mathsf{T} \tag{3.20}$$

Next, the heading and depth subsystem are given by,

$$\boldsymbol{x}_1 = [\boldsymbol{\nu}_1^\mathsf{T}, \psi]^\mathsf{T} \tag{3.21}$$

$$\boldsymbol{x}_2 = [\boldsymbol{\nu}_2^\mathsf{T}, \theta]^\mathsf{T} \tag{3.22}$$

Thus, the state spaces of the subsystems are,

$$\dot{\boldsymbol{x}}_1 = \boldsymbol{A}_1\boldsymbol{x}_1 + \boldsymbol{B}_1\boldsymbol{u}_1 + \boldsymbol{f}(\boldsymbol{x}_1) \tag{3.23}$$

$$\dot{\boldsymbol{x}}_2 = \boldsymbol{A}_2\boldsymbol{x}_2 + \boldsymbol{B}_2\boldsymbol{u}_2 + \boldsymbol{f}(\boldsymbol{x}_2) \tag{3.24}$$

Let us define the tracking error for heading and depth mode,

$$\tilde{\boldsymbol{x}}_1 = \boldsymbol{x}_1 - \boldsymbol{x}_{1d} \tag{3.25}$$

$$\tilde{\boldsymbol{x}}_2 = \boldsymbol{x}_2 - \boldsymbol{x}_{2d} \tag{3.26}$$

where $\boldsymbol{x}_{1d} = [0, r_d(t), \psi_d(t)]^\mathsf{T}$ and $\boldsymbol{x}_{2d} = [u_d(t), 0, q_d(t), \theta_d(t)]^\mathsf{T}$ are desired states. The desired sway and heave velocity cannot be specified as there is no independent control in sway, such that the $r_d(t) = \cos\theta\dot{\psi}_d(t)$, except $w_d(t)$ cannot be controlled independently of the other state vectors.

Now differentiating equation (3.25), (3.26) and substituting with equation (3.23), (3.24) gives,

$$\dot{\tilde{\boldsymbol{x}}}_1 = \boldsymbol{A}_1\boldsymbol{x}_1 + \boldsymbol{B}_1\boldsymbol{u}_1 + \boldsymbol{f}_1(\boldsymbol{x}_1) - \dot{\tilde{\boldsymbol{x}}}_{1d} \tag{3.27}$$

$$\dot{\tilde{\boldsymbol{x}}}_2 = \boldsymbol{A}_2\boldsymbol{x}_2 + \boldsymbol{B}_2\boldsymbol{u}_2 + \boldsymbol{f}_2(\boldsymbol{x}_2) - \dot{\tilde{\boldsymbol{x}}}_{2d} \tag{3.28}$$

Similar to the definition, time-varying sliding surfaces are defined as,

$$\sigma_1 = \boldsymbol{h}_1^\mathsf{T}\tilde{\boldsymbol{x}}_1 \tag{3.29}$$

$$\sigma_2 = \boldsymbol{h}_2^\mathsf{T}\tilde{\boldsymbol{x}}_2 \tag{3.30}$$

then the switching control can be obtained as,

$$\boldsymbol{u}_{1sw} = \frac{1}{\boldsymbol{h}_1^\mathsf{T}\boldsymbol{B}_1}(\boldsymbol{h}_1^\mathsf{T}\dot{\boldsymbol{x}}_{1d} - \boldsymbol{h}_1^\mathsf{T}\boldsymbol{f}_1(\boldsymbol{x}_1) - k_{1\sigma}\,\mathrm{sign}(\sigma_1)),$$

$$\boldsymbol{u}_{2sw} = \frac{1}{\boldsymbol{h}_2^\top \boldsymbol{B}_2}(\boldsymbol{h}_2^\top \dot{\boldsymbol{x}}_{2d} - \boldsymbol{h}_2^\top \boldsymbol{f}_2(\boldsymbol{x}_2) - k_{2\sigma}\,\mathrm{sign}(\sigma_2)),$$

To guarantee the stability of the controller for the heading and depth control, its derivative of control Lyapunov function then must satisfy by following equation (3.13) in section 3.2,

$$\begin{aligned} \dot{V}(\sigma_1) &= \sigma_1 \dot{\sigma}_1 \\ &= \sigma_1 \boldsymbol{h}_1^\top (\boldsymbol{A}_{1c}\boldsymbol{x}_1 + \boldsymbol{B}_1\boldsymbol{u}_1 + \boldsymbol{f}_1(\boldsymbol{x}_1) - \dot{\boldsymbol{x}}_{1d}) \\ &= -K_{\sigma_1}\sigma_1^2 + \sigma_1 \boldsymbol{h}_1^\top \boldsymbol{A}_{1c}\boldsymbol{x}_1 \\ &\leq -|K_{\sigma_1}|\sigma_1^2 \end{aligned} \tag{3.31}$$

and,

$$\begin{aligned} \dot{V}(\sigma_2) &= \sigma_2 \dot{\sigma}_2 \\ &= \sigma_2 \boldsymbol{h}_2^\top (\boldsymbol{A}_{2c}\boldsymbol{x}_2 + \boldsymbol{B}_2\boldsymbol{u}_2 + \boldsymbol{f}_2(\boldsymbol{x}_2) - \dot{\boldsymbol{x}}_{2d}) \\ &= -K_{\sigma_2}\sigma_2^2 + \sigma_2 \boldsymbol{h}_2^\top \boldsymbol{A}_{2c}\boldsymbol{x}_2 \\ &\leq -|K_{\sigma_2}|\sigma_2^2 \end{aligned} \tag{3.32}$$

where $\boldsymbol{h}^\top \boldsymbol{A}_c^\top \boldsymbol{x} = \lambda \boldsymbol{x}^\top \boldsymbol{h} = 0$ if $\boldsymbol{h}$ is chosen as right eigenvectors of $\boldsymbol{A}_c^\top$ for $\lambda = 0$. The derivative of the Lyapunov functions $\dot{V}(\sigma_1)$ and $\dot{V}(\sigma_2)$ of two subsystems are negative definite, thus they are rendered uniformly globally asymptotically stable (see appendix C for details).

3.3.1 Heading Subsystem

The heading subsystem presents the steering of the AUV which is concerned the AUV in x-y plane. The control input commands deflection of rudder. The heading subsystem comprises the sway velocity v, the yaw rate r, the heading angle ψ and the rudder deflection $\boldsymbol{u}_1$. Assuming an AUV moving forward with constant speed $u_0 = 1.3$ m/s, the linearised equation of motion for heading is given as follows,

$$\begin{bmatrix} m - Y_{\dot{v}} & mx_g - Y_{\dot{r}} & 0 \\ mx_g - N_{\dot{v}} & I_{zz} - N_{\dot{r}} & 0 \\ 0 & 0 & 1 \end{bmatrix} \begin{bmatrix} \dot{v} \\ \dot{r} \\ \dot{\psi} \end{bmatrix} = \begin{bmatrix} Y_v & Y_r - mu_0 & 0 \\ N_v & N_r - mx_g u_0 & 0 \\ 0 & 1 & 0 \end{bmatrix} \begin{bmatrix} v \\ r \\ \psi \end{bmatrix} + \begin{bmatrix} Y_\delta \\ N_\delta \\ 0 \end{bmatrix} \boldsymbol{u}_1. \tag{3.33}$$

Define the sliding surface for the heading subsystem,

$$\begin{aligned}\sigma_1 &= \boldsymbol{h}_1^{\mathsf{T}}(\boldsymbol{x}-\boldsymbol{x}_d),\\ &= s_1\tilde{v}+s_2\tilde{r}+s_3\tilde{\psi},\\ &= s_1(v-v_d)+s_2(r-r_d)+s_3(\psi-\psi_d).\end{aligned}$$

and the heading control law becomes,

$$\begin{aligned}\boldsymbol{u}_1 &= -\boldsymbol{k}_1^{\mathsf{T}}\boldsymbol{x}-K_\sigma\tanh(\frac{\sigma_1}{\Phi_1})\\ &= -k_{11}v-k_{12}r-k_{13}\psi-K_\sigma\tanh(\frac{\sigma_1}{\Phi_1})\end{aligned}$$

where a feedback gain $\boldsymbol{k}_1=[k_{11},k_{12},k_{13}]^{\mathsf{T}}$ for heading subsystem is determined by the pole placement method.

3.3.2 Depth Subsystem

The depth subsystem presents the depth motion of the AUV which is concerned the AUV in x-z plane. The control input commands deflection of sternplanes or bowplanes. The depth subsystem comprises the heave velocity w, the pitch angular velocity q, the pitch angle θ, the depth z and the sternplane deflection $\boldsymbol{u}_2$. Assuming an AUV moving forward with constant speed u_0, the linearised equation of motion in heave and pitch is given as follows,

$$\begin{bmatrix} m-Z_{\dot{w}} & -mx_g-Z_{\dot{q}} & 0 & 0\\ -mx_g-M_{\dot{w}} & I_{yy}-M_{\dot{q}} & 0 & 0\\ 0 & 0 & 1 & 0\\ 0 & 0 & 0 & 1\end{bmatrix}\begin{bmatrix}\dot{w}\\ \dot{q}\\ \dot{\theta}\\ \dot{z}\end{bmatrix} = \begin{bmatrix} Z_w & Z_q-mu_0 & 0 & 0\\ M_w & M_q-mx_gu_0 & -z_bW & 0\\ 0 & 1 & 0 & 0\\ 1 & 0 & -u_0 & 0\end{bmatrix}\begin{bmatrix}w\\ q\\ \theta\\ z\end{bmatrix} + \begin{bmatrix}Z_\delta\\ M_\delta\\ 0\\ 0\end{bmatrix}\boldsymbol{u}_2. \tag{3.34}$$

Define the sliding surface for the depth subsystem,

$$\begin{aligned}\sigma_2 &= \boldsymbol{h}_2^{\mathsf{T}}(\boldsymbol{x}-\boldsymbol{x}_d),\\ &= s_1\tilde{w}+s_2\tilde{q}+s_3\tilde{\theta}+s_4\tilde{z},\\ &= s_1(w-w_d)+s_2(q-q_d)+s_3(\theta-\theta_d)+s_4(z-z_d).\end{aligned}$$

and the heading control law becomes,

$$\begin{aligned}\boldsymbol{u}_2 &= -\boldsymbol{k}_2^{\mathsf{T}}\boldsymbol{x}-K_\sigma\tanh(\frac{\sigma_2}{\Phi_2})\\ &= -k_{21}w-k_{22}q-k_{23}\theta-k_{24}z-K_\sigma\tanh(\frac{\sigma_2}{\Phi_2})\end{aligned}$$

where a feedback gain $k_2=[k_{21},k_{22},k_{23},k_{24}]^{\mathsf{T}}$ for depth subsystem is determined by the pole placement method.

3.4 Case Study I

In this section, simulation results are implemented by using a design of sliding mode controllers as mentioned in section 3.3. Defining the parameters of a torpedo shaped AUV reported in [54] (see appendix D), the simulation of subsystems are implemented. In the heading control, the amplitude of heading angle is chosen as $\psi_d = 60°$. Figure 3.6 depicts the results of plots for sliding mode controller without disturbance. Figure 3.7 shows that the model of control system oscillated which is caused by disturbance. The disturbance is modelled as a random noise $0.01*\texttt{rand}(1)$ (see figure E.1) in each state of the channel. From simulation, sliding mode controller is able to provide accurate control for system without disturbance and also manage the heading for system with disturbance, only with small steady state errors.

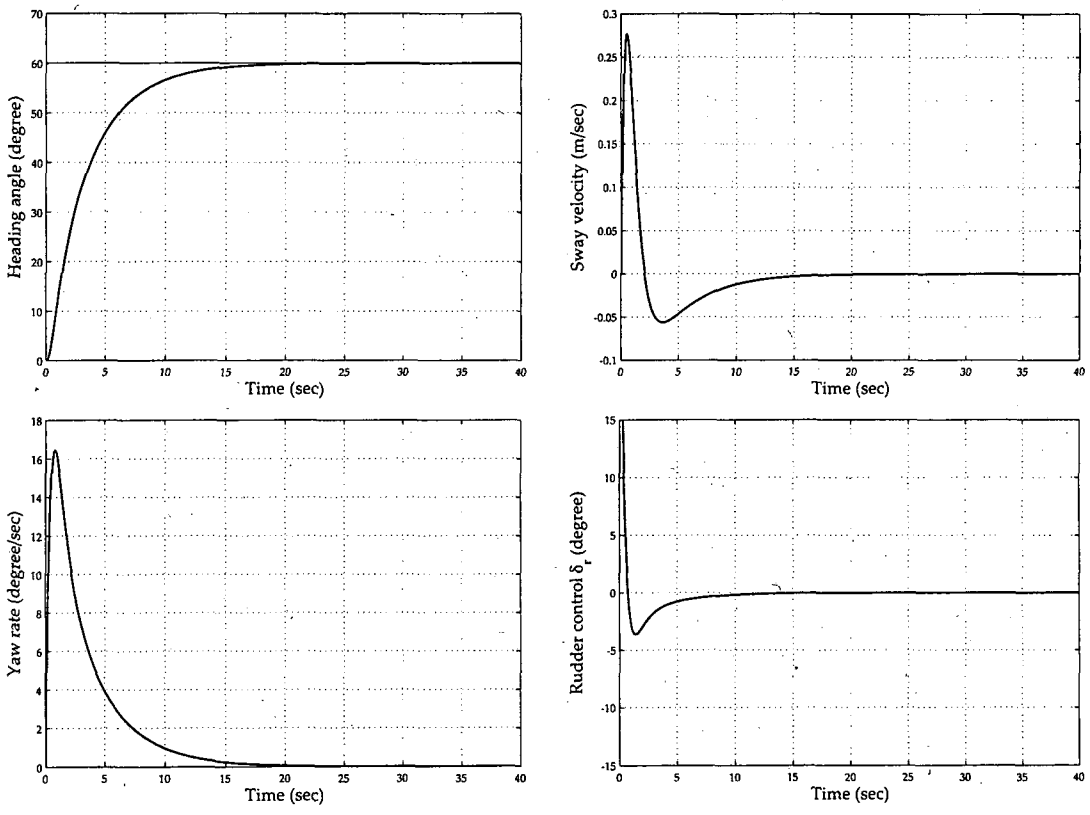

Figure 3.6: Heading control without disturbance. Letting the desired sway velocity v_d in heading be zero, the values of yaw rate r_d and heading angle ψ_d are different from those in path tracking. For course keeping, ψ_d is a constant, and then r_d is zero, whilst ψ_d and r_d normally follow certain dynamics for path tracking. By placing the poles at $[-0.6, -0.34, 0]^\mathsf{T}$, thus a set of linear feedback gains is $[-1.1485, 6.43e4, 0]^\mathsf{T}$.

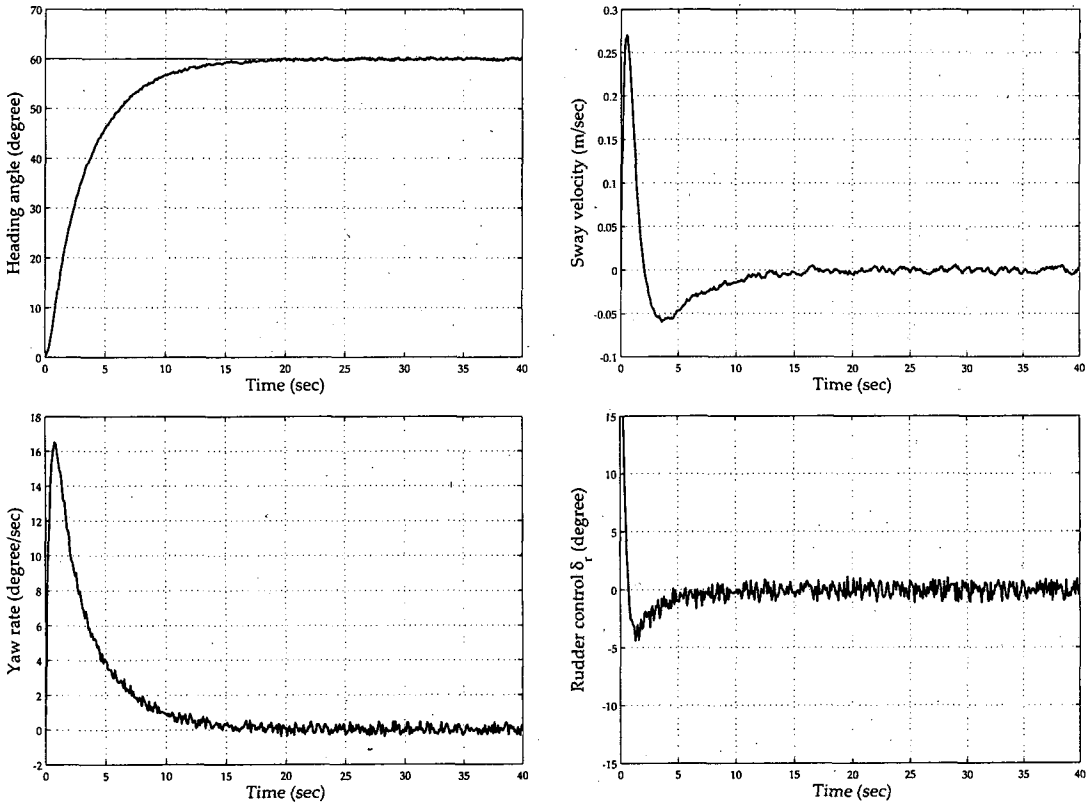

Figure 3.7: Heading control with disturbance. Letting the desired sway velocity v_d in heading be zero, the values of yaw rate r_d and heading angle ψ_d are different from those in path tracking. For course keeping, ψ_d is a constant, and then r_d is zero, whilst ψ_d and r_d normally follow certain dynamics for path tracking. By placing the poles at $[-0.6, -0.34, 0]^\mathsf{T}$, thus a set of linear feedback gains is $[-1.1485, 6.43e4, 0]^\mathsf{T}$. The standard SMC does not use much rudder control, and sway velocity and yaw rate are relatively small. The values of Root Mean Square (RMS) for heading and rudder control are $[55.9469, 2.6042]$.

In the depth control, the amplitude of desired depth is set as $z_d = 10$ metres, desired pitch angle θ_d and pitch rate q_d as zero. Figure 3.8 and 3.9 show the results of plots for the sliding mode controller with and without disturbances, respectively. From simulation, sliding mode controller is able to provide accurate control for system without disturbance and also manage the depth for system with disturbance, which still gives satisfactory results.

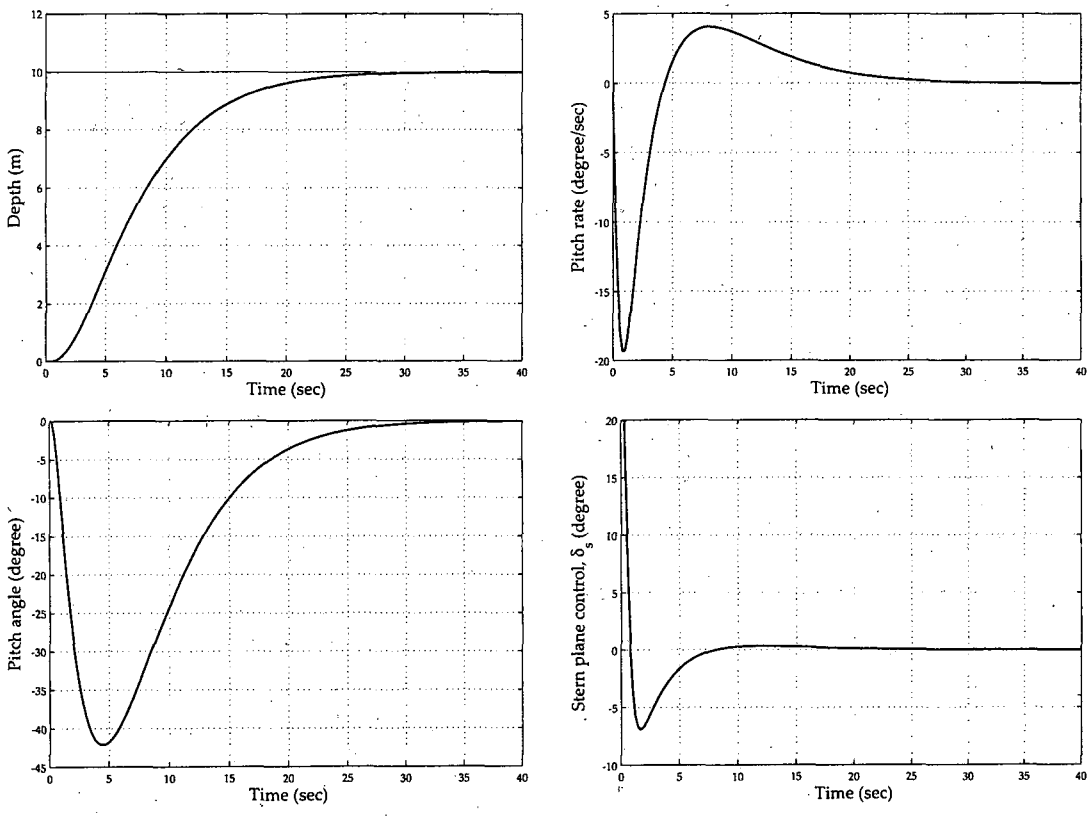

Figure 3.8: Depth control without disturbance. Letting the desired pitch rate q_d in depth be zero, the values of pitch angle θ_d and depth z_d are different from those in path tracking. For course keeping, z_d is a constant, and then q_d is zero, whilst z_d and θ_d normally follow certain dynamics for path tracking. By placing the poles at $[0, -0.25, -0.26]^\mathsf{T}$, thus a set of linear feedback gains is $[-0.4357, -0.0555, 0]^\mathsf{T}$.

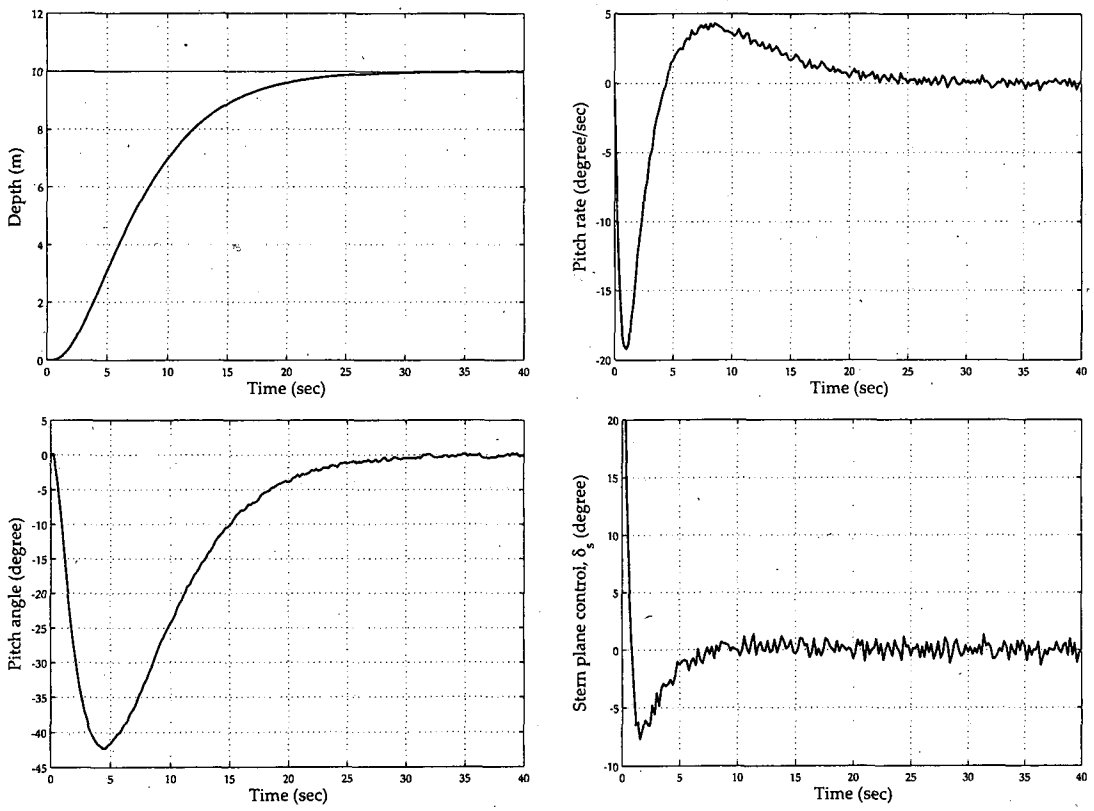

Figure 3.9: Depth control with disturbance. Letting the desired pitch rate q_d in depth be zero, the values of pitch angle θ_d and depth z_d are different from those in path tracking. For course keeping, z_d is a constant, and then q_d is zero, whilst z_d and θ_d normally follow certain dynamics for path tracking. By placing the poles at $[0, -0.25, -0.26]^{\mathsf{T}}$, thus a set of linear feedback gains is $[-0.4357, -0.0555, 0]^{\mathsf{T}}$. The standard SMC does not use much sternplane control, and pitch rate and pitch angle are relatively small. The values of RMS for depth and sternplane control are $[8.4759, 3.7031]$.

3.5 High-order Sliding Mode Control

Standard sliding mode controls used in the previous section have proved high accuracy and robustness with respect to external disturbances. On the other hand there are drawbacks: the so-called chattering phenomenon. It may excite high frequency vibration which degrades the performance of the control system. Recently, Levant [91], [92], [93] has developed a High-order Sliding Mode Control (HOSMC) which is able to avoid this chattering. Basically HOSMC acts on the high-order time derivatives. Whilst the method keeps the main advantage of the standard sliding mode, it also eliminates the chattering problem. There are a large number of recent references in the literature on this topic, for example unmanned aerial vehicle [46], electro-pneumatic actuator [78], [79], and underwater vehicle [123].

Consider a simple dynamic system and a sliding surface,

$$\dot{x} = a(x,t)x + b(x,t)u, \tag{3.35a}$$

$$\sigma = \widehat{\ }\sigma(x,t), \tag{3.35b}$$

where $x \in \mathbb{R}^n$, a, b and $\sigma \in \mathbb{R}^{n+1} \rightarrow \mathbb{R}$ are unknown smooth functions, $u \in \mathbb{R}$.

The standard sliding mode must be satisfied when the sliding surface is reached in a finite time,

$$\sigma = \dot{\sigma} = 0 \tag{3.36}$$

differentiating σ,

$$\begin{aligned} \frac{d\sigma}{dt} &= \frac{\partial\sigma}{\partial t} + \frac{\partial\sigma}{\partial x}\frac{dx}{dt}, \\ \dot{\sigma} &= \frac{\partial\sigma}{\partial t} + \frac{\partial\sigma}{\partial x}\dot{x}, \end{aligned} \tag{3.37}$$

differentiating $\dot{\sigma}$,

$$\begin{aligned} \frac{d\dot{\sigma}}{dt} &= \frac{\partial\dot{\sigma}}{\partial t} + \frac{\partial\dot{\sigma}}{\partial x}\frac{dx}{dt} + \frac{\partial\dot{\sigma}}{\partial x}\frac{du}{dt}, \\ \ddot{\sigma} &= \frac{\partial\dot{\sigma}}{\partial t} + \frac{\partial\dot{\sigma}}{\partial x}\dot{x} + \frac{\partial\dot{\sigma}}{\partial x}\dot{u}, \end{aligned} \tag{3.38}$$

The equations can be written as,

$$g_1(x,t) = \frac{\partial \dot{\sigma}}{\partial t} + \frac{\partial \dot{\sigma}}{\partial x}\dot{x}, \tag{3.39a}$$

$$g_2(x,t) = \frac{\partial \dot{\sigma}}{\partial x}, \tag{3.39b}$$

Define,

$$y_1 = \sigma, \tag{3.40a}$$

$$y_2 = \dot{\sigma}, \tag{3.40b}$$

It can be seen that,

$$\sigma^{(n)} = g_1(x,t) + g_2(x,t)u. \tag{3.41}$$

where $g_1(x,t)$ and $g_2(x,t)$ are uncertain functions that bound,

$$|g_1(x,t)| < \Gamma,$$

$$0 < \Psi_1 < g_2(x,t) < \Psi_2,$$

where Γ, Ψ_1 and $\Psi_2 > 0$.

Consider the nonlinear system (3.1) and the sliding manifold,

$$\mathcal{S} = \{(x,t) \in \mathbb{R}^m \times \mathbb{R} \quad | \quad \dot{\sigma} = \ddot{\sigma} = \cdots = \sigma^{(n-1)} = 0\} \tag{3.42}$$

The n^{th}-order sliding mode control allows the finite-time stabilisation to zero of the sling surface σ. This is to determine a discontinuous feedback control u providing a finite convergence to an n^{th}-order sliding mode. Similar to the 1^{st}-order sliding mode controller previously defined as $u = K_\sigma \operatorname{sign}(\sigma)$. Let us define $p > n$, the output n^{th}-order sliding mode satisfied [91], the structure of the controllers are therefore expressed as,

$$\begin{aligned} \mathcal{O}_{1,n} &= |\sigma|^{\frac{(n-1)}{n}}, \\ \mathcal{O}_{i,n} &= (|\sigma|^{\frac{p}{n}} + |\dot{\sigma}|^{\frac{p}{(n-1)}} + \cdots + |\sigma^{(i-1)}|^{\frac{p}{n-i+1}})^{\frac{(n-i)}{p}}, \\ \mathcal{O}_{n-1,n} &= (|\sigma|^{\frac{p}{n}} + |\dot{\sigma}|^{\frac{p}{(n-1)}} + \cdots + |\sigma^{(n-2)}|^{\frac{p}{2}})^{\frac{1}{p}}. \end{aligned} \tag{3.43a}$$

and,

$$\begin{aligned} \varpi_{0,n} &= \sigma, \\ \varpi_{1,n} &= \dot{\sigma} + \epsilon_1 \mathcal{O}_{1,n} \operatorname{sign}(\sigma), \\ \varpi_{i,n} &= \sigma^{(i)} + \epsilon_i \mathcal{O}_{i,n} \operatorname{sign}(\varpi_{i-1,n}). \end{aligned} \tag{3.43b}$$

where $i = 1, \cdots, n-1$ and $\epsilon_1, \cdots, \epsilon_{n-1}$ are positive constants.

Hence, the control laws (1^{st}-, 2^{nd}-order) can be constructed, when the condition of the sliding surface (equation (3.8)) $\sigma = 0$, $\dot{\sigma} = 0$ and $\ddot{\sigma} = 0$ is reached in a finite time. The control laws can be formulated,

$$u_{sw}^1 = -k_\sigma \operatorname{sign}(\sigma), \tag{3.44a}$$

$$u_{sw}^2 = -k_\sigma \operatorname{sign}(\dot{\sigma} + |\sigma|^{\frac{1}{2}} \operatorname{sign}(\sigma)). \tag{3.44b}$$

Such that the sliding mode control can be determined as similar to section 3.2. According to the algorithm, the trajectories on the 2^{nd}-order sliding mode is the so-called super-twist algorithm [124]. In this work, the 2^{nd}-order sliding mode algorithm is considered which the control law ensures that the trajectory converges in finite time towards the sliding surface whilst attenuating the chattering effect. The comparison studies between the standard and high-order sliding mode controller design for common decoupled subsystems (section 3.3) will be given in section 3.7.

3.6 State-Dependent Riccati Equation

State-Dependent Riccati Equation (SDRE) is a well established, accepted and effective methodology [140] for the synthesis of control laws for nonlinear systems. Literature and application using SDRE technique are found in double inverted pendulum [10], autonomous helicopters [11], unmanned air vehicles [118], multiple unmanned aerial vehicles [128], 2-DOFs helicopter [159].

Fundamentally the SDRE is derived to minimise the performance index,

$$J_0 = \frac{1}{2} \int_{t_0}^{\infty} (\boldsymbol{x}^\top \boldsymbol{Q}_x(\boldsymbol{x}) \boldsymbol{x} + \boldsymbol{u}^\top \boldsymbol{Q}_u(\boldsymbol{x}) \boldsymbol{u}) dt. \tag{3.45}$$

with respect to the state $\boldsymbol{x}$ and control $\boldsymbol{u}$ subject to the nonlinear dynamic system,

$$\dot{\boldsymbol{x}} = \boldsymbol{f}(\boldsymbol{x})\boldsymbol{x} + \boldsymbol{g}(\boldsymbol{x})\boldsymbol{u}. \tag{3.46}$$

which can be expressed in the State-Dependent Coefficient (SDC) form,

$$\dot{\boldsymbol{x}} = \boldsymbol{A}(\boldsymbol{x})\boldsymbol{x} + \boldsymbol{B}(\boldsymbol{x})\boldsymbol{u}. \tag{3.47}$$

There are many SDC parameterisation available for designing the control law. One of the most appropriate consideration for the system and control objectives is that the state-dependent controllability matrix which is of interest. The matrix is given by,

$$\boldsymbol{\mathcal{M}}(\boldsymbol{x}) = [\boldsymbol{B}(\boldsymbol{x}) \quad \boldsymbol{A}(\boldsymbol{x})\boldsymbol{B}(\boldsymbol{x}) \quad \ldots \quad \boldsymbol{A}^{(n-1)}(\boldsymbol{x})\boldsymbol{B}(\boldsymbol{x})] \tag{3.48}$$

In the linear case, matrix $\boldsymbol{\mathcal{M}}$ has full rank such that the system is controllable. However for the nonlinear case a parameterisation for $\boldsymbol{\mathcal{M}}$ that gives a full rank for which the system is to be controlled must be determined.

According to the Hamiltonian principle, the optimal control problem is considered,

$$H(\boldsymbol{x}, \lambda) = \frac{1}{2}(\boldsymbol{x}^{\mathsf{T}}\boldsymbol{Q}_x(\boldsymbol{x})\boldsymbol{x} + \boldsymbol{u}^{\mathsf{T}}\boldsymbol{Q}_u(\boldsymbol{x})\boldsymbol{u}) + \lambda^{\mathsf{T}}(\boldsymbol{A}(\boldsymbol{x})\boldsymbol{x} + \boldsymbol{A}(\boldsymbol{x})\boldsymbol{u}), \tag{3.49}$$

Referred to [21] for the properties of the SDRE method, the conditions for the optimal control are,

$$\dot{\lambda} = -\boldsymbol{Q}_x(\boldsymbol{x})\boldsymbol{x} - \left[\frac{\partial(\boldsymbol{A}(\boldsymbol{x})\boldsymbol{x})}{\partial \boldsymbol{x}}\right]^{\mathsf{T}}\lambda - \left[\frac{\partial(\boldsymbol{B}(\boldsymbol{x})\boldsymbol{u})}{\partial \boldsymbol{x}}\right]^{\mathsf{T}}\lambda; \tag{3.50a}$$

$$\dot{\boldsymbol{x}} = \boldsymbol{A}(\boldsymbol{x})\boldsymbol{x} + \boldsymbol{B}(\boldsymbol{x})\boldsymbol{u}; \tag{3.50b}$$

$$0 = \boldsymbol{Q}_u(\boldsymbol{x})\boldsymbol{u} + \boldsymbol{B}^{\mathsf{T}}(\boldsymbol{x})\lambda; \tag{3.50c}$$

The co-state or the Lagrange multiplier is assumed to be written in the form of $\lambda = \boldsymbol{P}(\boldsymbol{x})\boldsymbol{x}$. Using the form for λ in equation (3.50a), (3.50b) and (3.50c), a feedback control $\boldsymbol{u}$ = -$\boldsymbol{Q}_u^{-1}(\boldsymbol{x})\boldsymbol{B}^{\mathsf{T}}(\boldsymbol{x})$ $\boldsymbol{P}(\boldsymbol{x})\boldsymbol{x}$ is obtained. To find the matrix $\boldsymbol{P}(\boldsymbol{x})$, differentiating λ with respect to the time along the trajectory to obtain,

$$\begin{aligned} \dot{\lambda} &= \dot{\boldsymbol{P}}(\boldsymbol{x})\boldsymbol{x} + \boldsymbol{P}(\boldsymbol{x})\dot{\boldsymbol{x}}, \\ &= \dot{\boldsymbol{P}}(\boldsymbol{x})\boldsymbol{x} + \boldsymbol{P}(\boldsymbol{x})\boldsymbol{A}(\boldsymbol{x})\boldsymbol{x} - \boldsymbol{P}(\boldsymbol{x})\boldsymbol{B}(\boldsymbol{x})\boldsymbol{Q}_u^{-1}(\boldsymbol{x})\boldsymbol{B}^{\mathsf{T}}(\boldsymbol{x})\boldsymbol{P}(\boldsymbol{x})\boldsymbol{x}, \end{aligned} \tag{3.51}$$

where,

$$\dot{\boldsymbol{P}}(\boldsymbol{x}) = \sum_{i=1}^{n} \boldsymbol{P}_{\boldsymbol{x}_i}(\boldsymbol{x})\dot{\boldsymbol{x}}_i(t),$$

From equation (3.50a), (3.50b), (3.50c) and (3.51) it is found that,

$$\begin{aligned}\dot{\boldsymbol{P}}(\boldsymbol{x})\boldsymbol{x} + \boldsymbol{P}(\boldsymbol{x})\boldsymbol{A}(\boldsymbol{x})\boldsymbol{x} - \boldsymbol{P}(\boldsymbol{x})\boldsymbol{B}(\boldsymbol{x})\boldsymbol{Q}_u^{-1}(\boldsymbol{x})\boldsymbol{B}^{\mathsf{T}}(\boldsymbol{x})\boldsymbol{P}(\boldsymbol{x})\boldsymbol{x} \\ = -\boldsymbol{Q}_x(\boldsymbol{x})\boldsymbol{x} - \left[\boldsymbol{A}(\boldsymbol{x}) + \frac{\partial(\boldsymbol{A}(\boldsymbol{x})\boldsymbol{x})}{\partial \boldsymbol{x}}\right]^{\mathsf{T}} \boldsymbol{P}(\boldsymbol{x})\boldsymbol{x} - \left[\frac{\partial(\boldsymbol{B}(\boldsymbol{x})\boldsymbol{u})}{\partial \boldsymbol{x}}\right]^{\mathsf{T}} \boldsymbol{P}(\boldsymbol{x})\boldsymbol{x},\end{aligned} \tag{3.52}$$

rearranging equation (3.52),

$$\begin{aligned}\Bigg[\Big(\dot{\boldsymbol{P}}(\boldsymbol{x}) + \left[\frac{\partial(\boldsymbol{A}(\boldsymbol{x})\boldsymbol{x})}{\partial \boldsymbol{x}}\right]^{\mathsf{T}} \boldsymbol{P}(\boldsymbol{x}) + \left[\frac{\partial(\boldsymbol{B}(\boldsymbol{x})\boldsymbol{u})}{\partial \boldsymbol{x}}\right]^{\mathsf{T}} \boldsymbol{P}(\boldsymbol{x})\Big) \\ + \Big(\boldsymbol{A}^{\mathsf{T}}(\boldsymbol{x})\boldsymbol{P}(\boldsymbol{x}) + \boldsymbol{P}(\boldsymbol{x})\boldsymbol{A}(\boldsymbol{x}) - \boldsymbol{P}(\boldsymbol{x})\boldsymbol{B}(\boldsymbol{x})\boldsymbol{Q}_u^{-1}(\boldsymbol{x})\boldsymbol{B}^{\mathsf{T}}(\boldsymbol{x})\boldsymbol{P}(\boldsymbol{x}) + \boldsymbol{Q}_x(\boldsymbol{x})\Big)\Bigg]\boldsymbol{x} = 0,\end{aligned} \tag{3.53}$$

solving the SDRE which is simply given by,

$$\boldsymbol{A}^{\mathsf{T}}(\boldsymbol{x})\boldsymbol{P}(\boldsymbol{x}) + \boldsymbol{P}(\boldsymbol{x})\boldsymbol{A}(\boldsymbol{x}) - \boldsymbol{P}(\boldsymbol{x})\boldsymbol{B}(\boldsymbol{x})\boldsymbol{Q}_u^{-1}(\boldsymbol{x})\boldsymbol{B}^{\mathsf{T}}(\boldsymbol{x})\boldsymbol{P}(\boldsymbol{x}) + \boldsymbol{Q}_x(\boldsymbol{x}) = 0, \tag{3.54}$$

Thus, the following condition must be satisfied,

$$\dot{\boldsymbol{P}}(\boldsymbol{x}) + \left[\frac{\partial(\boldsymbol{A}(\boldsymbol{x})\boldsymbol{x})}{\partial \boldsymbol{x}}\right]^{\mathsf{T}} \boldsymbol{P}(\boldsymbol{x}) + \left[\frac{\partial(\boldsymbol{B}(\boldsymbol{x})\boldsymbol{u})}{\partial \boldsymbol{x}}\right]^{\mathsf{T}} \boldsymbol{P}(\boldsymbol{x}) = 0, \tag{3.55}$$

Equation (3.55) is referred to as the optimal criterion condition. Hence, nonlinear feedback control law can be constructed as,

$$\begin{aligned}\boldsymbol{u}_{eq} &= -\boldsymbol{K}(\boldsymbol{x})\boldsymbol{x}, \\ &= -\boldsymbol{Q}_u^{-1}(\boldsymbol{x})\boldsymbol{B}^{\mathsf{T}}(\boldsymbol{x})\boldsymbol{P}(\boldsymbol{x})\boldsymbol{x}.\end{aligned} \tag{3.56}$$

where $\boldsymbol{P}(\boldsymbol{x}) > 0$ is the positive semi-definite solution to the algebraic Riccati equation, $\boldsymbol{Q}_x(\boldsymbol{x}) = \boldsymbol{Q}_x^{\mathsf{T}}(\boldsymbol{x}) \geq 0$ is the state-dependent weight matrix and $\boldsymbol{Q}_u(\boldsymbol{x}) = \boldsymbol{Q}_u^{\mathsf{T}}(\boldsymbol{x}) > 0$ is the control weight matrix. Solving the algebraic Riccati equation in (3.54), feedback gain is therefore determined. The SDRE control produces a closed-loop system matrix $\boldsymbol{A}_c(\boldsymbol{x}) = (\boldsymbol{A}(\boldsymbol{x}) - \boldsymbol{B}(\boldsymbol{x})\boldsymbol{K})$. It is obvious that the sliding mode control (see section

3.2) consists of an equivalent and a switching term. Hence, the equivalent control in equation (3.56) can be solved. Then it can be used in the sliding mode control shown in equation (3.11). The work develops a method to select an optimal sliding surface by incorporating a SDRE technique. The controller design using a sliding mode and SDRE technique can be constructed as a block diagram shown in figure 3.10. Furthermore, it is interesting to develop the SDRE control law for an AUV, as such it would be suitable to find the SDC parameterisation available for designing the control.

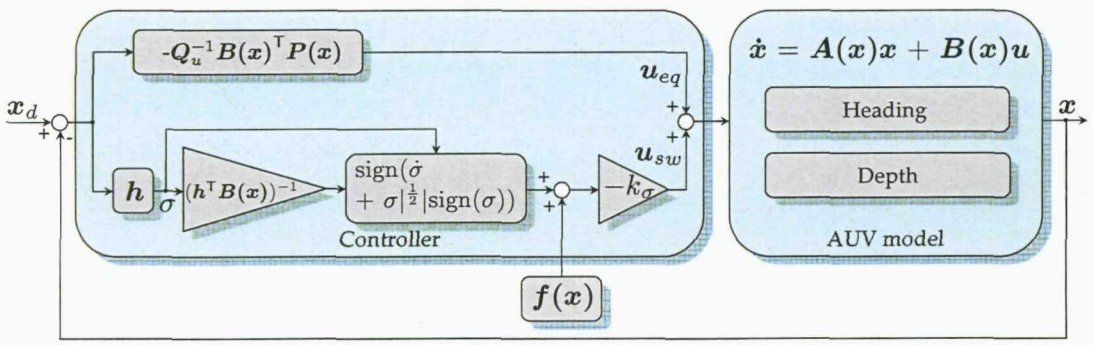

Figure 3.10: Block diagram of a high-order sliding controller with a use of state-dependent Riccati equation technique.

Consider the nonlinear equations of motion (see appendix B) in heading which are given as follows,

$$\begin{aligned} m[\dot{v} + ur + z_g qr + x_g \dot{r}] &= Y_{v|v|} v|v| + Y_{r|r|} r|r| \\ &\quad + Y_{\dot{v}} \dot{v} + Y_{\dot{r}} \dot{r} + Y_{ur} ur + Y_{uv} uv + Y_{uu} u^2 \delta_r, \\ I_{zz}\dot{r} + m[x_g(\dot{v} - wp + ur)] &= y_b B \sin\theta + N_{v|v|} v|v| + N_{r|r|} r|r| + N_{\dot{v}} \dot{v} \\ &\quad + N_{\dot{r}} \dot{r} + N_{ur} ur + N_{uv} uv + N_{uu} u_0^2 \delta_r, \\ \dot{\psi} &= r, \end{aligned} \tag{3.57}$$

The nonlinear dynamics in equation (3.57) can be represented in the state-dependent coefficient form,

$$\begin{aligned}\begin{bmatrix}\dot{v}\\ \dot{r}\end{bmatrix} &= \Pi_h^{-1}\begin{bmatrix}Y_{v|v|}|v| + Y_{uv}u & Y_{r|r|}|r| + Y_{ur}u + mu + mz_g q\\ N_{v|v|}|v| + N_{uv}u & N_{r|r|}|r| + N_{ur}u\end{bmatrix}\begin{bmatrix}v\\ r\end{bmatrix}\\ &\quad +\Pi_h^{-1}\begin{bmatrix}Y_{uu}\\ N_{uu}\end{bmatrix}u_0^2\delta_r + \begin{bmatrix}0\\ 0\end{bmatrix}[\psi] + \Pi_h^{-1}y_b B\sin\theta, \qquad (3.58)\\ &\equiv \boldsymbol{A}_{h1}(\boldsymbol{x})\begin{bmatrix}w\\ q\end{bmatrix} + \boldsymbol{A}_{h2}(\boldsymbol{x})[\psi] + \boldsymbol{B}_{h1}(\boldsymbol{x})\delta_r + \boldsymbol{c}_{h1},\end{aligned}$$

and,

$$\begin{aligned}[\dot{\psi}] &= [1][r] + [0][\psi],\\ &\equiv \boldsymbol{A}_{h3}(\boldsymbol{x})[r] + \boldsymbol{A}_{h4}(\boldsymbol{x})[\psi],\end{aligned} \qquad (3.59)$$

where,

$$\Pi_h = \begin{bmatrix}m - Y_{\dot{v}} & mx_g - Y_{\dot{r}}\\ mx_g - N_{\dot{v}} & I_{zz} - N_{\dot{r}}\end{bmatrix}, \qquad (3.60)$$

It can be seen that,

$$\begin{aligned}\dot{\boldsymbol{x}}_1 &= \begin{bmatrix}\boldsymbol{A}_{h1}(\boldsymbol{x}) & \boldsymbol{A}_{h2}(\boldsymbol{x})\\ \boldsymbol{A}_{h3}(\boldsymbol{x}) & \boldsymbol{A}_{h4}(\boldsymbol{x})\end{bmatrix}\boldsymbol{x} + \begin{bmatrix}\boldsymbol{B}_{h1}(\boldsymbol{x})\\ 0\end{bmatrix}\delta_r + \begin{bmatrix}\boldsymbol{c}_{h1}\\ 0\end{bmatrix}, \qquad (3.61)\\ &\equiv \boldsymbol{A}_h(\boldsymbol{x}) + \boldsymbol{B}_h(\boldsymbol{x})(\boldsymbol{u}) + \boldsymbol{c}_h.\end{aligned}$$

Now consider the nonlinear equations of motion (see appendix B) in heave and pitch which are given as follows,

$$\begin{aligned}m[\dot{w} - uq - z_g q^2 - x_g\dot{q})] &= (W - B)\cos\theta + Z_{w|w|}w|w| + Z_{q|q|}q|q|\\ &\quad + Z_{\dot{w}}\dot{w} + Z_{\dot{q}}\dot{q} + Z_{uq}uq + \quad + Z_{uw}uw + Z_{uu}u^2\delta_s,\\ I_{yy}\dot{q} + m[z_g wq - x_g(\dot{w} - uq)] &= -(x_g W - x_b B)\cos\theta - (z_g W - z_b B)\sin\theta\\ &\quad + M_{w|w|}w|w| + M_{q|q|}q|q| + M_{\dot{w}}\dot{w} + M_{\dot{q}}\dot{q}\\ &\quad + M_{uq}uq + M_{uw}uw + M_{uu}u_0^2\delta_s,\\ \dot{\theta} &= q,\\ \dot{z} &= w\cos\theta - u\sin\theta,\end{aligned} \qquad (3.62)$$

The nonlinear dynamics in equation (3.62) can be represented in the state-dependent coefficient form,

$$\begin{aligned}
\begin{bmatrix} \dot{w} \\ \dot{q} \end{bmatrix} &= \Pi_d^{-1} \begin{bmatrix} Z_{w|w|}|w| + Z_{uw}u & Z_{q|q|}|q| + mu + mz_g q \\ M_{q|q|}|q| + M_{uw}u & M_{q|q|}|q| + M_{uq}u - m(z_g w + x_g u) \end{bmatrix} \begin{bmatrix} w \\ q \end{bmatrix} \\
&\quad + \Pi_d^{-1} \begin{bmatrix} 0 & \theta^{-1}(W-B)(\cos\theta - 1) \\ 0 & \theta^{-1}(x_b B - x_g W)(\cos\theta - 1) - \theta^{-1}(z_g W - z_b B)\sin\theta \end{bmatrix} \begin{bmatrix} z \\ \theta \end{bmatrix} \\
&\quad + \Pi_d^{-1} \begin{bmatrix} Z_{uu} \\ M_{uu} \end{bmatrix} u_0^2 \delta_s + \Pi_d^{-1} \begin{bmatrix} (W-B) \\ (x_g W - x_b B) \end{bmatrix}, \\
&\equiv \boldsymbol{A}_{d1}(\boldsymbol{x}) \begin{bmatrix} w \\ q \end{bmatrix} + \boldsymbol{A}_{d2}(\boldsymbol{x}) \begin{bmatrix} z \\ q \end{bmatrix} + \boldsymbol{B}_{d1}(\boldsymbol{x})\delta_s + \boldsymbol{c}_{d1},
\end{aligned} \tag{3.63}$$

and,

$$\begin{aligned}
\begin{bmatrix} \dot{z} \\ \dot{\theta} \end{bmatrix} &= \begin{bmatrix} \cos\theta & 0 \\ 0 & 1 \end{bmatrix} \begin{bmatrix} w \\ q \end{bmatrix} + \begin{bmatrix} 0 & -\theta^{-1}\cos\theta \\ 0 & 0 \end{bmatrix} \begin{bmatrix} z \\ \theta \end{bmatrix}, \\
&\equiv \boldsymbol{A}_{d3}(\boldsymbol{x}) \begin{bmatrix} w \\ q \end{bmatrix} + \boldsymbol{A}_{d4}(\boldsymbol{x}) \begin{bmatrix} z \\ \theta \end{bmatrix},
\end{aligned} \tag{3.64}$$

where,

$$\Pi_d = \begin{bmatrix} m - Z_{\dot{w}} & -mx_g - Z_{\dot{q}} \\ -mx_g - M_{\dot{w}} & I_{yy} - M_{\dot{q}} \end{bmatrix}, \tag{3.65}$$

It can also be seen that,

$$\begin{aligned}
\dot{\boldsymbol{x}}_2 &= \begin{bmatrix} \boldsymbol{A}_{d1}(\boldsymbol{x}) & \boldsymbol{A}_{d2}(\boldsymbol{x}) \\ \boldsymbol{A}_{d3}(\boldsymbol{x}) & \boldsymbol{A}_{d4}(\boldsymbol{x}) \end{bmatrix} \boldsymbol{x} + \begin{bmatrix} \boldsymbol{B}_{d1}(\boldsymbol{x}) \\ 0 \end{bmatrix} \delta_s + \begin{bmatrix} \boldsymbol{c}_{d1} \\ 0 \end{bmatrix}, \\
&\equiv \boldsymbol{A}_d(\boldsymbol{x}) + \boldsymbol{B}_d(\boldsymbol{x})(\boldsymbol{u}) + \boldsymbol{c}_d.
\end{aligned} \tag{3.66}$$

3.7 Case Study II

Comparative results implemented using computer simulation between a standard SMC and HOSMC-SDRE technique are illustrated in this section. The computer implementation is similar to case study I where was detailed in the previous section,

whilst the parameters for SDRE technique are defined according to the nonlinear model (see equation (3.61)), (3.66). Responses to control law for heading and depth control subsystem are compared in figures 3.11, 3.12 and 3.13, 3.14, respectively and shown in figure E.2, E.3, E.4 and E.5 (see appendix E). Further studies have carried out how the controllers can cope with the changes of hydrodynamic coefficients. By varying the hydrodynamics term from 0%, 0.01%, 0.1%, 1% and 2% in each state, figure 3.15 and 3.16 show the comparison of simulation results in heading and depth subsystem with the design of SMC, HOSMC and SDRE-HOSMC controller.

3.8 Summary

This chapter has presented the finding of a sliding mode controller for two subsystems, namely heading and depth subsystems of an AUV. Comparisons of performance for each subsystem with and without disturbance are demonstrated by computer simulations using MATLAB®. They have shown that promising results provide accurate control for the tracking problem. However the problem of chattering effect is a concern but can be avoided. This can be done by using the high-order sliding mode. Improved performance have been shown, whilst retaining the main characteristic of the standard sliding mode control. Its previous restriction due to chattering effect has been prevented. The use of an optimal controller for such a subsystem control by a state-dependent Riccati equation has been introduced. An integration of a high-order sliding mode and state-dependent Riccati equation method gives a controller a great deal of promise for the nonlinear system with a noise model and uncertainties of hydrodynamics changes for underwater vehicle applications. The simulation studies show that the values of RMS reduces from 2.6042 (SMC) to 2.1759 (HOSMC) and 1.4066 (SDRE-HOSMC) in the heading control and from 3.6851 (SMC) to 2.5571 (HOSMC) and 1.7713 (SDRE-HOSMC) in the depth control.

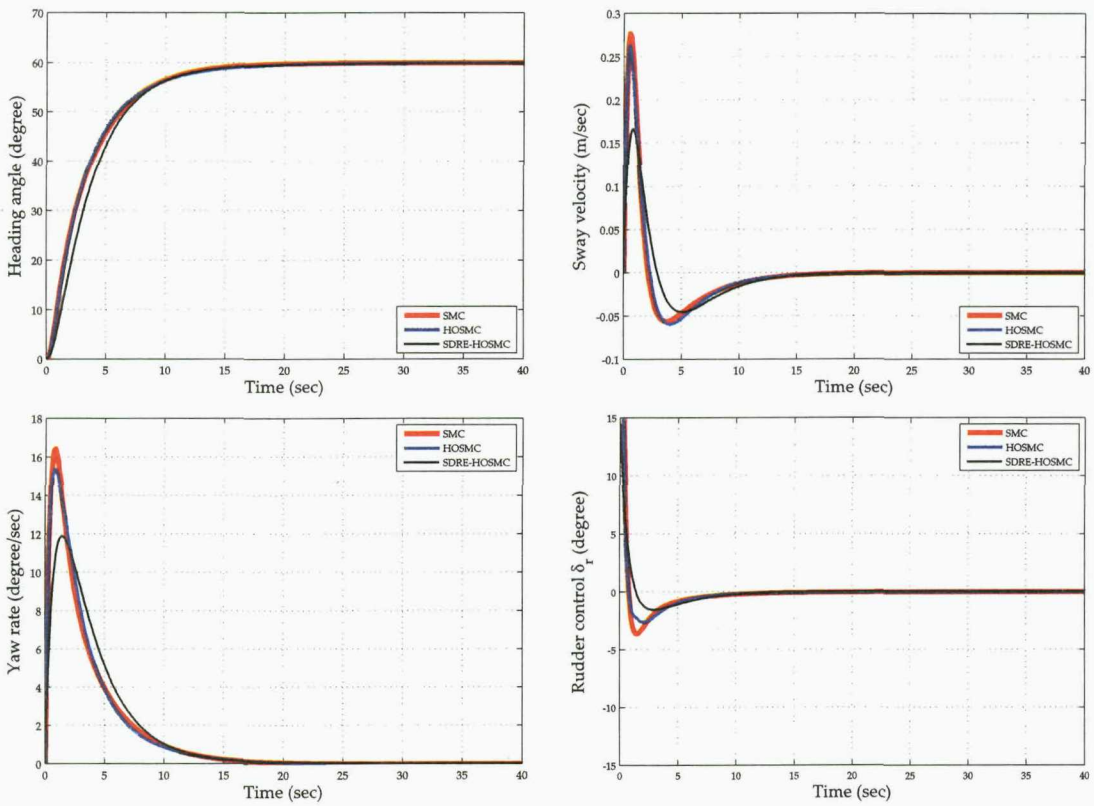

Figure 3.11: Heading control using SMC (see section 3.2), HOSMC (see section 3.5) and SDRE-HOSMC (see section 3.6) without disturbance.

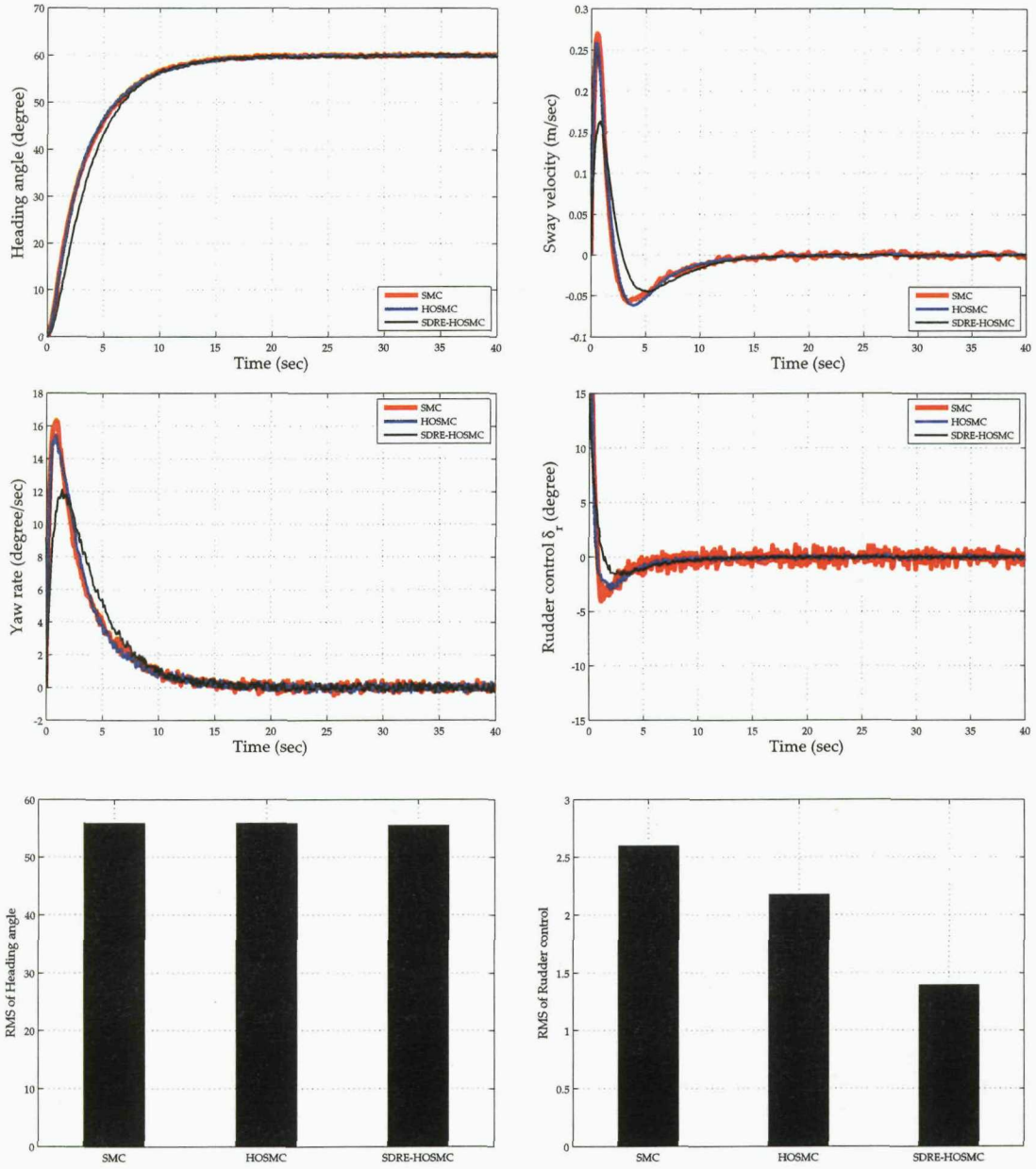

Figure 3.12: Heading control using SMC, HOSMC and SDRE-HOSMC techniques with disturbance modelled as 0.01∗`rand`(1) (see section 3.4). Bar graphs show that values of RMS for heading angle and rudder control are [55.9469, 55.9633, 55.5446] and [2.6042, 2.1759, 1.4066], respectively.

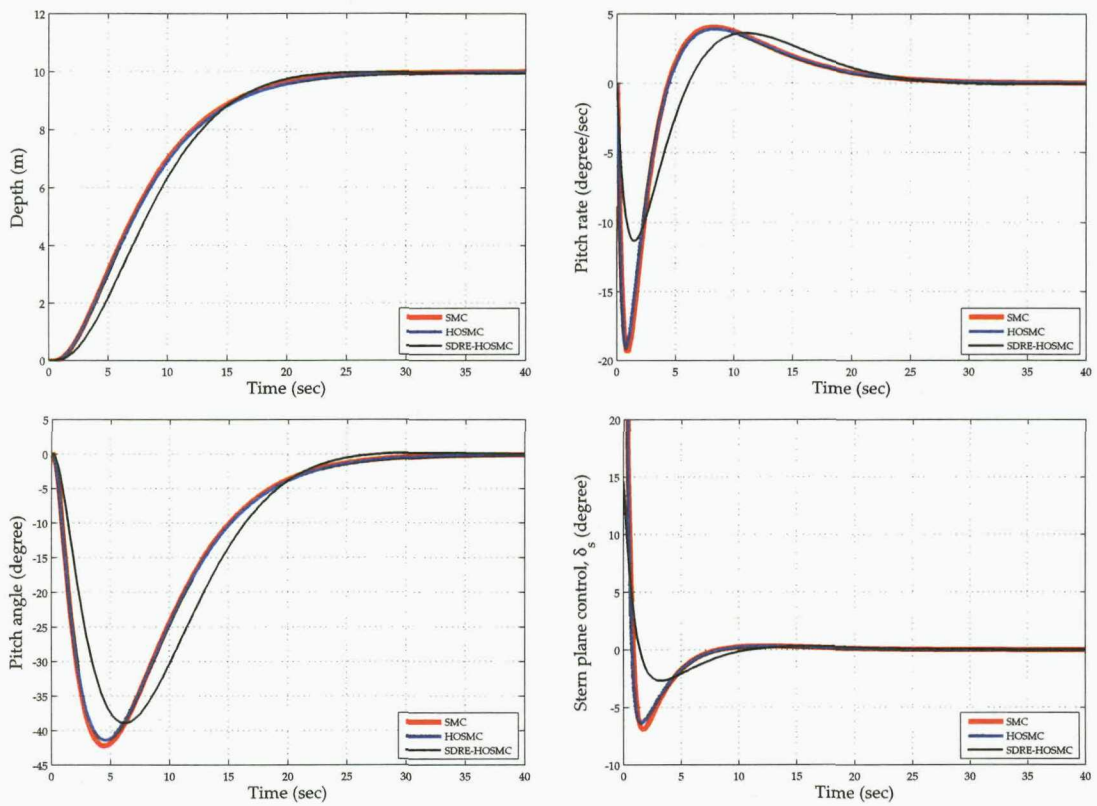

Figure 3.13: Depth control using SMC (see section 3.2), HOSMC (see section 3.5) and SDRE-HOSMC (see section 3.6) without disturbance.

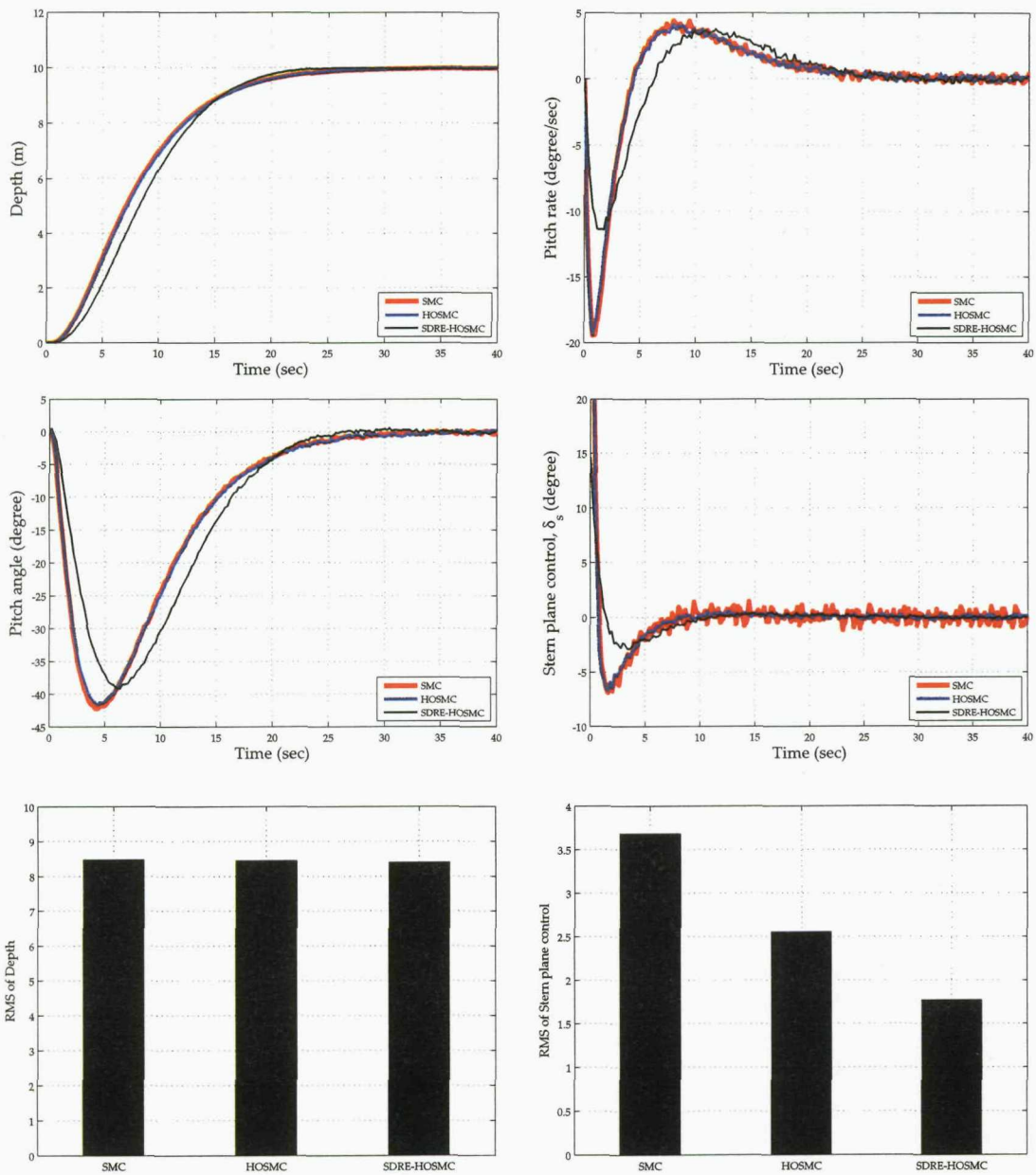

Figure 3.14: Depth control using SMC, HOSMC and SDRE-HOSMC techniques with disturbance modelled as 0.01∗`rand`(1) (see section 3.4). Bar graphs show that values of RMS for depth and sternplane control are [8.4761, 8.4561, 8.4020] and [3.6851, 2.5571, 1.7713], respectively.

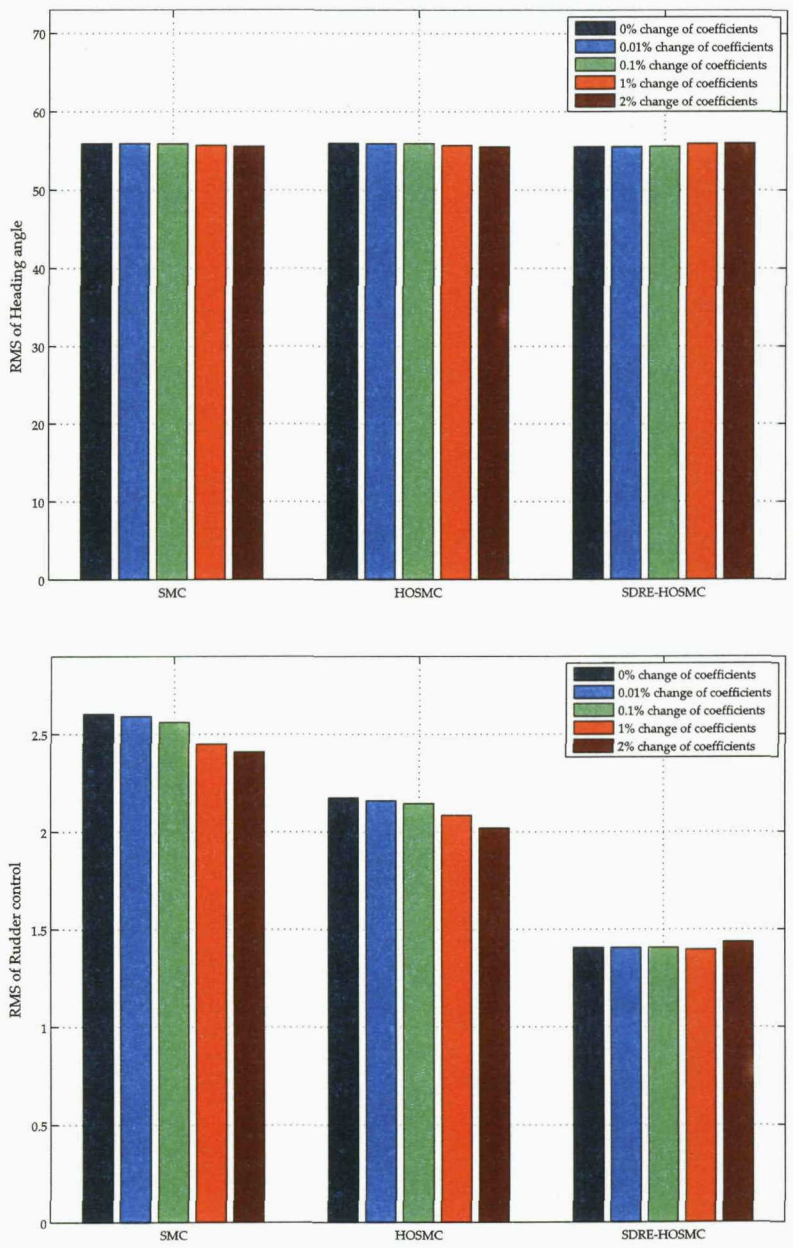

Figure 3.15: Study considers the changes of the hydrodynamic coefficients ($Y_{\dot{v}}$, $Y_{\dot{r}}$, Y_v, Y_r, $N_{\dot{v}}$, $N_{\dot{r}}$, N_v, N_r, Y_δ, N_δ) by 0%, 0.01%, 0.1%, 1% and 2% in heading control. Bar graphs show values of RMS for heading (top) that are [55.9469, 55.9353, 55.912, 55.7008, 55.5658] using SMC, [55.9633, 55.9562, 55.9189, 55.7004, 55.5282] using HOSMC and [55.5446, 55.5381, 55.5768, 55.9271, 55.9876] and SDRE-HOSMC, whilst RMS for rudder control (bottom) are [2.6042, 2.592, 2.5616, 2.4511, 2.4103] using SMC, [2.1759, 2.161, 2.1463, 2.0857, 2.0199] using HOSMC and [1.4066, 1.4058, 1.4061, 1.3959, 1.4352] using SDRE-HOSMC.

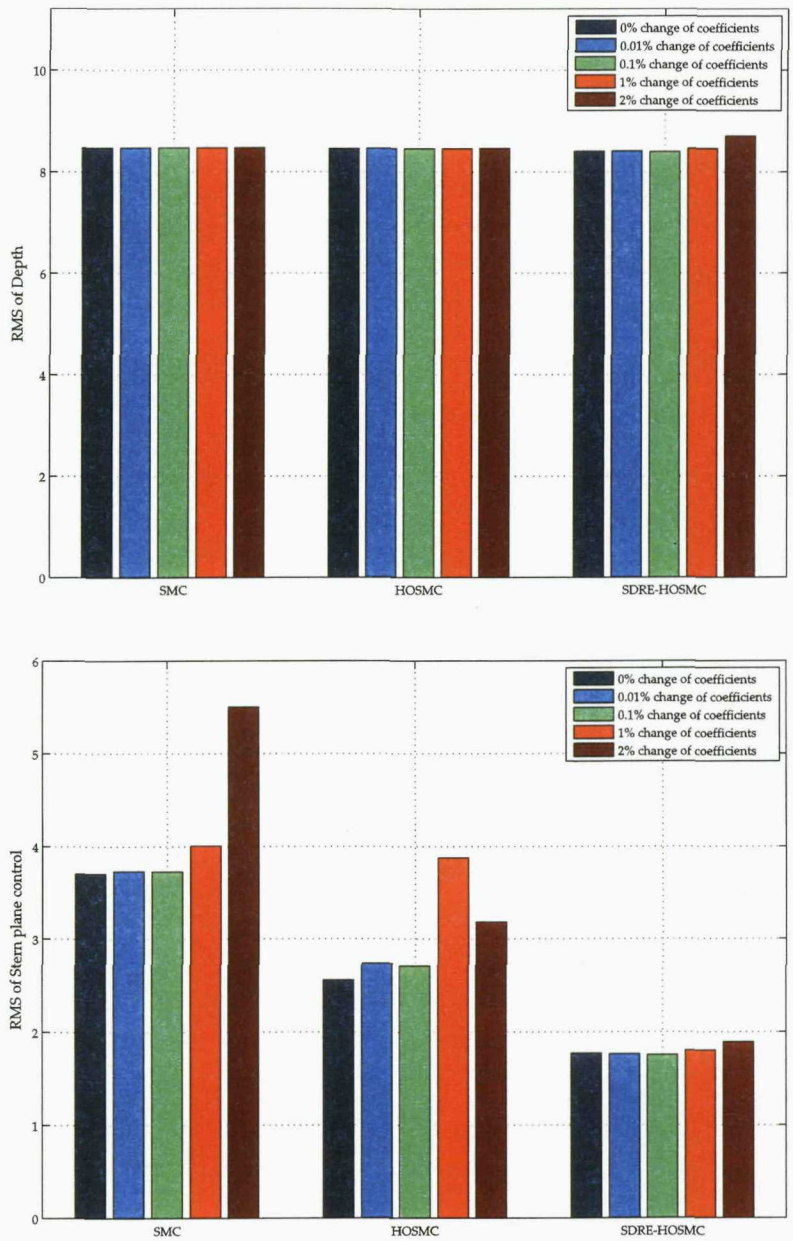

Figure 3.16: Study considers the changes of the hydrodynamic coefficients ($M_{\dot{q}}$, M_q, N_r, M_δ) by 0%, 0.01%, 0.1%, 1% and 2% in depth control. Bar graphs show values of RMS for depth (top) that are [8.4759, 8.476, 8.4759, 8.4758, 8.4761] using SMC, [8.4561, 8.4583, 8.4566, 8.4548, 8.4599] using HOSMC and [8.402, 8.4063, 8.4003, 8.4616, 8.7067] and SDRE-HOSMC, whilst RMS for sternplane control (bottom) are [3.7031, 3.7323, 3.7281, 4.0055, 5.5011] using SMC, [2.5571, 2.7364, 2.7071, 3.877, 3.1803] using HOSMC and [1.7713, 1.7636, 1.7533, 1.8019, 1.8906] using SDRE-HOSMC.

Chapter 4

Trajectory Generation

4.1 Overview of Chapter

Autonomous homing and docking play an important rôle in long-term underwater explorations and surveys. The autonomous docking preparation mission for an AUV involves a vehicle and a dock station matching both position, orientation and velocity. Hence, path planning is required for the mission. In this chapter, a predefined trajectory for homing and docking using a vector field method based on a conventional artificial potential field motion planning is proposed. Section 4.2 discusses previous works on various homing and docking. An overview of path planning is explained in section 4.3. Conventional potential field, vector field and the improved vector field are detailed in section 4.4, 4.5 and 4.7 respectively. Strategy for homing and docking proposed in this research is considered in section 4.6. A definition for safe trajectory is given in section 4.8. Section 4.9 shows simulation results. A chapter summary can be found in section 4.10.

4.2 Reviews of Homing and Docking

In long-term underwater applications, an AUV should be an autonomous system. This means that the functionality of homing and docking is therefore required for a complete system. Homing and docking operation are important for the task of recharging power and transferring data which are limited by on-board energy storage and on-board data storage. The key problem of underwater homing and docking tasks is accurately stabilising between the positions and orientations of the AUV and the platform. In this section, literature for homing and docking tasks for various applications are explored:

- In a mission of homing and docking, a number of researchers have studied and developed hardware implementations. Singh *et al.* [132] have proposed a docking methodology for underwater vehicle networks. A model of behaviour composed of a finite number of states and actions based on data from sensors equipped both on the vehicles and on the station have been used for a docking mission. A hardware failure detection system ensures successfully docking operations. Unfortunately, no results for the implementation were discussed in this paper.

- Cowen *et al.* [22] have used a small and simple docking structure using light emitting optical trackers. However, its technique is limited by water clarity and depths. Hutchins and Roque [55] have utilised sonar sensors for measuring orientations. The filtering and control methods for docking operations have been developed. Three processes comprising pursuit, proportional navigation and linear-quadratic regulation have been used for intercepting the mission and the docking operator assures an AUV to precisely reach the target. By using a short range position system based on a sonar, Evans *et al.* [36] have developed a docking mission guidance for an ROV applicable of precise alignment to the docking station.

- In addition to improving the mission, methods in intelligent control are also considered. Kato and Endo [68] have presented a fuzzy algorithm of the docking guidance and control for unmanned submersibles. The guidance consists of two steps are: (i) rough guidance based on fuzzy algorithms provides prearrangement of the vehicle near the docking target and; (ii) precise guidance based on sonar and transponders give a precise distance and target poses. Numerical simulations illustrated in the paper have shown that an underwater vehicle follows a precise course and places close to the docking target. Feng *et al.* [38] have developed a neural network simulator for safe, economic and reliable low speed AUV docking operations. A learning algorithm allows an adaptive controllability for a docking procedure.

- Since position and orientation of AUV near a docking platform are accurately required, Feezor *et al.* [37] have proposed electromagnetic homing systems for the AUV guidance. The AUV is equipped with sensors to follow magnetic fields transmitted from such a system into the docking entrance. Trials in homing and docking were successfully implemented in this concept.

- Rae *et al.* [117], [137] have studied position, depth and speed controllers based on fuzzy logic rules in a docking mission to a moving or stationary target submarine. For a moving target, an AUV may therefore be sluggish in response due to large inertia caused from currents. White *et al.* [153] have further considered a virtual docking funnel guiding an AUV closer to the centre of the docking station. A virtual funnel is constructed by a use of three based-line sonar. The planning mission has been carried out using a fuzzy behaviour based control system.

- The first study in homing planning using biologically-inspired strategies have been carried out by recent researchers [102], [150]. Visual based navigation of insects can be explained by the snapshot model [80] and average landmark

vector model [102]. Two most important techniques are similar but the method provides more compact representation. In the landmark vector model, unit vectors represent a position of the robot toward each landmark features. Details in the application for mobile robot homing could be found in works of Moller *et al.* [102], [103], Ushera *et al.* [145] and Wei *et al.* [150].

- It can be seen from the previous research that there is still a wide open in the homing and docking path generation and control design for an AUV. Inspired by a virtual funnel and an average landmark model, Jantapremjit and Wilson [62], [63] have extended works in path generation using a vector field method, including a control system for homing and docking . Details of the concept are given in the following sections.

4.3 Planning

In the field of robotics, motion planning is expressed as the process of choosing a motion and associated input forces and torques in 6-DOFs whilst all constraints are satisfied. In marine applications, motion planning deals with the problem of finding a suitable path and control inputs to drive an AUV from an initial state to a final state whilst it has to satisfy physical-based dynamic constraints. However both kinematic and dynamic constraints must be considered simultaneously [85]. In the literature of motion planning, the configuration space is a set of all possible collision-free configurations for the robot [84]. There are common two motion planning algorithms namely, explicit and implicit motion planning. The first method involves the explicit computation of trajectory of the system in order to produce a set point for the low-level control. It focuses on randomized algorithms which can solve a high-dimensional configuration space. There are several algorithms that are applied to those problems, such as the randomized potential field method and the probabilistic road-map method. A Rapidly-exploring Random Tree (RRT) is a randomized algorithm designed for path

planning problems [86] which can applied to nonholonomic and kinodynamic planning. Tan *et al.* [142] have proposed a motion planning on an incremental stochastic planning method based on RRT algorithms which are available for both holonomic and nonholonomic underwater vehicles. The second method is implicit motion planning which has implicit motion planning in which trajectory and the control action are not explicitly computed before the motion occurs. One of examples is an potential field algorithm [69]. The potential field algorithm was developed in this article to specify the robot interaction with the environment and how it responds to the sensory information. This method comes to the attention because of its simplicity and less computation. The basic algorithm is detailed in the following section.

Motion Planning and Artificial Potential Field Method

Artificial potential field methods are attractive among researchers in robotics, due to its mathematical simplicity and elegance [69]. The method can be implemented quickly and provide reasonable results without requiring heavy computational resources. It can be applied for real-time control as it requires only local gradient information. The potential field method was first proposed by Khatib [69]. Motion planning using gradient information provides a potential function as an input that drives a vehicle to its desired trajectory while avoiding obstacle collision. This is attractive to work carried out for homing and docking task.

4.4 Artificial Potential Field

The artificial potential field technique is an approach that breaks up the free space into a fine grid which is then searched for a free path. Each grid element is assigned a **potential**, where the goal and neighbouring elements are assigned an **attractive potential** and obstacles possess a **repulsive potential**. This ensures that the path created moves towards the goal whilst steering clear of any obstacles.

4.4.1 Potential Fields

The potential field approach treats the target position as an attractive well, where the minimum is at the target and treats obstacles as a high potential hill that creates a repulsive force. Assuming the vehicle is a point mass and moves in 2D space. Its position in the workspace is denoted by $q = [x, y]^{\mathsf{T}}$. The overall potential is the sum of these two types,

$$U_{total}(q) = U_{att}(q) + U_{rep}(q). \tag{4.1}$$

where $U_{att}(q)$ and $U_{rep}(q)$ denote the attractive and repulsive artificial potential function , thus the field of artificial forces can be further determined by,

$$\mathcal{F}_{total}(q) = -\nabla U_{att}(q) - \nabla U_{rep}(q). \tag{4.2}$$

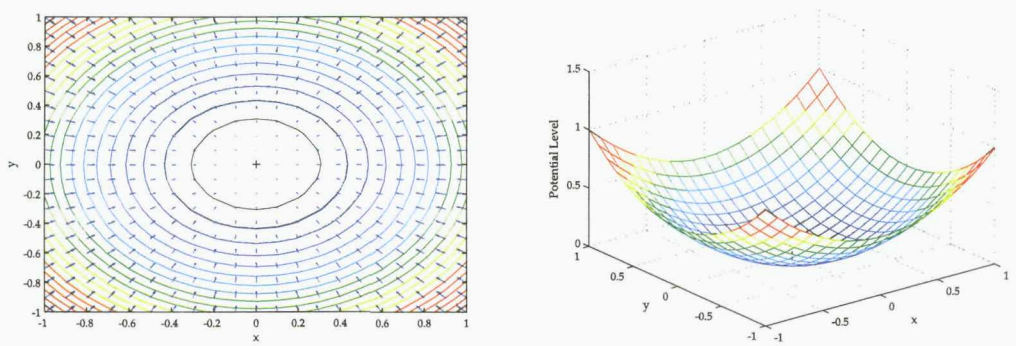

(a) (b)

Figure 4.1: (a) Gradient plot of attractive field, (b) Attractive potential field in 3D plot with $\xi_a = 1$, $m = 2$.

Attractive Potential Field

The attractive potential field gives the negative gradient flows pointed toward the target in the workspace.

$$U_{att}(q) = \frac{1}{2}\xi_a \|q - q_{target}\|^m. \tag{4.3}$$

where $\xi_a > 0$ is scaling factor, $\|\cdot\|$ represents the Euclidean distance and $m = 1$ or 2. For $m = 1$, the attractive potential is conic in the shape where $m = 2$ the attractive potential is parabolic in shape. A typical attractive potential field with $\xi = 1$ and $m = 2$ is shown in figure 4.1.

Repulsive Potential Field

On the other hand, the repulsive potential field gives the negative gradient flows pointed away from the obstacle in the workspace.

$$U_{rep}(q) = \begin{cases} \frac{1}{2}\xi_r(\frac{1}{\rho(q,q_o)} - \frac{1}{\rho_0}), & \text{if } \rho(q,q_o) \leq \rho_0; \\ 0, & \text{if } \rho(q,q_o) > \rho_0. \end{cases} \tag{4.4}$$

where $\xi_r > 0$ is positive scaling factor, $\rho(q, q_o)$ defines the minimal distance from the vehicle q to the obstacle, q_o denotes the point on the obstacle such that the distance between this point and the vehicle is minimal between the vehicle and the obstacle and ρ_0 is positive constant denoting the distance of influence of the obstacle. A repulsive potential field with $\xi_r = 1$ and $\rho_0 = 1.2$ is shown in figure 4.2.

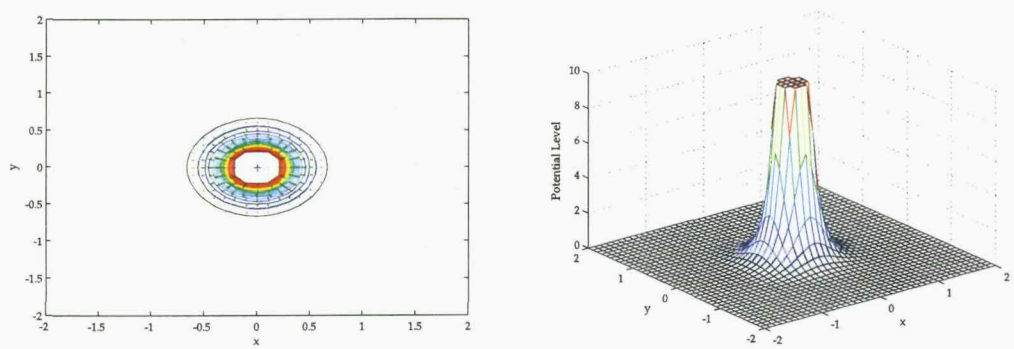

(a) (b)

Figure 4.2: (a) Gradient plot of repulsive field, (b) Repulsive potential field in 3-D plot with $\xi_r = 1$, $\rho_0 = 1.2$.

4.4.2 Limitation with Potential Field Method

Conventional potential field which is created from some potential functions can have local minima and therefore it creates a trapped situation for the motion of the vehicle. Fundamentally local minima are created at points where the gradient of an attraction function for the target has the same magnitude and is reversed to the gradient of a repulsive function for an obstacle. Local minima can be caused by either one obstacles or combination of obstacle. An example of local minima results from two closely space obstacles shown in figure 4.3. There are various efforts aimed at overcoming the local minimum problem. Those efforts fall into two categories: (i) establishing artificial potential fields that do not have local minima other than at the goal position; (ii) developing methods for avoiding from local minima. Details of works in those categories can be found in [20], [120], [162] and [86], [116], respectively.

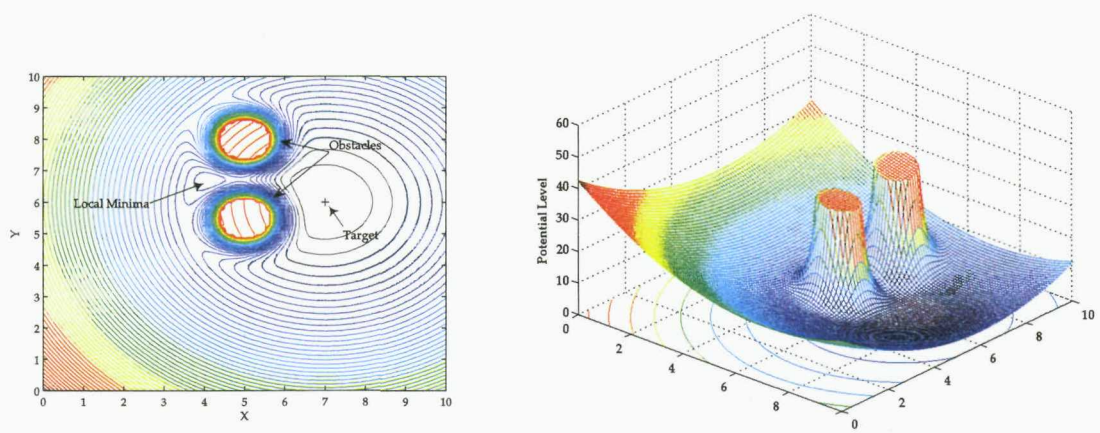

(a) (b)

Figure 4.3: (a) Contour plot of potential field showing a local minima, (b) 3D plot in space configuration.

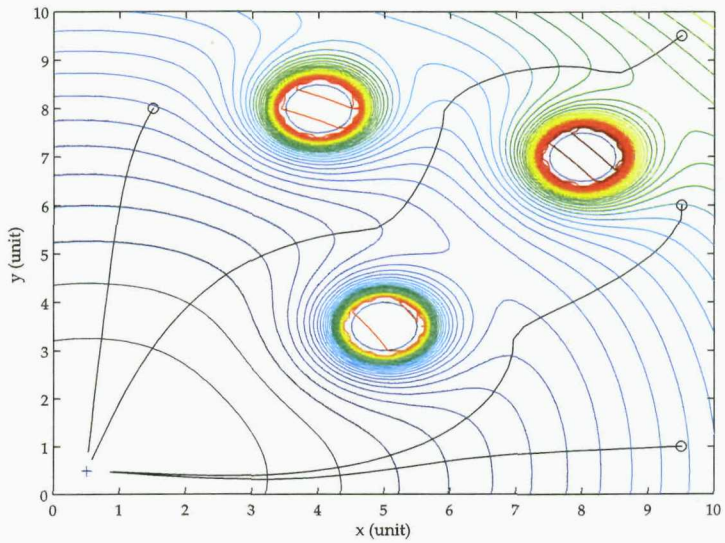

(a)

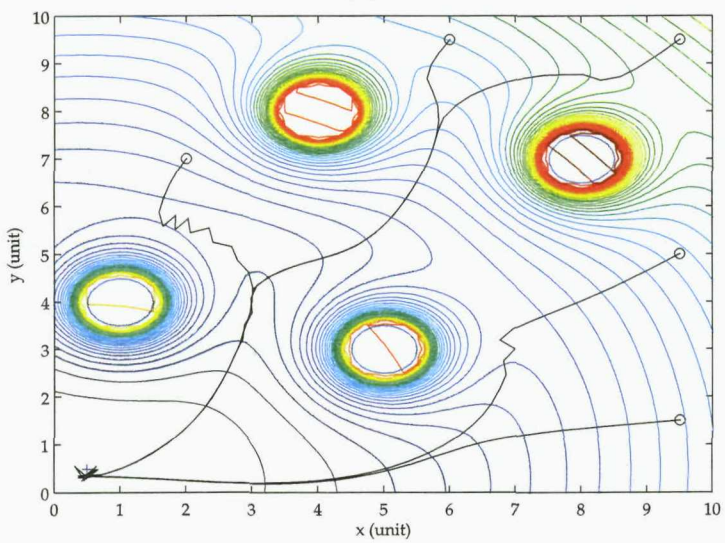

(b)

Figure 4.4: Simulation results of trajectory planning on iso-contour using a potential field method with (a) Three obstacles, (b) Four obstacles. The ○ in figures denote the starting points of the trajectories.

4.4.3 Trajectory Planning in a Workspace with Obstacles

In the case study of trajectory planning using a conventional potential field method. Figure 4.4 (a) shows the contour plot of the potential field and also the trajectory in workspace with three obstacles. Figure 4.4 (b) shows the trajectories created in a workspace with four obstacles. Unfortunately, some of those trajectories are unable to reach the target point (figure 4.4 (a)) and cause oscillation around the target point (figure 4.4 (b)). The conventional potential field is useful enough for homing stage guiding a vehicle converged to a certain location as a destination whilst avoiding the obstacles. Extending the conventional potential field, the vector field method is presented in the following section. This method is used in the docking preparation stage which would shape the trajectory and place a vehicle near the destination point with proper orientations.

4.5 Vector Field Method

A vector field inspired by a method from the visual based navigation of insects explained by [80] and the average landmark vector model [102] based on a conventional artificial potential field [69] is proposed in this work. The vector field for predefined trajectory provides a more compact representation detailed in the following sections.

4.5.1 Vector Field

From a conventional potential field method, a new potential field function is simply considered,

$$U_i(q) = \|q_i - q\|, \tag{4.5}$$

where $\|\cdot\|$ represents the Euclidean norm, hence a potential function of N sensor nodes is,

$$U(q) = \sum_{i=1}^{N} U_i(q) = \sum_{i=1}^{N} \|q_i - q\|, \tag{4.6}$$

where $U(q)$ is a potential function, $q_i \in \mathbb{R}^N$ is the vector of the position point toward sensor node N_i, differentiating equation (4.6), gives,

$$\nabla U(q) = -\sum_{i=1}^{N} \frac{q_i - q}{\|q_i - q\|}, \tag{4.7}$$

It is now defined that $\mathcal{Q}$ is a vector with unit length point towards sensor network N_i is,

$$\mathcal{Q} = \sum_{i=1}^{N} \frac{q_i - q}{\|q_i - q\|} \tag{4.8}$$

and the orientation is,

$$\theta_i = \text{atan}(\frac{\nabla U_{yi}(q)}{\nabla U_{xi}(q)}) \tag{4.9}$$

Now it is interesting to know how many of sensor nodes would be needed to generate clear area for an AUV to be fall down to. Computation simulations illustrated in figure 4.5 show results of a vector field distribution around the sensor networks in the workspace. The distributions can be plotted by using equation (4.7), where $N = 1, 2, 3, 4, 5$ is number of sensor nodes. It can be seen that potentials converge to a minimum at the centre of the valley. Obviously a minimum of three sensor node provides a clear valley thus it is helpful in docking procedure.

4.5.2 Weighted Vector Field

By extending a set of constant weights to a set of varying weights for a vector field in equation (4.7), a better shape of the predefined path can be generated. This is enhanced an achievement to a desired target. A central sensor node is greater meaning for a vehicle to perform docking manoeuvre, the algorithm therefore gives a higher weight than other sensor nodes. Basically, a weighted vector field is denoted by a vector point towards the sensor nodes. Briefly, a path should fall into the centre of the valley; this is because the path would not give too sharp turn and then the second weighted set allows an AUV to approach closer to the dock (details can be found in section 4.6). Assuming each vector (from an AUV points towards each sensor node)

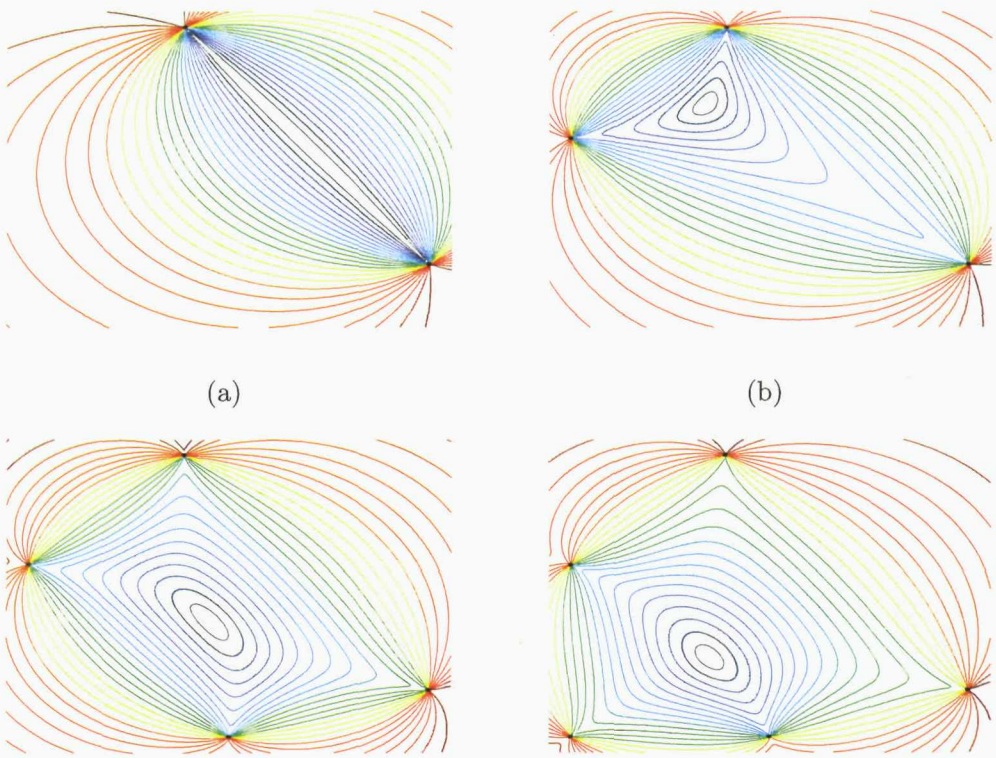

(a) (b)

(c) (d)

Figure 4.5: The level sets of the vector field for: (a) Two sensor nodes, (b) Three sensor nodes, (c) Four sensor nodes, (d) Five sensor nodes. The • in the figures denote the sensor location. From equation (4.7), q_i is the position of each sensor node, whilst q is the position of interest. It can be seen that a minimum of three nodes provides a clear valley.

has its own weight hence a set of weight can be used as path shaping for a trajectory. The equation of a vector with a weight set is,

$$\mathcal{Q} = \sum_{i=1}^{N} \varrho_i \frac{q_i - q}{\|q_i - q\|}, \tag{4.10}$$

where ϱ_i is the weight of each corresponding sensor node N_i.

Figure 4.6 depicts a distribution of $\mathcal{Q}$ that is effected by using various constant weights. The level set shows a convergence to the central valley of the convex hull shown in figure 4.6 (a) whilst it converges closer to the centre node in a valley illustrated in figure 4.6 (b). This would give an excellent opportunity for a vehicle to perform a docking preparation. Figure 4.7 shows a comparison of distributions of potential field using a conventional and a vector field method in 2D and 3D. Figure 4.8 (a)-(f) show plots in various ranges of workspace size using the proposed vector field method. The level sets also illustrate a convergence to the centre area in every case of workspace size.

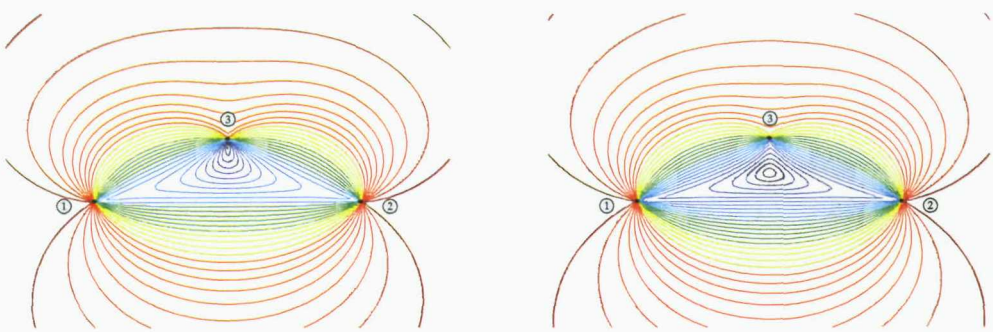

(a) (b)

Figure 4.6: The level set of the vector field using (a) Constant weights set of $\varrho_1 = 0.8$, $\varrho_2 = 0.8$, $\varrho_3 = 0.5$, (b) Constant weight set of $\varrho_1 = 1$, $\varrho_2 = 1$, $\varrho_3 = 1.3$. Node 1 and 2 are represented as • on the left- and right-hand side, respectively whilst the centre • depicts Node 3.

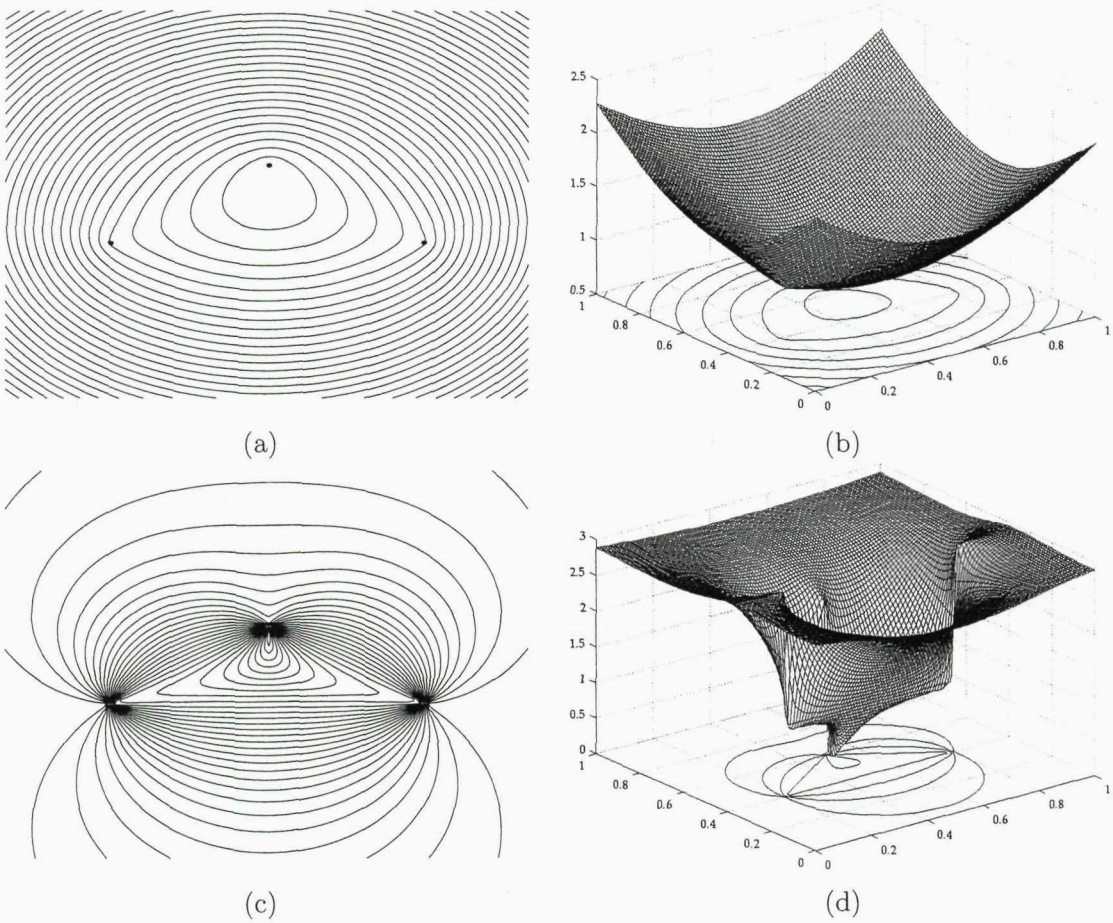

Figure 4.7: Level sets of a potential function U, norm of a vector field $|\mathcal{Q}|$. Convention potential field: (a) Contour plot, (b) 3D plot. Vector field: (c) Contour Plot, (d) 3D plot. The three sensor nodes are represented as •.

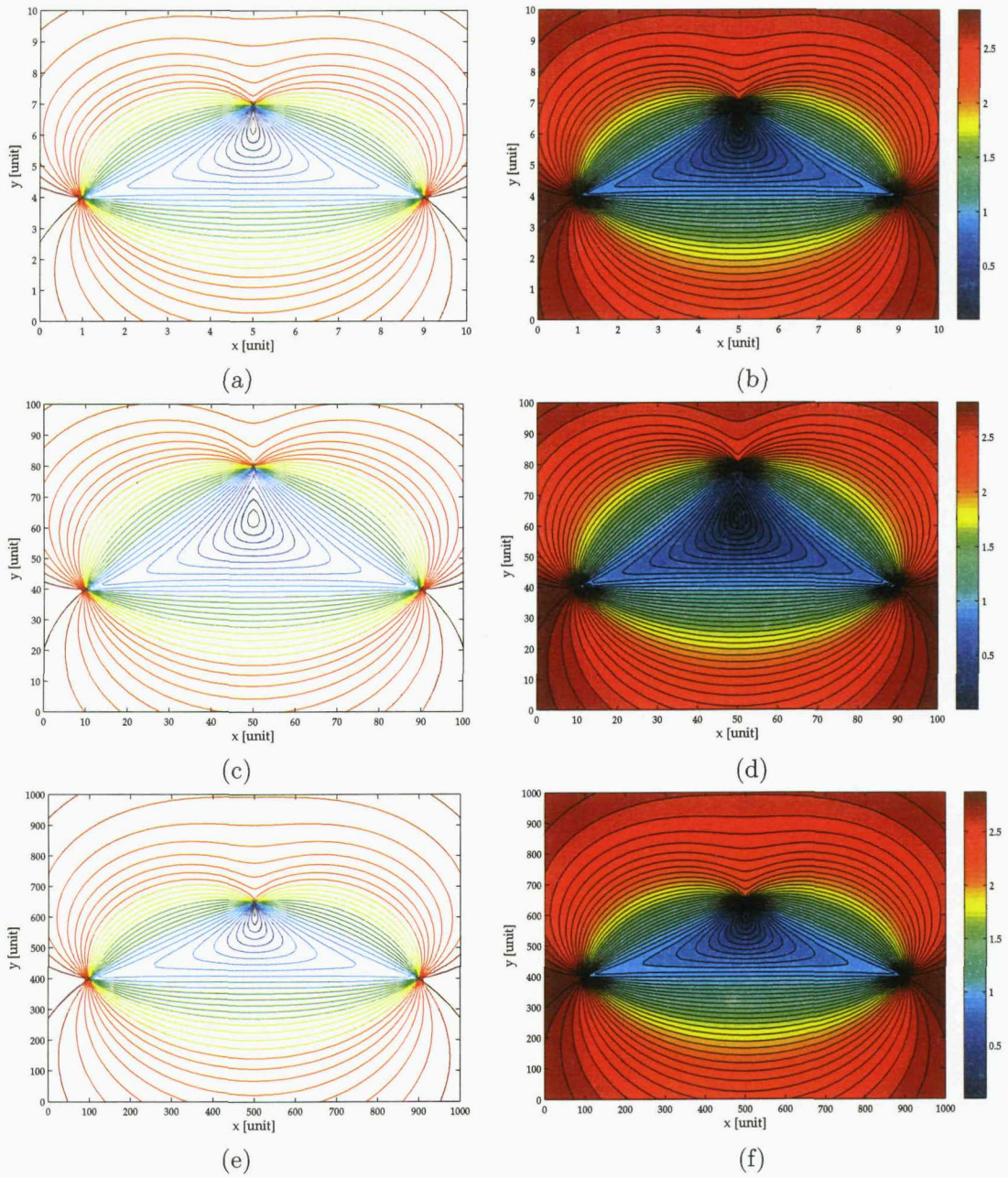

Figure 4.8: Plots of contour and potentials in color map for various cases: (a)-(b) small (c)-(d) medium (e)-(f) large size of workspace and different distance between nodes. The plots shows a convergence to the a confine area near the central valley for every case.

4.6 Homing and Docking Strategy

In this section, a homing and docking strategy is presented. A simple diagram depicted in figure 4.9 shows how an AUV performs either the homing or the docking strategy. Firstly, an AUV is located far away from a docking station where a distance between an AUV and the station satisfies $|q| > 2D$, D is a radius between the dock $\mathcal{N}_3$ and the sensor network $\mathcal{N}_1$, $\mathcal{N}_2$. With this condition an AUV should be able to do the homing strategy L_H by using an artificial potential field path generation method as previously detailed. Secondly, when $|q| \leq 2D$ it is suitable for an AUV to perform docking preparation strategy L_D. The distance $2D$ should allow an AUV enough distance and time for desired position and orientation at the dock. The docking strategy is detailed in the following section.

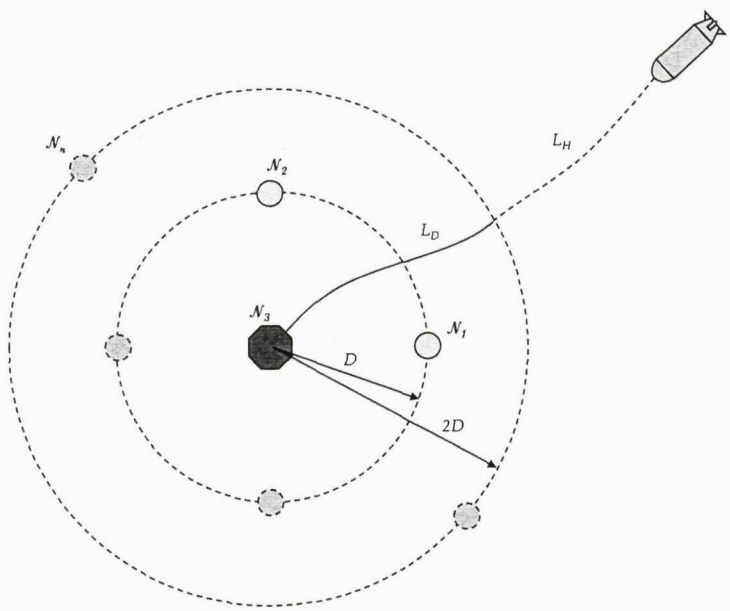

Figure 4.9: Illustration of a diagram shows how an AUV would be able to perform homing and docking strategy. Sensor nodes are at $\mathcal{N}_1$, $\mathcal{N}_2$ and the dock is at $\mathcal{N}_3$.

4.6.1 Homing Strategy

As mentioned previously, the homing trajectory is modelled with the conventional artificial potential method. With a use of acoustic sensor networks such as the acoustic Long-Baseline system, a virtual AUV is assumed to be is able to track the negative gradient field generating a predefined path until it reaches the minimum potential.

4.6.2 Docking Strategy

In the docking strategy, it is more challenging than the homing task since it requires more precision in position and orientation at the docking station. The docking strategy is divided into two stages: docking preparation and final docking stages. Firstly a precise path is generated using a virtual AUV for a relative position and orientation between a vehicle and a platform. Secondly, a AUV is kept within a safe velocity in order to avoid a possible serious impact at platform in the latter stage. A visual docking which is not considered in this work is a possible method that is used to perform a final attachment to a docking station.

The docking preparation is now considered by using a path generation with the vector field method. According to a weighted vector field which is proposed for trajectory planning, the vector (see figure 4.10) is now computed,

$$\vec{q} = \sum_{i=1}^{N} \varrho_i \vec{p}_i. \tag{4.11}$$

As modelling of the vector field, three sensor nodes should be available to the AUV for measuring both position and orientation in the environment. Figure 4.7 shows the level set and 3D plot of a conventional potential field and a vector field with a constant weight. By comparison, the difference between two methods are clearly displayed.

Suppose a vehicle equipped with sensors, so it is more convenient to compute the minimum potential force as,

$$\nabla U_{\min} = \min(\sum \nabla U(q)), \tag{4.12}$$

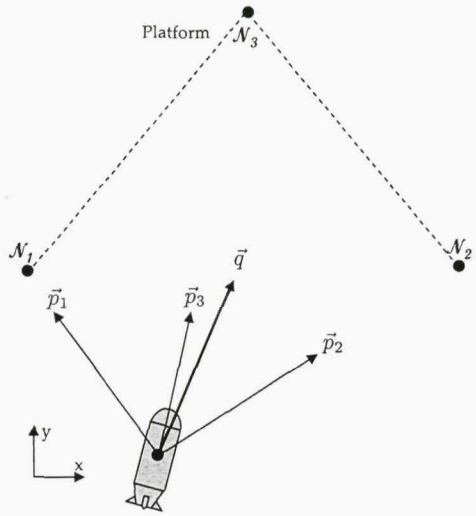

Figure 4.10: Illustration of the weighted vector for three sensor nodes in workspace. Vector $\vec{q}$ is a sum of all unit vectors $\vec{p}_1$, $\vec{p}_2$ and $\vec{p}_3$ with each weight of each corresponding sensor node.

where $min(\cdot)$ returns the minimum vector among all ∇U. Minimising the sum of potentials to each node, a vector will fall down to the area with respect to a level set of $|\mathbf{Q}|$ and then converge to a minimum. Assuming that the position $\vec{q}_{\min}$ of the target with minimum potential field is determined, the objective is to design such that,

$$\lim_{t\to\infty} |\vec{q} - \vec{q}_{min}| = \epsilon \tag{4.13}$$

The algorithm starts determining the gradient of the potential functions related to all sensor nodes as shown in figure 4.11(a) leading a trajectory for a virtual vehicle approaching the target along the gradient flows toward a single minimum potential. Figure 4.11(b) shows that a virtual vehicle approaching an area where its potential field converges toward the minimum. Then the algorithm drives the vehicle to achieve both position and orientation along a computed trajectory resulting in a docking manoeuvre as shown in figure 4.11(c). The summary of path generation using vector fields is shown in Algorithm 1.

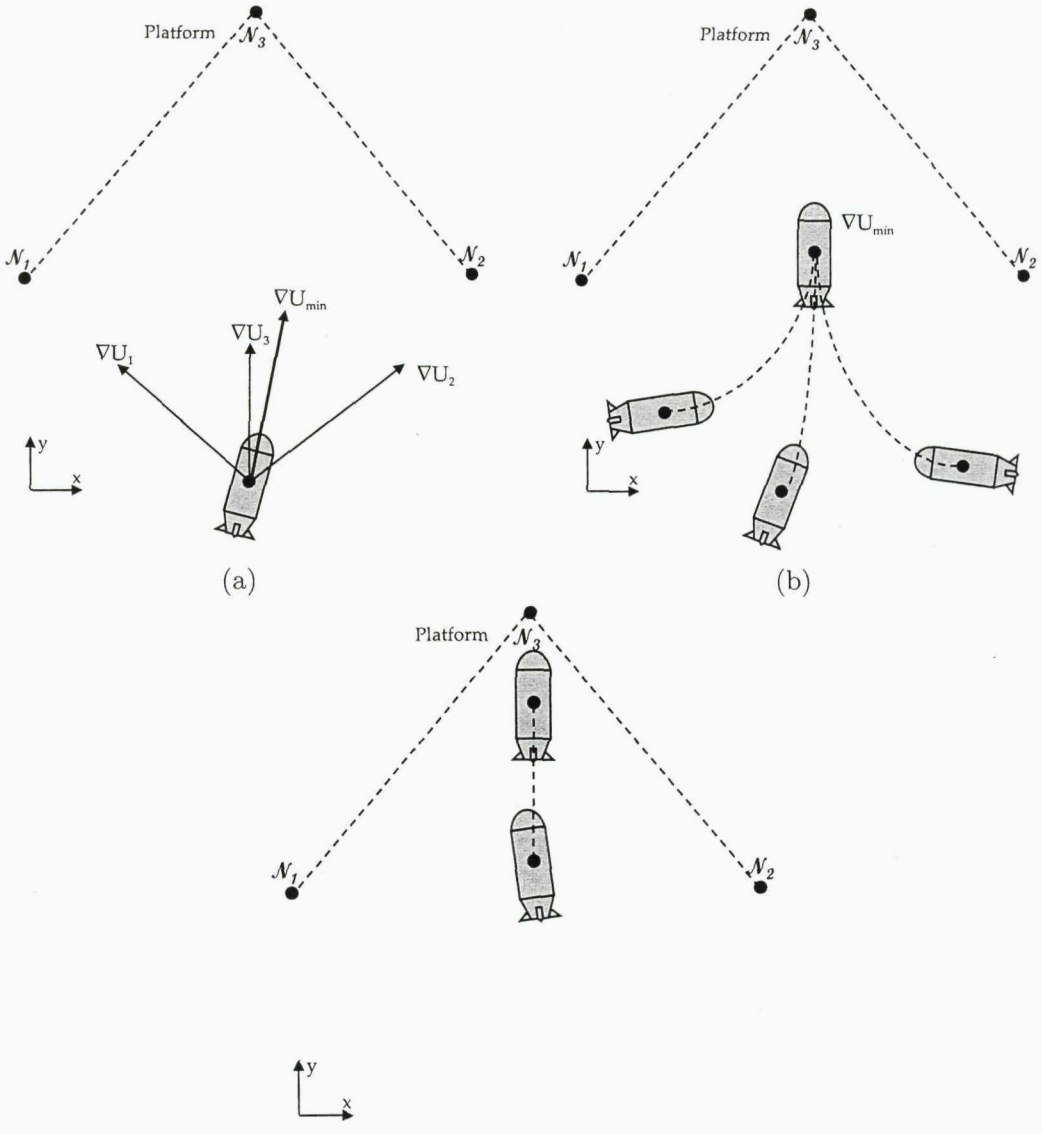

Figure 4.11: Illustration of how a path can be generated using a vector field method during a docking preparation. A virtual AUV is influenced by sensor nodes $\mathcal{N}_1$, $\mathcal{N}_2$ which are represented by •, and a docking platform located at $\mathcal{N}_3$: (a) Summing all vector fields: a virtual AUV is to determine the minimum potential force, (b) A virtual AUV visits a valley where is around the centre area in the convex hull, (c) After approaching close to the target, an virtual AUV is able to perform a docking at the station.

Algorithm 1 Path Generation using Vector Field

Require: Given a set z of n points in 2D or 3D: $z = [x_n, y_n] \in \mathbb{R}^2$ or $z = [x_n, y_n, z_n] \in \mathbb{R}^3$, search for ∇U_{min}, as follows:

$\nabla U_1 \leftarrow \dfrac{q_1 - z}{\|q_1 - z\|}$

$\nabla U_2 \leftarrow \dfrac{q_2 - z}{\|q_2 - z\|}$

$\nabla U_3 \leftarrow \dfrac{q_3 - z}{\|q_3 - z\|}$

$\nabla U_{min} \leftarrow \min(\Sigma \nabla U)$

Require: Given $\nabla U_{\min}$, construct path (waypoints), as follows:

if $\|\vec{q}_j - \nabla U_{\min}\| \geq \epsilon$ **then**

  $\nabla U_{1i} \leftarrow \varrho_1 \dfrac{q_1 - q_j}{\|q_1 - q_j\|}$

  $\nabla U_{2i} \leftarrow \varrho_2 \dfrac{q_2 - q_j}{\|q_2 - q_j\|}$

  $\nabla U_{3i} \leftarrow \varrho_3 \dfrac{q_3 - q_j}{\|q_3 - q_j\|}$

  $\vec{q}_j \leftarrow$ sum of all vectors from AUV, points towards each node

  $j \leftarrow j + 1$

end if

4.7 Switching Weighted Vector Field

In order to improve a docking preparation manoeuvre, a switching weighted technique is proposed for controlling a virtual vehicle's path with proper orientations during the docking preparation stage. Firstly, a virtual vehicle is driven towards the middle of a convex hull by using the first weight set ϱ_1 and once the vehicle is aligned at the centre of the valley and then a second set of weight ϱ_2 is applied for a final docking manoeuvre (see figure 4.12). The switching weighted equation can be expressed as,

$$\varrho_i \doteq \varrho_{i,1}(1 - \Lambda) + \varrho_{i,2}\Lambda, \tag{4.14}$$

and,

$$\Lambda = \begin{cases} 0, & \text{if } \Delta < \Delta_0; \\ \frac{\Delta - \Delta_0}{\Delta_s}, & \text{if } \Delta_0 \leq \Delta \leq (\Delta_0 + \Delta_s); \\ 1, & \text{if } \Delta > (\Delta_0 + \Delta_s); \end{cases} \tag{4.15}$$

where Δ_s is a switching period and $\varrho_{i,1}$, $\varrho_{i,1}$ are sets of weight at N_i sensor nodes in stage 1 and stage 2.

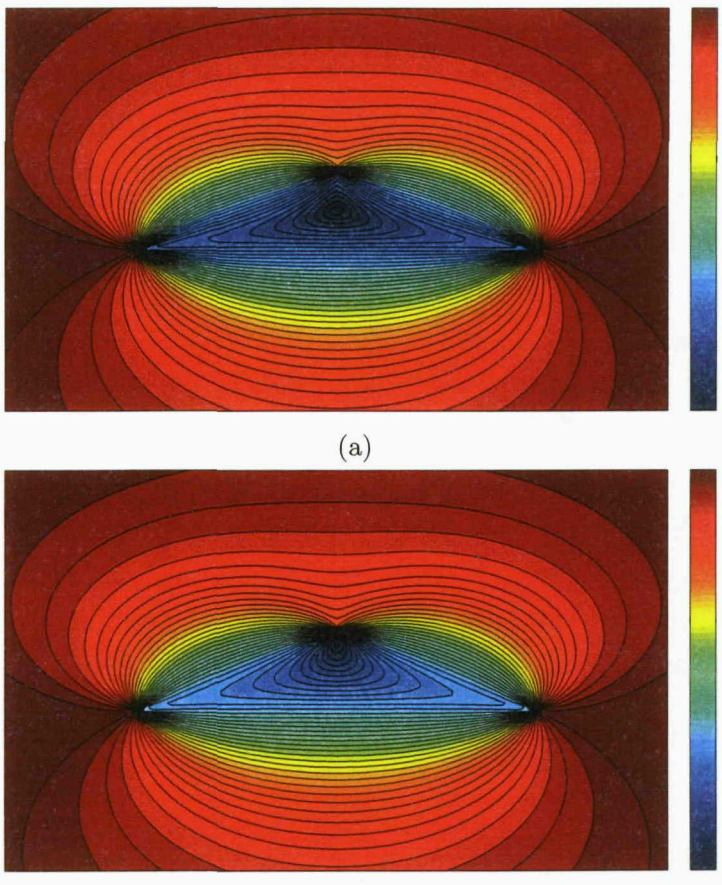

(a)

(b)

Figure 4.12: Colour maps of the potentials using the vector field method with switching weight sets (a) Stage 1 with a weight set of [0.8 , 0.8, 0.5] , (b) Stage 2 with a weight set of [1, 1, 1.3]. The area of minimum potentials (dark blue) moves from the centre nearer to the docking station.

4.8 Safe Trajectory

The concept of the vector field method provides a convergence to a destination point therefore the feasibility of the trajectory generation is guaranteed. The total of potential field function is a sum of all sensor networks. It is obvious that the sum of this function is convex. It therefore can be concluded that all trajectories following the negative gradient will decreasingly moving toward a minima. For example, a virtual AUV may fall into a concavity without able to exit from that concavity. A scenario is shown in figure 4.13. Indeed, it can be observed that trajectories enter in the area (shown as the cone shape) where all trajectories radially converge to the target.

Definition 4.1. *(Safety): The virtual vehicle is in a safe state at time t if that state lies on the trajectory $\mathcal{Q}$ or if from that state there exists an obstacle free trajectory of all length $\mathcal{Q}$ ending at a destination point. Safety is therefore defined as being in such a safe trajectory.*

4.9 Simulation Results

In this section, simulations using MATLAB® for predefined path planning are illustrated. Figure 4.14 shows two example of vector field around straight and circular line. The vector fields represent the desired direction to the desired paths (linear and circular). Figure 4.15 shows trajectories generated by the conventional potential field and the vector field. It is obvious that the vector field allows trajectories converge to a centre of convex hull. Figure 4.16 shows the simulation of trajectories employing the time-varying switching weighted set. The improved method generates paths which provide better orientation directing to a target. These smoother path would allow an AUV to track much easier.

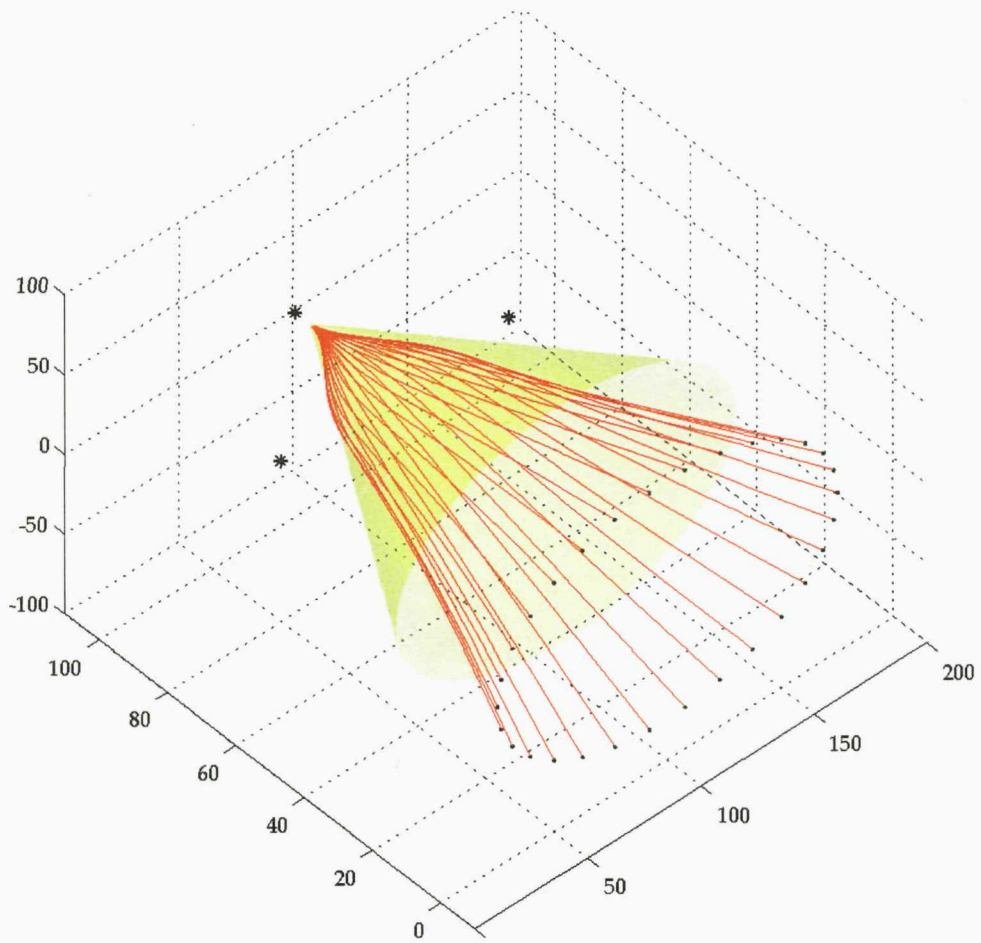

Figure 4.13: Illustration of trajectories entering in a cone shape. A set of initial points is shown as $\cdot$, whilst the center $*$ is the target. It can be seen that all trajectories converge into the centre of the cone shape.

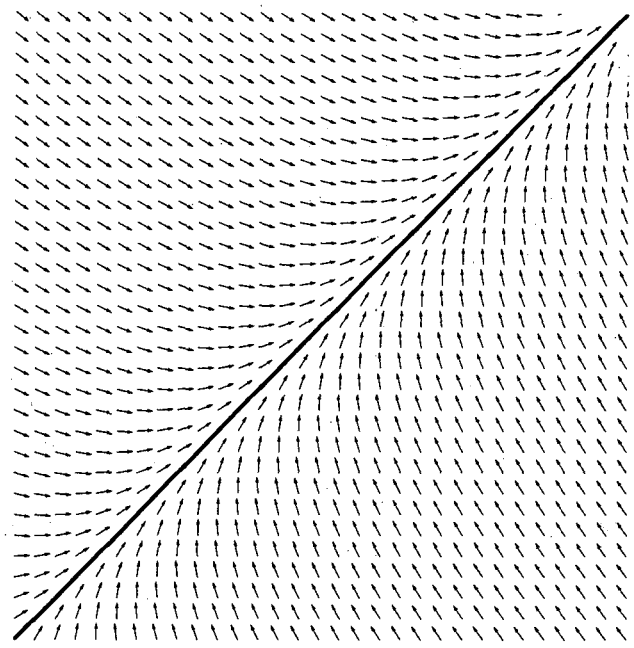

(a)

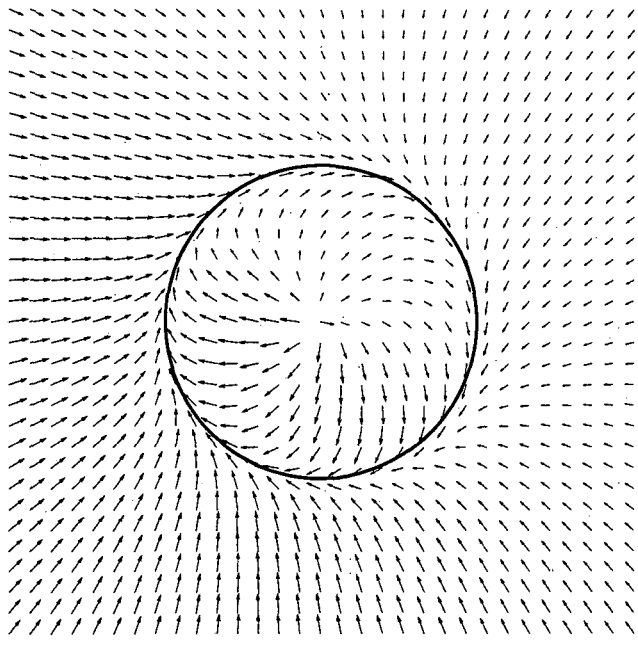

(b)

Figure 4.14: Vector field plots for (a) straight line (b) circular line.

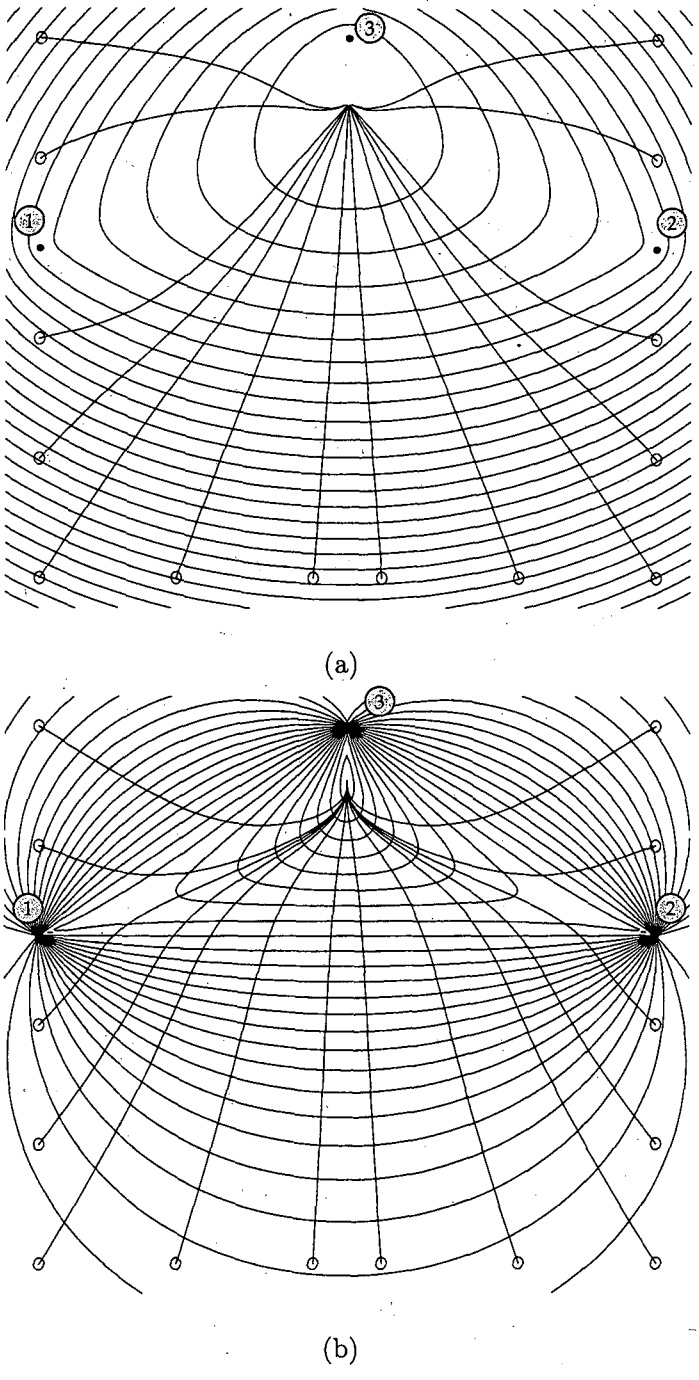

Figure 4.15: Generating trajectories on potential distributions using (a) Conventional potential field method, (b) Vector field method. References of Node 1 and 2 are represented as • on the left- and right-hand side, respectively whilst the centre • depicts Node 3. Starting points depicts as ○.

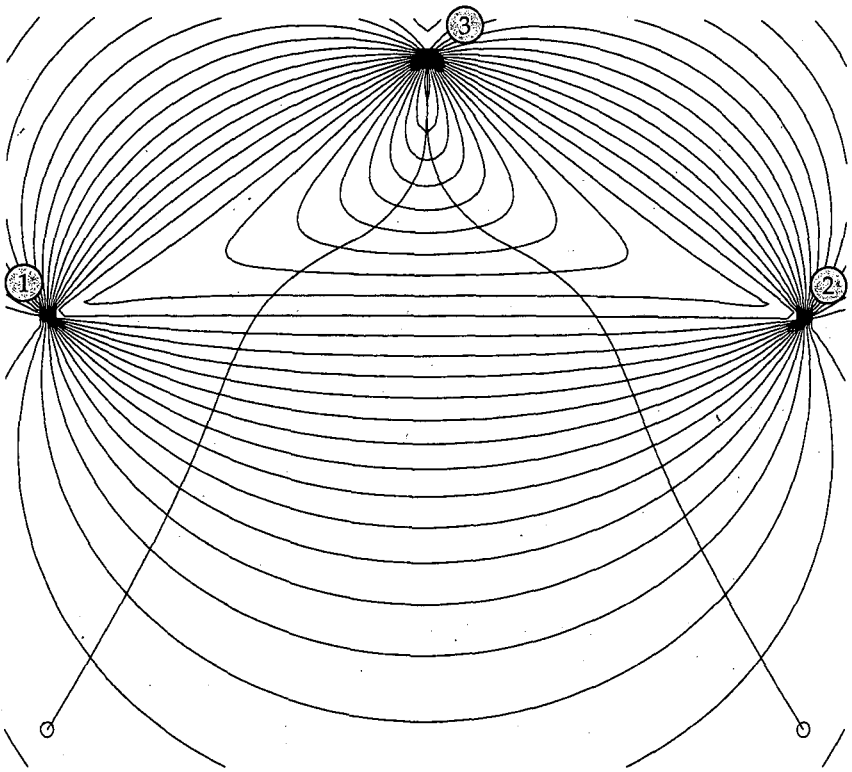

Figure 4.16: Trajectory generated using a vector field with a switching weighted set. References of Node 1 and 2 are represented as • on the left- and right-hand side, respectively whilst the centre • depicts Node 3 represented as a destination. Starting points depicts as ○. The first weight set $\varrho_1 = 0.8$, $\varrho_2 = 0.8$, $\varrho_3 = 0.5$ is used for a converge trajectory to a centre area far from the sensor nodes. Then a time-varying switching weight function gives the smooth trajectory by shaping AUV's orientations. Finally, the second set of weight $\varrho_1 = 1$, $\varrho_2 = 1$, $\varrho_3 = 1.3$ is applied for precise positions and proper orientations at the docking station.

4.10 Summary

This chapter describes a method for a path generation in homing and docking tasks. The vector field is used to determine a predefined trajectory. The main advantage of this method is the minimum field at the centre of a convex hull that is very useful for aligning an AUV in both position and orientation closer to the target. Safe trajectory is also provided by the proposed concept. With the proposed method of weighted vector and switching weighted vector, a smooth trajectory is permitted. Consequently the path following and tracking problem will be easier. In the following chapter this concept will be detailed.

Chapter 5

Guidance-Control Approach

5.1 Overview of Chapter

Given a path to be followed, the aim is to construct a control system that forces the AUV to converge along the path and drive it closed to the destination. This chapter documents the current research effort and a framework for guidance-control in the field of path following using an integration of line-of-sight guidance and sliding mode controller. Section 5.2 briefly discusses the problem in guidance-control for docking task. Literature in trajectory tracking and path following are given in section 5.3 and 5.4 respectively. In section 5.5, a novel guidance-control approach based on Line-of-Sight guidance and sliding mode control is proposed. This is followed by an optimal guidance law for orientation, which is given in section 5.6. Simulation studies are described in section 5.7 and a summary of the chapter is presented in section 5.8.

5.2 Problem Statement

In many marine applications, they is considerable interest in the development of advanced methods for marine control system. A simple block diagram of the system can be shown in figure 5.1. Furthermore, motion control is concentrated into three problems, namely stabilisation, trajectory tracking and path following. Stabilisation refers to stabilising a vehicle at a point in the output space. Trajectory tracking aims to make a vehicle track a desired time-parameterised reference trajectory in the output space. Path following is to make a vehicle converge to and follow a desired spatial path in the output space, without any temporal specification. In the following sections, an introduction of path-following and tracking problem is discussed. Generally speaking, guidance-control problem is usually approached as two separate tasks. The first task, denoted the kinematic or path following, is to reach and follow a desired trajectory. In the second task, it is to satisfy dynamic behavior along the path, for example a desired speed. This task is usually specified as an assignment for the speed. It is useful in the development of an approach for steering an AUV along the predefined trajectory with a desired speed for accurate homing and docking tasks in a long-term mission.

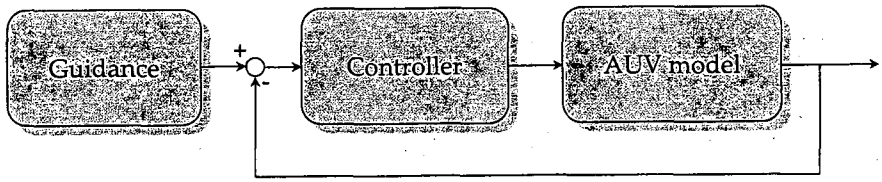

Figure 5.1: Basic block diagram for an underwater vehicle's guidance and control system.

5.3 Trajectory Tracking

A general dynamic system can be expressed in the ordinary differential equation,

$$\dot{x} = f(x, u) \tag{5.1}$$

where $f \in \mathbb{R}^{m \times n}$ is the nonlinear function, $x \in \mathbb{R}^m$ is the state vector, $u \in \mathbb{R}^n$ is the control and $\dot{x}$ is the time derivative of the state. The output can be related to the state as following,

$$y = h(x) \tag{5.2}$$

where $y(t) \in \mathbb{R}^m$ is the output of the system that is to be tracked along a desired trajectory.

In trajectory tracking problems, a designed control law is to ensure that a system is able to track desired trajectory. Let $y_d(t)$ be a bounded desired output. The tracking problem is to design a input vector such that it makes $y(t)$ converge to $y_d(t)$,

$$\lim_{t \to \infty} (y(t) - y_d(t)) = 0, \tag{5.3}$$

where the desired output $y_d(t)$ is defined as a point that moves as a function with respect to time in space. Tracking $y(t)$ is to follow desired trajectory $y_d(t)$ and its derivative is given by $\dot{y}_d(t)$.

Numerous underwater applications using various techniques for solving the tracking problem are reported in the literatures (see summary in Table 5.1):

- Pettersen and Fossen [114] have demonstrated results of the dynamic positioning problems for a surface vessel. They have shown that underactuated surface vessel cannot be asymptotically stabilised by a continuous time-invariant feedback law. A time-varying feedback control law with integral action is therefore proposed to provides such a stability. An integral control is introduced in the control law in order to mimimise the stationary errors and oscillation of the

ship. However the experiments have shown that the control law did not give the desired behaviour.

- Alonge *et al.* [5] have presented a cascade control scheme for an underwater vehicle. The method combines a vehicle kinematic model for forcing the model to follow the trajectory and a dynamic control law for forcing the vehicle to track along the reference trajectory with an assigned speed. An observer based on a PI controller is implemented to obtain a speed of the vehicle. The simulation depicted a controller forces a heading of vehicle to track along the path with small error in position and orientation.

- Behal *et al.* [9] have proposed a continuous, time varying tracking controller based on the Lyapunov stability to control position and orientation tracking error of a surface vehicle. The proposed controller yields global uniformly stability which gives a small error in tracking/regulation problem. Only mathematical modelling has been given in the paper.

- Aguiar and Hespanha [2] have discussed the problem of position tracking problems for underactuated underwater vehicles. They have proposed an algorithm based on the Lyapunov stability criteria, an integral backstepping which satisfies global stability and exponential convergence. The rotation matrix representation is modelled in the group of rotations in three dimensions $SO(3)$. Thus, the control law does not suffer from geometric singularities.

- Godhavn [48] has presented an optimal trajectory using an underactuated surface vehicle. The path is created by a technique using splines. The control law combines feedback linearisation and recursive backstepping for global exponential stabilisation of its line and orbit trajectories. Due to the controller structure, the orientation of the vehicle is not controlled. The output states are reduced to 2-DOFs, thus tracking control problem is fully actuated. Similarly, Toussaint *et al.* [143] have used an integrator backstepping of trajectory

tracking for underactuated surface vehicle forced to follow the reference path by using generalized forces.

- Repoulias and Papadopoulos [119] have combined state-feedback linearisation, backstepping and nonlinear damping approaches. The method is for stabilising an AUV's motion in horizontal plane and for minimising error in trajectory tracking problems. Based on Lyapunov stability, the controller has guaranteed stability in complex hydrodynamics and damping terms.

- The studies of underactuated surface vessels with 3-DOFs for tracking control are considered in [66], [89] and [96]. Its globally uniformly asymptotically stabilisation (see appendix C) is derived for position and heading tracking control. However, its limitation to non-zero curvature is unable to be used for straight-line tracking. A cascade backstepping controller based on Lyapunov stability is developed in the paper. Various results that achieve full state control based on 3-DOFs marine vessel are reported.

- A global output-feedback controller for an ODIN spherical underwater vehicle in horizontal plane has been developed in [26]. The controller is designed on Lyapunov direct method and backstepping technique. Numerical simulations have been illustrated.

- A waypoint tracking of a straight-line at constant surge speed is considered in [45]. The closed loop system control law is proved to be global κ-exponentially stable. Similarly Pettersen and Lefeber [115] have proposed a waypoint tracking control law which is related to LOS method but which are ad-hoc methods for which, to authors' knowledge, stability and convergence of tracking error have not been proved. A heading- and cross- tracking for straight-line using cascade system theory is developed that guarantees global asymptotic stability.

Table 5.1: Summary of research for tracking trajectory

Reference	Vehicle	Control laws	Results
[2]	Hovercraft/ Underwater vehicle	Lyapunov stability/ backstepping	Simulation in 2D, 3D
[5]	Underactuated Underwater vehicle	Cascade scheme	Simulation in 3D
[9]	Surface vessel	Lyapunov-based control	Mathematical modelling
[26]	Underwater vehicle	Output feedback/ Backstepping	Simulation in 2D
[45], [115]	Surface vessel	Cascade theory	Simulation in 2D
[48], [143]	Surface vessel	Feedback linearisation/ Backstepping	Path simulation in 2D
[66], [89], [96]	Surface vessel	Cascade backstepping	Simulation in 2D
[114]	Surface vessel	Time-varying feedback control law	Experiments
[119]	Surface vessel	State-feedback/ Backstepping	Simulation in 2D

5.4 Path Following

Path following is the problem of making a vehicle converge to and follow a given path, without any temporal demands [3]. In this problem, an entire path is considered rather than a single point. A path is given as a set of coordinates. Now considering $y_d(\chi)$ defined as a continuous parameterisation [133] by the path variable χ, thus the path can be represented by,

$$Q_p = \{y \in \mathbb{R}^m : \exists \chi \in \mathbb{R} \quad \text{such that} \quad y = y_d(\chi)\} \tag{5.4}$$

The path following problem aims to design a function such that an input vector $u(t)$ in equation (5.1) makes $y(t)$ converge to and track the path with nonzero motion.

Example 5.1. *A parameterised path is defined as $\eta_d(\chi) \in \mathbb{R}^m$ with $m \geq 1$ parameterised by a continuous path variable χ [39].*

A vehicle in 3-DOFs is defined:

$$\eta_d = [x_d(\chi), y_d(\chi), \psi_d(\chi)]^\mathsf{T} \tag{5.5}$$

A vehicle in 6-DOFs is defined:

$$\eta_d = [x_d(\chi), y_d(\chi), z_d(\chi), \phi_d(\chi), \theta_d(\chi), \psi_d(\chi)]^\mathsf{T} \tag{5.6}$$

Table 5.2: Summary of research for path following

Reference	Guidance	Control laws	Results
[16]	Line-of-Sight	Backstepping	Simulation in 2D, 3D
[3], [32]	Serret-Frenet coordinate	Backstepping	Simulation in 2D
[33], [34], [35], [82], [83]	Serret-Frenet coordinate	Backstepping	Simulation in 3D
[133], [134]	Maneuvering	Backstepping	Simulation in 3D
[24], [25], [27], [28]	Waypoint guidance	Backstepping	Mathematical model

Preliminary work in the field of land vehicle controls is referred to [125]. The Lyapunov method is used as a power tool for nonlinear path-following. Although the proposed method has been successfully implemented for a land vehicle, it may not be true for marine vehicles. This is due to the fact that non-dimensional hydrodynamic terms play a key rôle in the motion. Therefore, motion control of path-following for marine vehicle requires advance methodologies for accurate path-following that is able to take explicitly into account the nonlinear hydrodynamic terms influenced by ocean currents and wave action. The literatures (see summary in Table 5.2) are discussed by followings,

- Breivik and Fossen [16] have discussed the problem of path following in marine application. They studied the action of helmsman and surface vessel. A waypoint representation is basically designed by reducing 3-DOFs (positions and heading) to 2-DOFs (yaw and speed) [54]. A similar method has proposed using

the Line-of-Sight projection tracking waypoints by considering a heading and surge speed. The controller is designed using the backstepping method which will guarantee stability.

- In [3] a planar path following controller is designed for the dynamic model of a marine vessel. This static solution takes explicitly into account constant but unknown currents and it guarantees global convergence of the position and heading error to zero. As explicitly shown in [32], reference paths are not required to have constant curvature. The path of the model is represented by the Serret-Frenet coordinate frame. Remarkably the same design methodology may be extended to solve also the 3D path following problem. A backstepping based on Lyapunov function again guarantees a stability.

- A development of a combined feature of trajectory tracking and path following for marine vehicle can be found in [33], [34], [35]. The method models the vehicle in term of the Serret-Frenet reference. A control based on backstepping techniques is designed and numerical implemented by using a hovercraft.

- A nonlinear control method for accurate path following and path tracking in underwater vehicle application is developed by [83], [82]. The definition of variables used a simplified 2-DOFs vehicle is built on Serret-Frenet reference frame. A virtual target is to be tracked along the path by the real vehicle. Controller is designed by using recursive backstepping method. The controller guarantees global asymptotic convergence of the vehicleŠs trajectory to the path. Trajectory simulation results are illustrated the performance of the proposed controller.

- Similar to these works is that of Skjetne [133], [134] which develops an output manoeuvering method composed of two tasks: forcing the output to converge to the desired path (kinematics) and then secondly satisfying a desired speed

assignment along the path (dynamics). A marine vehicle simulation is shown in the paper.

- In [25] *et al.*, based on Lyapunov's direct method and backstepping technique guarantee global asymptotic stability of a predefined path at a desired speed. The paper is concerned with unknown parameters along a given path under environmental disturbances induced by wave, wind and ocean current.

- The off-diagonal terms of the inertia and damping matrices are considered in [24], [28] for underactuated ships. Path tracking control law that is allowed to be a curve including a straight line is based on Lyapunov direct method and backstepping technique. However, extended work on controller design in [27] for trajectory tracking for 3-DOFs model ship is proved that guarantees global κ-exponential stability.

5.5 Guidance-Control Law

Based on various literature a guidance based control for following the path has been reviewed in previous sections. Consider the manoeuvering problem which constructs an update law for the path and forces the path speed to follow the desired speed. The objective can be then classified into two main problems: kinematics and dynamics.

Definition 5.1. *(Maneuvering problem [133]) Two tasks are:*

- **Kinematics**: *Let $y_d(\chi)$ be a desired output (positions and orientations). For any continuous function $\chi(t)$. The tracking problem is then to design a control system of the vehicle to make y converge to and eventually follow $y_d(\chi)$ that is,*

$$\lim_{t\to\infty} |y(t) - y_d(\chi(t))| = 0 \tag{5.7}$$

- **Dynamics**: *Let $u_d(t)$ be a desired speed. The design of control system is to force the speed $\dot{\chi}$ of the vehicle to converge to a desired speed $u_d(\chi, t)$, that is,*

$$\lim_{t\to\infty} |\dot{\chi} - u_d(\chi(t), t)| = 0 \tag{5.8}$$

Various guidance and control strategies are considered in the communities. Before continuing, two common guidance systems are briefly given:

I. Waypoint guidance is commonly used both for marine and aerial vehicles [113]. A path defined by a series of waypoints in 2D cartesian coordinates,

$$\text{Waypoints} = [(x_0, y_0, z_0), (x_1, y_1, z_1), \ldots, (x_n, y_n, z_n)]$$

II. Line-of-Sight guidance is widely used in marine applications [39]. For a surface vessel, the vector is defined as $\eta = [x, y, \psi]^\intercal$ where $[x, y]$ is the position and ψ is the heading angle. Hence, the desired path for each vessel is given in equation (5.5), where the desired heading is computed as,

$$\psi_d(\chi) = \text{atan}\,\frac{y_d(\chi)}{x_d(\chi)}$$

Guidance-control system is of interest in the aerial and marine applications. Previous works can be briefly discussed as following.

- Ryoo *et al.* [121] have proposed an optimal waypoint guidance for an unmanned aerial vehicle. The method determines optimal angle passing through waypoints for the energy impact-angle-control guidance law. In the work by Nelson *et al.* [111], a guidance based path following is developed for an unmanned aerial vehicle. The method constructs vector fields around the path. A sliding mode controller allows a vehicle to follow a straight and circular path.

- Encarnação and Pascoal [32] have proposed a concept of the path following technique using a backstepping controller. The path following is built on the Serret-Frenet frame. Due to complexity of system equation, the method is only valid to the case of the vehicle motion is closed to horizontal and vertical planes.

- Similarly Lapierre *et al.* [83] have presented a control law for a path following of an AUV in 2D. Kinematics is developed in the Serret-Frenet coordinate. The problem in a singularity in the model is resolved by adding an extra degree of freedom for a controller.

- Breivik and Fossen [17], [18], [19] have developed a unified control for a marine vehicle. The concept consists of a model-based velocity controller based on backstepping technique and a Line-of-Sight guidance. Simulation shows 2D and 3D examples of an AUV able to converge to and follow a desired path through non-zero speed assignment.

- Bøhaug and Pettersen [13] have developed a waypoint guidance for path tracking and following for an underwater vehicle. A cascade controller gives a condition for a stability in path tracking to desired waypoints. An improved LOS technique for an AUV has been introduced by Bøhaug *et al.* [12]. Optimal cross-track controller is considered for minimising the error and providing the smooth final approach trajectory. A model predictive guidance is constructed to determine a minimum of the look-ahead distance. This allows an achievement of high convergence rate for cross-track errors.

5.5.1 Control Law

A controller designed for AUV control needs to be robust to deal with external disturbance and model uncertainties (as discussed in chapter 2). However, a simple model is required, thus computational time will be relatively short. Basically a controller that is decoupled into two common subsystems of heading and depth has been proposed [64]. An extension version of the subsystem in a velocity control (see figure 5.2) is expressed in this section. The sliding mode controller (see chapter 3) is chosen.

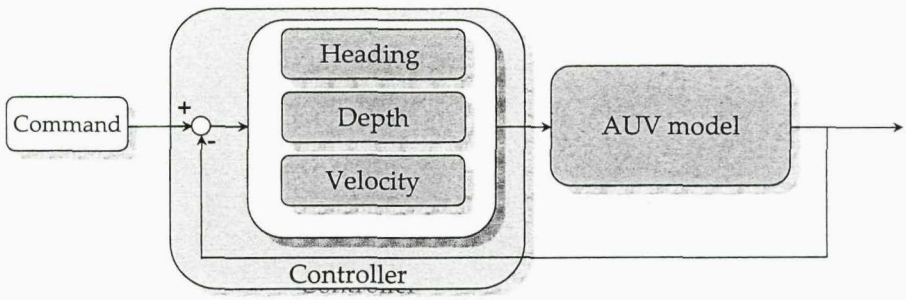

Figure 5.2: Block diagram of a control system.

Case Study

To demonstrate an example of the guidance-control system, the control signal $\bar{u}_{(.)}$ can be simplified and chosen as,

$$\begin{aligned} \bar{u}_u &= -k_u(u - u_d) + \dot{u}_d, \\ \bar{u}_\psi &= \psi - k_\psi(u \sin\theta \cos\psi) - k_{\sigma_\psi} \operatorname{sat}(\frac{\tilde{\psi}}{\Phi_\psi}), \\ \bar{u}_\theta &= \theta - k_\theta(u \sin\theta) - k_{\sigma_\theta} \operatorname{sat}(\frac{\tilde{\theta}}{\Phi_\theta}), \end{aligned} \tag{5.9}$$

where u_d is desired surge speed and k_u, k_ψ, k_θ, k_{σ_ψ}, $k_{\sigma_\theta} > 0$ and $\tilde{\psi} = \psi - \psi_d$, $\tilde{\theta} = \theta - \theta_d$ and $\Phi_\psi, \Phi_\theta > 0$.

5.5.2 Guidance Law

In this section a guidance based on the Line-of-Sight integrated with the waypoint concept (see chapter 4). A guidance system is shown in figure 5.3. First, define the position vector, $p = [x, y, z]^\mathsf{T} \in \mathbb{R}^3$ in the inertial reference frame. The position error $e_d = [e_x, e_y, e_z]^\mathsf{T} \in \mathbb{R}^3$ is defined as the transformation between the inertial-frame based position and the inertial-frame based desired position denoted as p_d, and,

$$e_d = \boldsymbol{R}_d^\mathsf{T}(p - p_d) \tag{5.10}$$

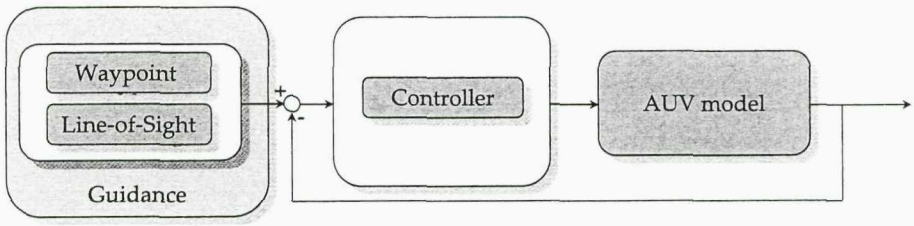

Figure 5.3: Block diagram of a guidance system.

where the rotation matrix $\boldsymbol{R}_d$ is given by,

$$\boldsymbol{R}_d = \boldsymbol{R}_d(\psi)\boldsymbol{R}_d(\theta), \tag{5.11}$$

The position error rate $\dot{e}_p$ is obtained by taking the time derivative of equation (5.10),

$$\dot{e}_d = \dot{\boldsymbol{R}}_d^{\mathsf{T}}(p - p_d) + \boldsymbol{R}_d^{\mathsf{T}}(\dot{p} - \dot{p}_d), \tag{5.12}$$

substituting for $\dot{\boldsymbol{R}}_d = \boldsymbol{R}_d\ \boldsymbol{S}(\omega)$, and $\dot{p}_d = \boldsymbol{R}_d v_d$, and $\dot{p} = \boldsymbol{R}_p v_p$ and using $\boldsymbol{R}^{\mathsf{T}}\boldsymbol{R}= \boldsymbol{I}$ and a relative rotation matrix $\boldsymbol{R}= \boldsymbol{R}_d^{\mathsf{T}}\ \boldsymbol{R}_p$,

$$\begin{aligned} \dot{e}_d &= (\boldsymbol{R}_d\boldsymbol{S}(\omega))^{\mathsf{T}}(p - p_d) + \boldsymbol{R}_d^{\mathsf{T}}(\dot{p} - \dot{p}_d) \\ &= (\boldsymbol{R}_d\boldsymbol{S}(\omega))^{\mathsf{T}}(p - p_d) + \boldsymbol{R}_d^{\mathsf{T}}(\boldsymbol{R}_p v_p - \boldsymbol{R}_d v_d) \\ &= \boldsymbol{S}^{\mathsf{T}}(\omega)e_d + \boldsymbol{R}^{\mathsf{T}}v_p - v_d. \end{aligned} \tag{5.13}$$

Given the candidate Lyapunov function $V_e = \frac{1}{2}e^{\mathsf{T}}e$, then its derivative is obtained,

$$\begin{aligned} \dot{V}_e &= e_d^{\mathsf{T}}\dot{e}_d \\ &= e_d^{\mathsf{T}}(\boldsymbol{S}^{\mathsf{T}}(\omega)e_d + \boldsymbol{R}^{\mathsf{T}}v_p - v_d) \\ &= e_d^{\mathsf{T}}(\boldsymbol{R}^{\mathsf{T}}v_p - v_d), \end{aligned} \tag{5.14}$$

where $e_d^{\mathsf{T}}\ \boldsymbol{S}^{\mathsf{T}}(\omega)e_d = 0$, and let us define $v_p = [u_d, 0, 0]^{\mathsf{T}}$, thus,

$$\dot{V}_e = e_y u_d \sin\psi_d \cos\theta_d - e_z u_d \sin_d \theta_d. \tag{5.15}$$

The aim of path following method is to allow an AUV to follow a predefined path (waypoints) which is represented by a series of vehicle's coordinates joined by line

segments. As described earlier a number of techniques have been developed to solve this problem. The Line-of-Sight guidance technique [39] is intuitive and widely used in the application for path following of an underwater vehicles both in 2D and 3D. Line-of-sight guidance is chosen and can be characterised by,

$$\psi_d = \text{atan}(\frac{-e_y}{\triangle}), \tag{5.16a}$$

$$\theta_d = \text{atan}(\frac{e_z}{\sqrt{e_y^2 + \triangle^2}}), \tag{5.16b}$$

where $\triangle > 0$ is referred to a look-ahead distance, and the initial conditions $y(t_0)$, $z(t_0) > 0$ where t_0 is the initial time. The yaw and pitch angle are bounded,

$$\begin{aligned} \psi_{min} &\leq \psi_d \leq \psi_{max} \\ \theta_{min} &\leq \theta_d \leq \theta_{max} \end{aligned}$$

substituting (5.16a), (5.16b) into (5.15),

$$\begin{aligned} \dot{V}_e &= e_y u_d \sin\psi_d \cos\theta_d - e_z u_d \sin\theta_d \\ &\leq e_y |u_d| |\sin(\text{atan}\tfrac{-e_y}{\triangle})| |\cos(\text{atan}\tfrac{e_z}{\sqrt{e_y^2+\triangle^2}})| \\ &\qquad -e_z |u_d| |\sin(\text{atan}\tfrac{e_z}{\sqrt{e_y^2+\triangle^2}})| \\ &\leq -e_y |u_d| |\sin(\text{atan}\tfrac{e_y}{\triangle})| - e_z |u_d| |\sin(\text{atan}\tfrac{e_z}{\sqrt{e_y^2+\triangle^2}})| \\ &\leq -e_y^2 |\gamma_\psi| - e_z^2 |\gamma_\theta|. \end{aligned}$$

where $\lim_{x\to 0} \cos(x) = 1$, $\lim_{x\to 0} \sin(x) = x$ and $\gamma_\psi, \gamma_\theta$ are constant parameters. Since $\dot{V}_e$ is negative definite, the error vector e is rendered uniformly globally asymptotically stable if $u_d > 0$, ψ_d and θ_d are defined as in equations (5.16a), (5.16b) for all initial conditions. Moreover, with the control laws developed using the sliding mode control developed in section 5.5.1, such that the goal of the path following using LOS is ensured that,

$$\begin{aligned} \tilde{u} &= u - u_d \rightarrow 0, \\ \tilde{\theta} &= \theta - \theta_d \rightarrow 0, \\ \tilde{\psi} &= \psi - \psi_d \rightarrow 0, \end{aligned}$$

Algorithm 2 shows how the Line-of-Sight guidance can be computed. It is to determine the commanded yaw and pitch angle for an AUV. By combining the control law (section 5.5.1) and the guidance law (section 5.5.2), an AUV is able to follow the predefined path with a desired surge speed.

Algorithm 2 Line-of-Sight Path Following Guidance

Require: Given a set of waypoints $p_d = [w_{xi}, w_{yi}, w_{zi}] \in \mathbb{R}^3$, determine commanded yaw ψ^c and pitch angle θ^c, as follows:

$\psi \leftarrow \text{atan}(-\frac{w_{y2} - w_{y1}}{w_{x2} - w_{x1}})$

$\theta \leftarrow \text{atan}(\frac{w_{z2} - w_{z1}}{\sqrt{(w_{x2} - w_{x1})^2 + (w_{y2} - w_{y1})^2}})$

$e \leftarrow \boldsymbol{R}^{\mathsf{T}}(p - p_d)$

$\psi_d \leftarrow \text{atan}(-\frac{e_y}{\triangle})$

$\theta_d \leftarrow \text{atan}(\frac{e_z}{\sqrt{e_y^2 + \triangle^2}})$

$p^* \leftarrow \frac{(p - w_1)^{\mathsf{T}}(w_2 - w_1)}{\|w_2 - w_1\|}$ calculate position of an AUV

if $p^* > 1$ **then**

  switch to next waypoint

else

  $\psi^c \leftarrow \psi - \psi_d$

  $\theta^c \leftarrow \theta - \theta_d$

end if

5.6 Optimal Waypoint Guidance Law

Given waypoints by the path generation with the vector field concept, the LOS guidance connects the current waypoint and the next waypoint in the guidance system. Finding the optimal path gives a smooth command transition. The optimality of the entire path thorough all waypoints is discussed in this section. The concept of the method is to regulate the path via orientation angle by a linear quadratic regulator. The cost function for the optimisation problem $J_{(\cdot)}$ is defined by optimising over the

yaw and pitch angle at each waypoint,

$$\begin{aligned} J_\psi &= \min \sum_{i=1}^{n} J_i(\psi_{i-1} - \psi_i), \\ J_\theta &= \min \sum_{i=1}^{n} J_i(\theta_{i-1} - \theta_i), \end{aligned} \tag{5.17}$$

Define the choice of ψ and θ for the optimisation problem,

$$\begin{aligned} \psi_i &= \psi_{i1} + \tfrac{1}{2}\Delta\psi_i, \\ \Delta\psi_i &= \psi_{i2} - \psi_{i1}, \end{aligned} \tag{5.18}$$

and,

$$\begin{aligned} \theta_i &= \theta_{i1} + \tfrac{1}{2}\Delta\theta_i, \\ \Delta\theta_i &= \theta_{i2} - \theta_{i1}, \end{aligned} \tag{5.19}$$

where ψ_{i1}, θ_{i1} and ψ_{i2}, θ_{i1} are measured from waypoint $i-1$ to waypoint i and from waypoint i to waypoint $i+1$, respectively. Figure 5.4 shows snapshots an AUV following the three consecutive waypoints using optimal orientation through out these waypoints.

5.7 Simulation Results

Simulations for the predefined path following using the Line-of-Sight guidance for a docking task are illustrated. Figure 5.5 and 5.6 show comparisons of 2D simulations of trajectory generation using a conventional artificial potential field and a vector field employed a set of constant weights and switching weights. With a switching weight set, an AUV is able to follow and converge to the path closely aligning in both position and orientation to the destination.

Figure 5.7 considers the vehicle moving along the predefined path operating with the constant speed at 1.3 m/s whilst the speed of an AUV in figure 5.10 converges from 1.3 m/s to 0.5 m/s. The tracking error for yaw and pitch angles for constant and variable speed are illustrated in figures 5.8 and 5.11.

The statistic results for 3D path following can be summarised. Table 5.8 shows an AUV moving at constant speed resulting an average position error of [-0.095, 0.851, 0.033] and an average yaw and pitch angle error of -0.151° and -0.160°, respectively. Table 5.8 shows an AUV moving at variable speed resulting an average position error of [-0.112, 1.038, 0.0014] and an average yaw and pitch angle error of -0.053° and -0.114°, respectively.

5.8 Summary

This chapter presents the development of a control and guidance system for an AUV's homing and docking mission. The main contributions of this chapter can be summarised as follows. A predefined trajectory generated by using the vector field method for homing and docking is presented in previous chapter to provide a vehicle and a platform matching both position and orientation, while the LOS guidance law gives an AUV to converge and follow the path. The sliding mode controller is proposed to provide system's stability. It guarantees that an AUV using the integrated control-guidance system able to converge to a desired path and its speed. Entire path through all waypoints is optimised over yaw and pitch angle. The statistic simulation shows that the proposed guidance-control law successfully gives the AUV to follow the path and converge to the destination (docking platform) with small errors in positions and orientations.

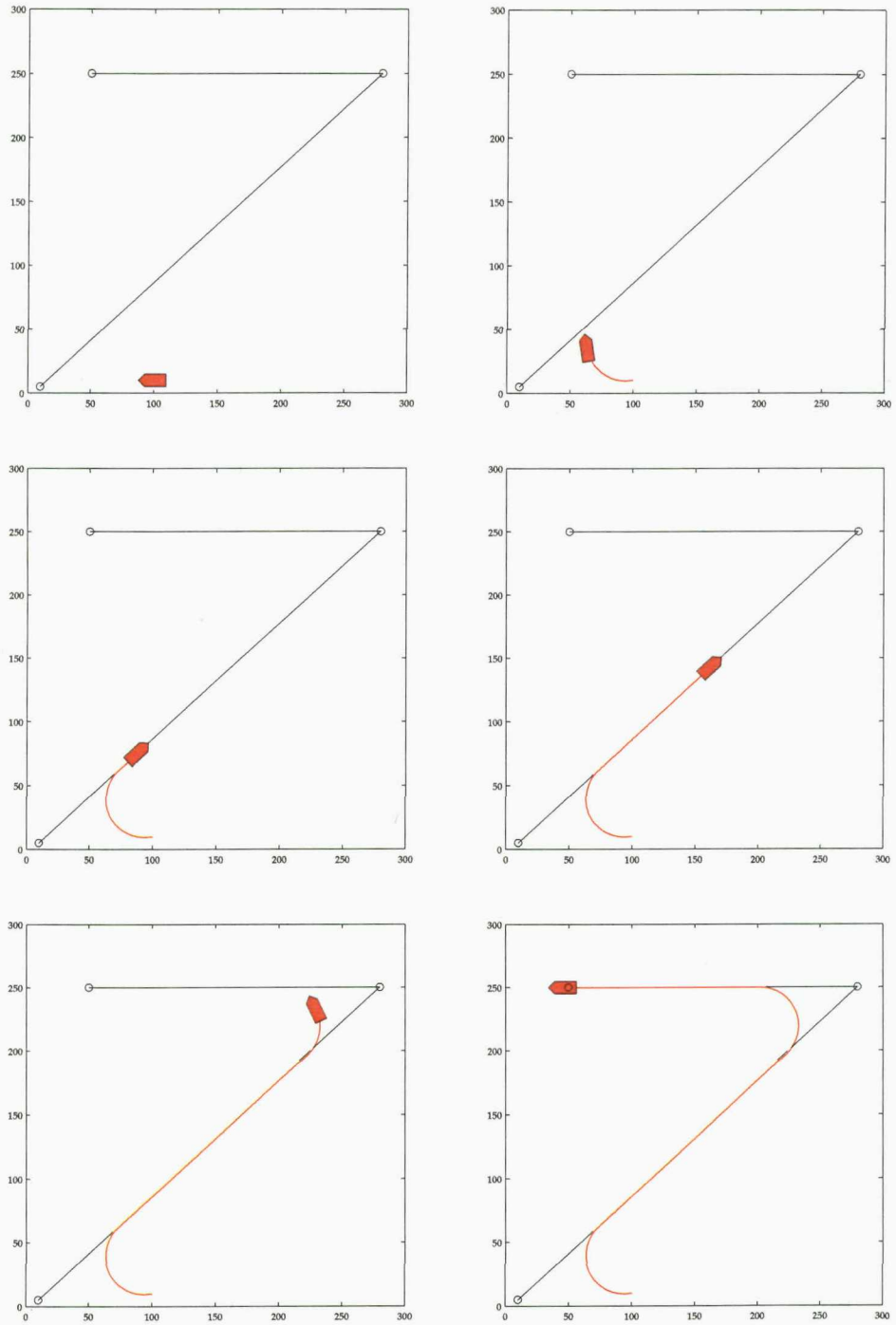

Figure 5.4: Snapshots of a path following three consecutive (denoted as ○) with a use of optimal waypoint guidance law and LOS technique in 2D. An AUV is moving with a constant speed at 1.3 m/s where the red line depicts the vehicle's moving path.

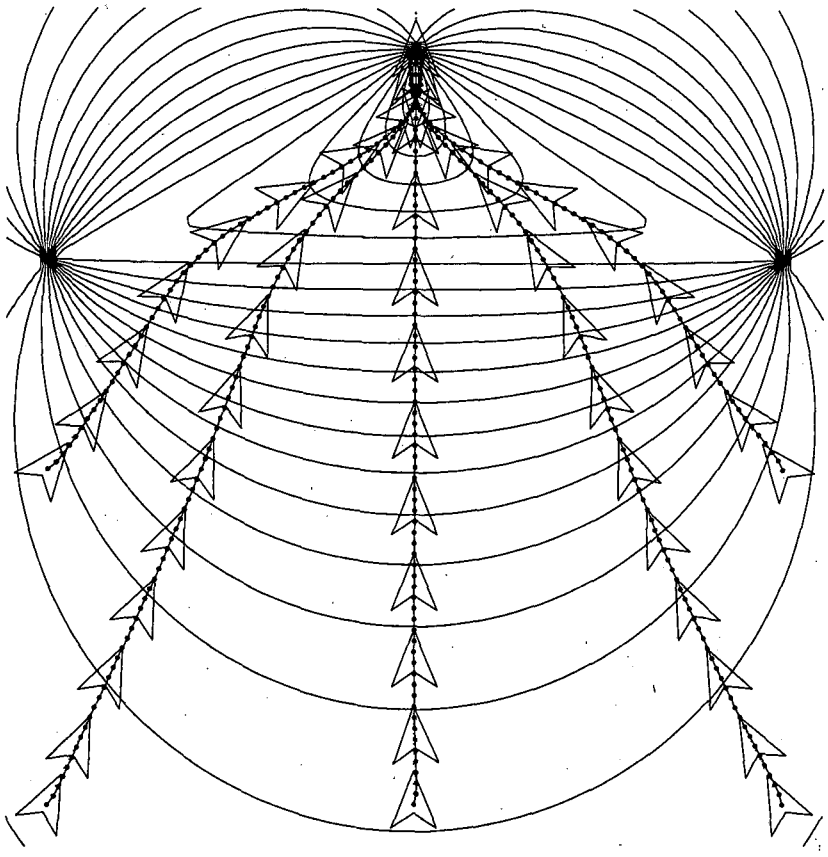

Figure 5.5: Simulations of path following using LOS guidance using an AUV model in potential distribution plots. Predefined trajectories are generated by a vector field technique with a constant weighted set $\varrho_1 = 0.8$, $\varrho_2 = 0.8$, $\varrho_3 = 0.5$. An AUV's speed is 1.3 m/s which each step of the motion is shown in $\cdot$. Sensor node 1 and 2 are represented as $\bullet$ on the left- and right-hand side, respectively whilst the centre $\bullet$ depicts the destination point.

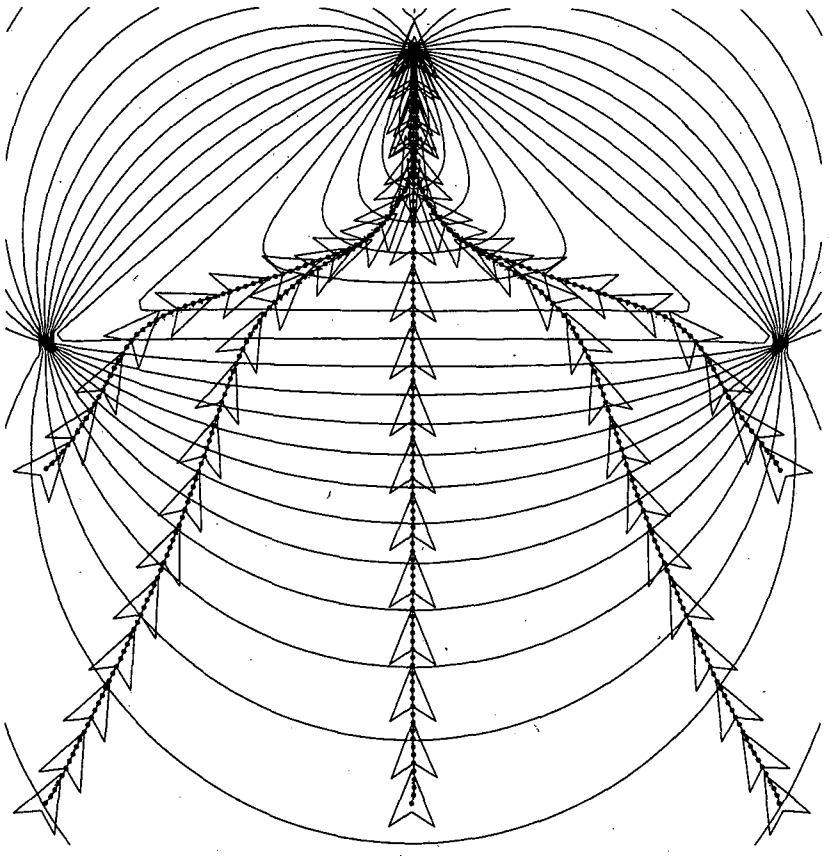

Figure 5.6: Simulations of path following using LOS guidance using an AUV model in potential distribution plots. Predefined trajectory is generated by switching weighted sets [0.8, 0.8, 1.5], [1, 1, 1.5]. An AUV's speed is 1.3 m/s which each step of the motion is shown in ·. Sensor node 1 and 2 are represented as • on the left- and right-hand side, respectively whilst the centre • depicts the destination point. The path generation using switching weighted sets allows an AUV to align with more proper orientation at the dock.

Table 5.3: Statistic results of position and orientation errors between the AUV and the dock in 3D during the docking preparation stage: an AUV is moving at a constant speed of 1.3 m/s.

Test	$\triangle x$ (cm)	$\triangle y$ (cm)	$\triangle z$ (cm)	$\triangle \psi$ (deg)	$\triangle \theta$ (deg)
1	-0.803	0.992	0.014	-2.429	-0.071
2	-0.571	0.540	0.037	-2.029	-0.183
3	0.571	0.530	0.044	2.037	-0.211
4	0.801	0.984	0.013	2.423	-0.054
5	-0.795	0.941	0.026	-2.460	-0.135
6	-0.565	0.510	0.068	-2.030	-0.341
7	0.567	0.501	0.079	2.044	-0.373
8	0.798	0.936	0.026	2.470	-0.108
9	-0.859	1.729	-0.010	-1.387	0.040
Mean	-0.095	0.851	0.033	-0.151	-0.160

Table 5.4: Statistic results of position and orientation errors between the AUV and the dock in 3D during the docking preparation stage: an AUV is moving with an initial speed of 1.3 m/s and converges to a final desired speed of 0.5 m/s.

Test	$\triangle x$ (cm)	$\triangle y$ (cm)	$\triangle z$ (cm)	$\triangle \psi$ (deg)	$\triangle \theta$ (deg)
1	-0.795	1.567	0.005	-3.105	-0.038
2	-0.590	1.184	0.015	-2.744	-0.120
3	0.563	0.676	0.020	3.116	-0.167
4	0.725	0.565	0.006	4.157	-0.045
5	-0.790	1.517	0.010	-3.174	-0.074
6	-0.587	1.156	0.028	-2.764	-0.224
7	0.558	0.647	0.036	3.109	-0.294
8	0.721	0.516	0.011	4.189	-0.087
9	-0.809	1.512	-0.002	-3.264	0.020
Mean	-0.112	1.038	0.014	-0.053	-0.114

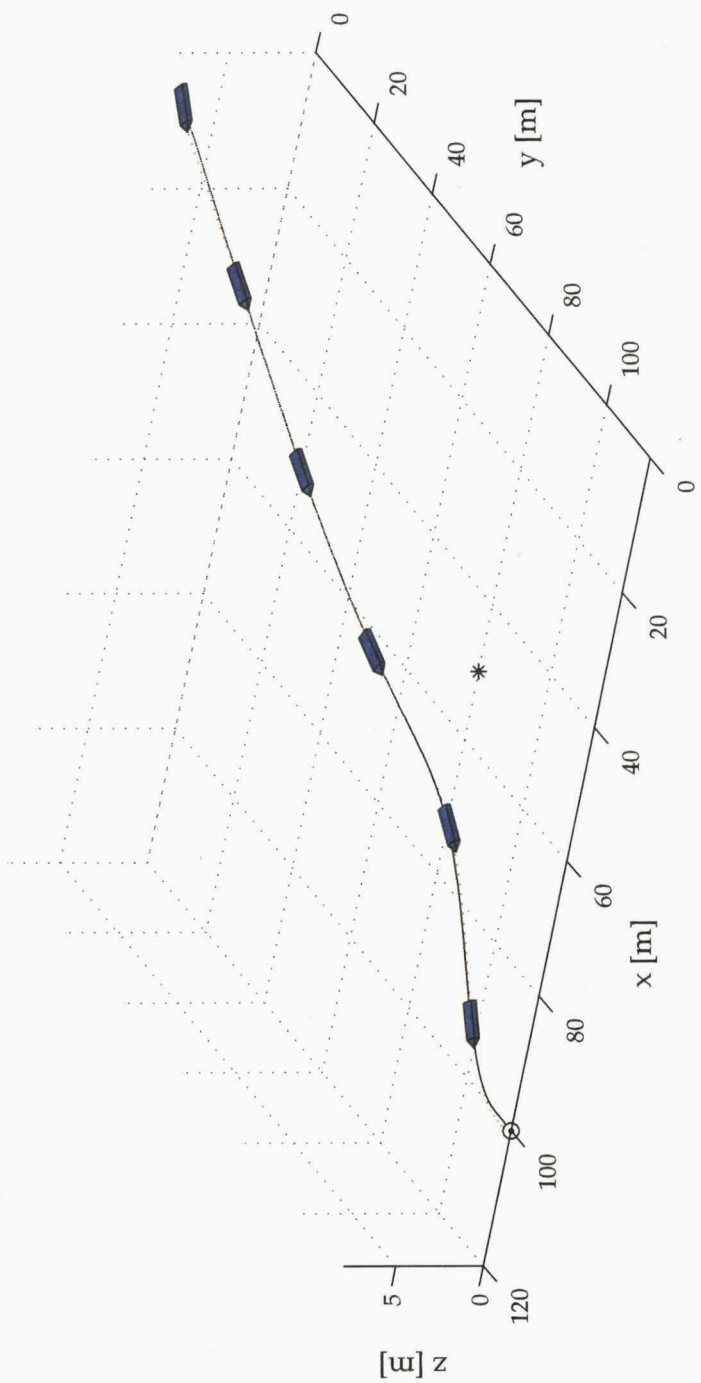

Figure 5.7: A vehicle is moving at a constant speed follows 3D path generated by using the vector field method. Locations of a dock and one of the sensor nodes are represented by ∘ and ∗, respectively. Black line and red dots depict the predefined path and the AUV's path, respectively.

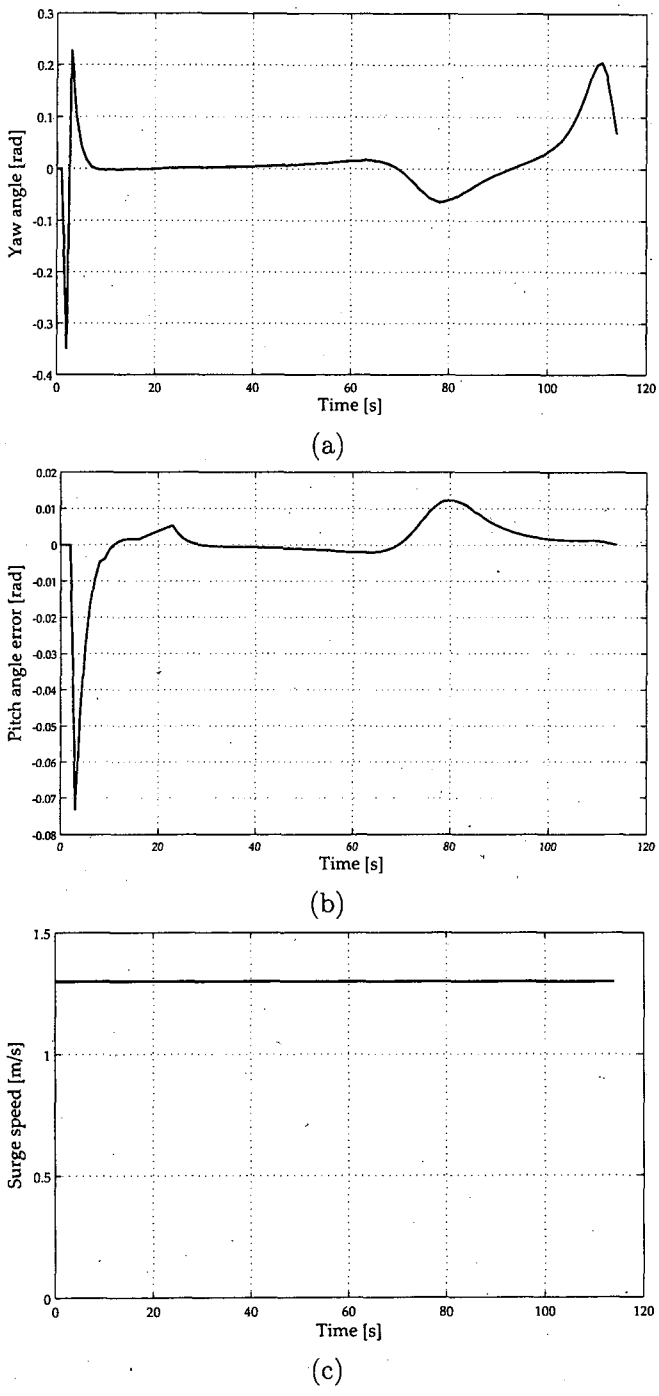

Figure 5.8: Errors in (a) yaw angle, (b) pitch angle and (c) surge velocity tracking comparison when an AUV moving at a constant speed of 1.3 m/s.

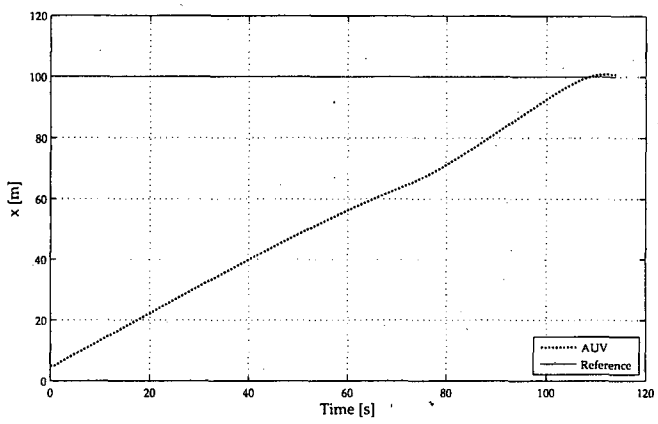

(a)

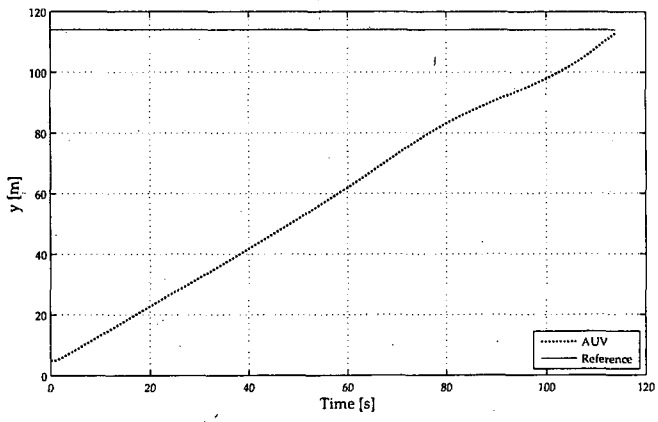

(b)

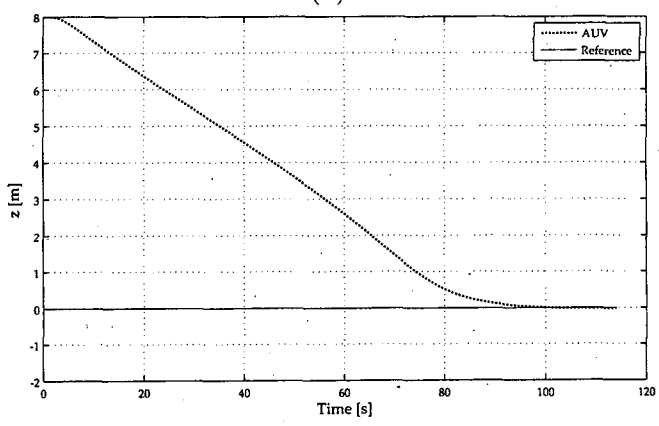

(c)

Figure 5.9: Errors along x-axis, y-axis and z-axis.

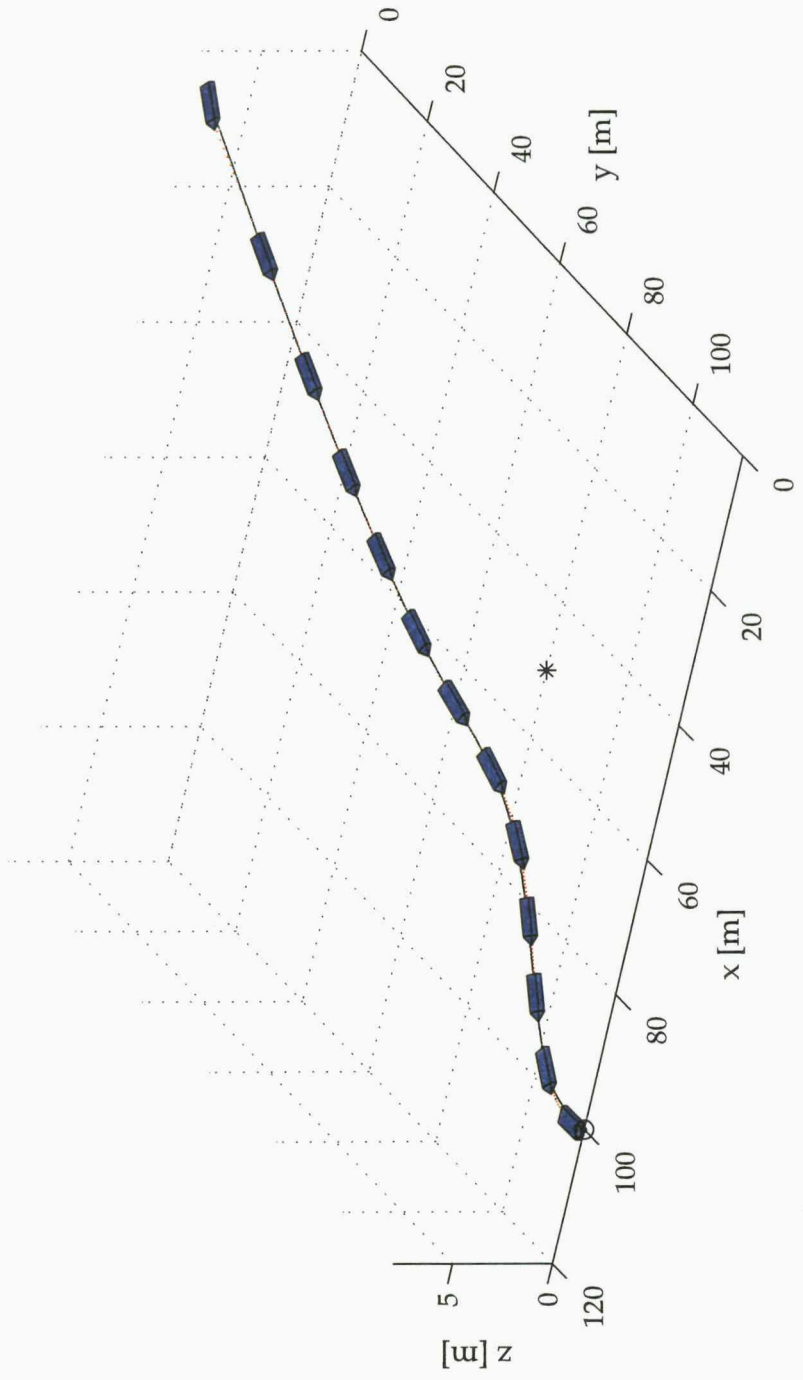

Figure 5.10: A vehicle is following 3D path generated by using the vector field method. The speed of an AUV converges from 1.3 m/s to a desired speed of 0.5 m/s. Locations of docking station and one of the sensor nodes are represented by ∘ and ∗, respectively. Black line and red dots depicts predefined path and AUV's path, respectively

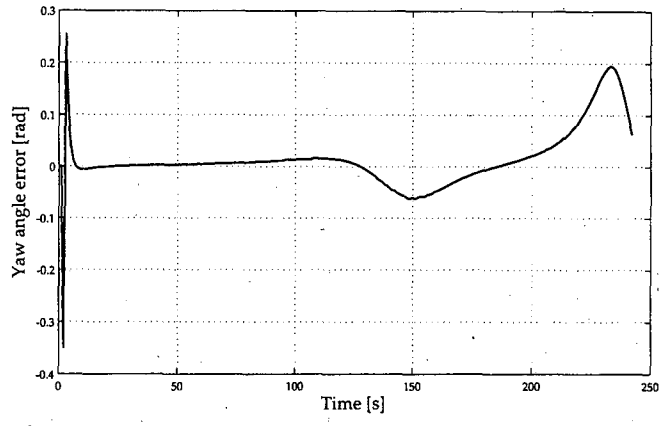

(a)

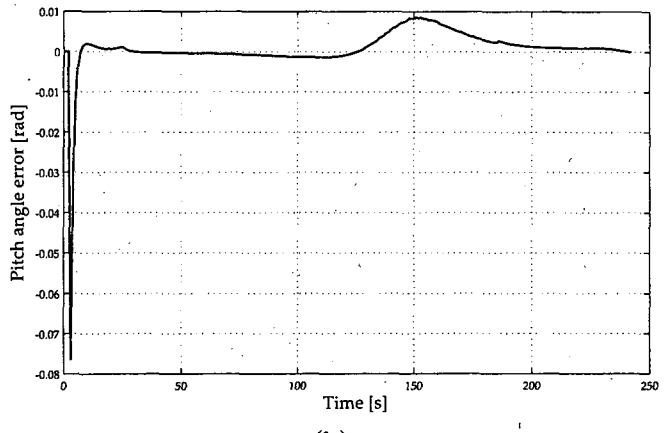

(b)

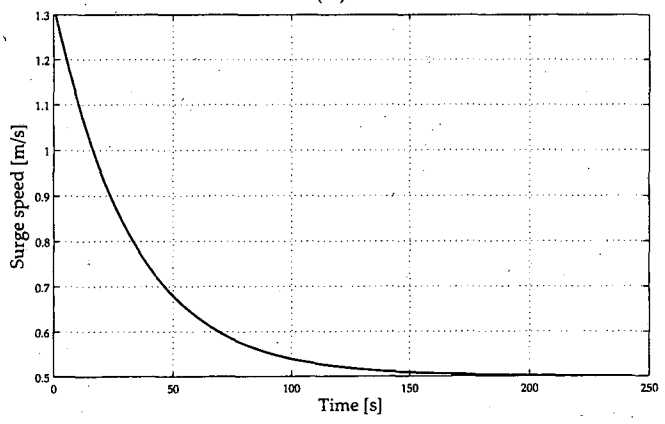

(c)

Figure 5.11: Errors in (a) yaw angle, (b) pitch angle and (c) surge velocity tracking comparison when an AUV is moving and converging to a desired speed of 0.5 m/s.

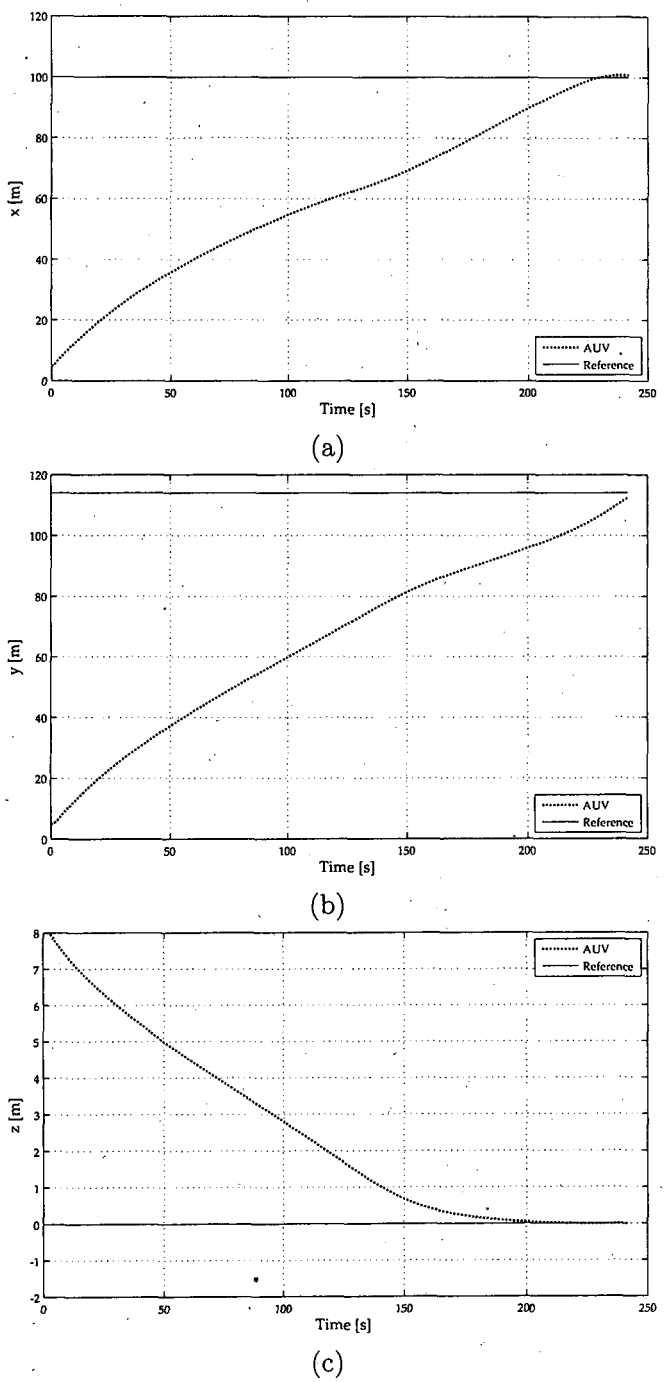

Figure 5.12: Errors along x-axis, y-axis and z-axis.

Chapter 6

Conclusion and Future Work

6.1 Conclusion

This thesis has studied several issues in robust and optimal control, path planning and path following for autonomous vehicles in long-term underwater application. At the beginning of this thesis, the subject of control techniques and its development is introduced and reviewed, following by the highlight of the research issues and research goals. The strategy is combined together such that the problems can be tackled. A comprehensive literature review of the development of control algorithm and advantages/disadvantages of the different control schemes developed for marine vehicles is studied. In addition, reviews of current research in motion planning, trajectory tracking and path following are briefly given in each chapter. Several problems in homing and docking are discussed. A mathematical model for kinematics and dynamics of a fully coupled six degrees of freedom of a marine vehicle is detailed and used through out the research. This was followed by three technical chapters, mainly focused on the development of the robust sliding mode control and its improvement with optimality, the strategy for homing and docking trajectory planning using the artificial potential

field method and the vector field technique, and the integrated system. The three main objectives have been achieved and can be summarised,

I. A design of decoupled subsystems using a standard sliding mode controller for an underwater vehicle is proposed. This is a general controller designed for a use of trajectory tracking problems. The second controller uses a high-order time derivative. The major advantage of the high-order sliding mode over the standard sliding mode controller is that it eliminates the chattering effects that would cause harm to mechanical parts of the vehicle. This is followed by the studies of optimal technique for the controllers. The proposed method uses a state-dependent Riccati equation for each subsystems. The most significant result was the solution for optimal control for the sliding mode. It is shown that the technique gives good performance results whilst keeping the main characteristics of the sliding mode with small chattering phenomenon.

II. This work considers a trajectory planning for a guidance system solving a docking problem in a marine vehicle. Whilst the conventional potential field allows the AUV to return to the home station, the extended work of the vector field method enables a system to generate a predefined trajectory required for docking manoeuvre. An enhanced method of weighted vector field and switching weighted vector field are introduced. They provide a smoother path for an AUV to achieve the desired docking station matching both position and orientation.

III. The final work presents a new guidance-control approach for homing and docking tasks. An integration of the Line-of-Sight guidance law and the sliding mode control law is proposed. The approach gives an AUV the ability to follow and converge to the predefined path with the following desired speed profiles whilst ensuring stability. Simulation results successfully demonstrate the capability of the proposed approach.

6.2 Recommendations for Future Work

This will be an active research in the field of underwater vehicle application in the future due to an increasing in a number of vehicles in education, commercial and military research. It is also observed that an increasing number of workshops and special sessions in major conferences in diverse areas. Whilst the proposed algorithm in this thesis could be immediately beneficial to AUVs, there are still improvements and extensions that can be made:

- The present approach did not consider the navigational system. Integration of the measurement model could lead to improved performance and made it usable in the real world.
- Real-time guidance and the navigation system for positions and attitude estimate would be possible for trajectory tracking in the real implementation.
- The proposed method could be used in other applications. For instance, the concept can be applied to an autonomous aerial refueling for unmanned vehicles. Rendezvous of multiple vehicles at space docking station are also considerable interest in this problem.

Bibliography

[1] A. P. Aguiar, "Nonlinear motion control of nonholonomic and underactuated systems," Ph.D. dissertation, Department of Electrical Engineering, Instituto Superior Técnico, Lisbon, Portugal, 2002.

[2] A. P. Aguiar and J. P. Hespanh, "Position tracking of underactuated vehicles," *Proceeding of American Control Conference*, pp. 1988–1993, 2003.

[3] M. Aicardi, G. Casalino, G. Indiveri, A. Aguiar, P. Encarnação, and A. Pascoal, "A planar path following controller for underactuated marine vehicles," *Proceeding of 9th IEEE Mediterranean Conference on Control and Automation*, 2001.

[4] J. Akhtman, M. Furlong, P. Jantapremjit, A. Palmer, A. Phillips, S. Sharkh, S. Turnock, and S. Veres, "Scotomas: University of southampton entry into the 2007 student autonomous underwater challenge - Europe," *The 9th Unmanned Underwater Vehicle Showcase (UUVS 2007)*, no. 10, 2007.

[5] F. Alonge, F. D'Ippolito, and F. M. Raimondi, "Trajectory tracking of underactuated underwater vehicles," *Proceedings of the 40th IEEE Conference on Decision and Control*, vol. 5, no. 4-7, pp. 4421–4426, 2001.

[6] G. Antonelli, *Underwater Robots: Motion and Force Control of Vehicle-Manipulator Systems*. Germany: Springer, 2003.

[7] G. Antonelli and S. Chaverini, "Adaptive tracking control of underwater vehicle-manipulator systems," *Proceedings of the IEEE International Conference on Control Applications*, pp. 1089–1093, 1998.

[8] Atlas Maridan, "Atlas Maridan product specification," 2001, available at http://www.maridan.dk/.

[9] A. Behal, D. M. Dawson, W. E. Dixon, and Y. Fang, "Tracking and regulation control of an underactuated surface vessel with nonintegrable dynamics," *IEEE Transactions on Automatic Control*, vol. 47, no. 3, pp. 495–500, 2002.

[10] A. Bogdanov, "Optimal control of a double inverted pendulum on a cart: report," December 2004, OGI School of Science and Engineering, Oregon Health and Science University, Beaverton, OR, USA.

[11] A. Bogdanov, E. Wan, and G. Harvey, "SDRE flight control for X-Cell and R-Max autonomous helicopters," *43rd IEEE Conference on Decision and Control*, vol. 2, pp. 1196–1203, 2004.

[12] E. Bøhaug, K. Y. Pettersen, and A. Pavlov, "An optimal guidance scheme for cross-track control of underactuated underwater vehicles," *Proceedings of 14th Mediterranean Conference on Control and Automation*, pp. 1–5, 2006.

[13] E. Bøhaug and K. Pettersen, "An optimal guidance scheme for cross-track control of underactuated underwater vehicles," *Proceedings of 44th IEEE Conference on Decision and Control, and the European Control Conference*, pp. 4028–4034, 2005.

[14] B. Borovic, O. Kuljaca, and F. Lewis, "Neural net underwater vehicle dynamic positioning control," *Proceedings of 9th Mediterranean Conference on Control and Automation*, 2001.

[15] D. M. Boskovic and M. Krstic, "Global attitude/position regulation for underwater vehicles," *International Journal of Systems Science*, vol. 30, no. 9, pp. 939–946, 1999.

[16] M. Breivik and T. I. Fossen, "Path following of straight lines and circles for marine surface vessels," *Proceedings of the 6th IFAC CAMS*, pp. 65–70, 2004.

[17] ——, "Principles of guidance-based path following," *Proceedings of the 4th IEEE Conference on Decision and Control and the European Control Conference*, pp. 627–634, 2005.

[18] ——, "A unified control concept for controlling a marine surface vessel through the entire speed envelop," *Proceedings of the 13th Mediterranean Conference on Control and Automation*, pp. 1518–1523, 2005.

[19] ——, "A unified control concept for autonomous underwater vehicles," *Proceedings of the 2006 American Control Conference*, pp. 4920–4926, 2006.

[20] H. Choset, K. Lynch, S. Hutchinson, G. Kantor, W. Burgard, and L. Kavraki, *Principles of Robot Motion: Theory, Algorithms and Implementation.* Massachusettes, USA: The MIT Press, 2005.

[21] J. R. Cloutier, "State-dependent Riccati equation techniques: An overview," *Proceedings of the 1997 American Control Conference*, vol. 2, pp. 932–936, 1997.

[22] S. Cowen, S. Briest, and J. Dombrowski, "Underwater docking of autonomous undersea vehicles using optical terminal guidance," *MTS/IEEE Conference Proceedings on Oceans*, vol. 2, pp. 1143–1147, 1997.

[23] J. J. Craig, *Introduction to robotics: mechanics and control.* MA, USA: Addison-Wesley.

[24] K. D. Do, Z. P. Jiang, and J. Pan, "Underactuated ship global tracking under relaxed conditions," *IEEE Transactions on Automatic Control*, vol. 47, pp. 1529–1536, 2002.

[25] ——, "A robust adaptive path following of underactuated ships," *Automatica*, no. 40, pp. 929–944, 2004.

[26] K. D. Do, Z. P. Jiang, J. Pan, and H. Nijmeijer, "A global output-feedback controller for stabilization and tracking of underactuated ODIN: A spherical underwater vehicle," *Automatica*, vol. 40, no. 1, pp. 117–124, 2004.

[27] K. D. Do and J. Pan, "Global tracking control of underactuated ships with off-diagonal terms," *Proceedings of the 42nd IEEE Conference an Decision and Control*, pp. 1250–1255, 2003.

[28] ——, "Underactuated ships follow smooth paths: Full state-feedback," *IEEE Conference on Decision and Control*, pp. 14–17, 2004.

[29] M. W. Dunnigan, D. M. Lane, A. C. Clegg, and I. Edwards, "Hybrid position/force control of a hydraulic underwater manipulator," *IEEE Proceedings Control Theory and Applications*, vol. 143, no. 2, pp. 145–151, 1996.

[30] M. W. Dunnigan and G. T. Russell, "Evaluation and reduction of the dynamic coupling between a remotely operated vehicle and a manipulator," *IEEE Journal of Oceanic Engineering*, vol. 3, no. 23, pp. 260–273, 1998.

[31] O. Egeland and J. T. Gravdahl, *Modeling and Simulation for Automatic Control.* Norway: Marine Cybernetics, 2002.

[32] P. Encarnação and A. Pascoal, "3D path following for autonomous underwater vehicle," *Proceedings of 39th IEEE Conference on Decision and Control*, 2000.

[33] ——, "Path following for autonomous marine craft," *Proceedings of MCMC'2000 - 5th IFAC Conference on Manoeuvring and Control of Marine Craft*, pp. 117–122, 2000.

[34] ——, "Path following for marine vehicles in the presence of unknown currents," *Proceedings of SYROCO'2000 - 6th International IFAC Symposium on Robot Control*, pp. 469–474, 2000.

[35] ——, "Combined trajectory tracking and path following control for dynamic wheeled mobile robots," *Proceedings of b'02 - 15th IFAC World Congress on Automatic Control*, 2002.

[36] J. C. Evans, K. M. Keller, J. S. Smith, P. Marty, and O. V. Rigaud, "Docking techniques and evaluation trials of the SWIMMER AUV: an autonomous deployment AUV for work-class ROVs," *MTS/IEEE Oceans Conference Proceedings*, vol. 1, pp. 520–528, 2001.

[37] M. Feezor, F. Sorrell, P. Blankinship, and J. Bellingham, "Autonomous underwater vehicle homing/docking via electromagnetic guidance," *MTS/IEEE Conference Proceedings on Oceans*, vol. 26, no. 4, pp. 547–555, 1997.

[38] X. Feng, B. Qiu, and D. Yun, "A graphic simulator for autonomous underwater vehicle docking operations," *Proceedings on Oceans Engineering for Today's Technology and Tomorrow's Preservation*, vol. 1, pp. 152–157, 1994.

[39] T. I. Fossen, *Guidance and Control of Ocean Vehicles.* England: John Wiley and Sons Ltd., 1994.

[40] T. I. Fossen and O. Fjellstad, "Robust adaptive control of underwater vehicles: A comparative study," *Proceeding of the 3rd IFAC Workshop on Control Applications in Marine Systems (CAMS'95)*, pp. 66–74, 1995.

[41] T. I. Fossen and O.-E. Fjellstad, "Nonlinear modelling of marine vehicles in 6 degrees of freedom," *International Journal of Mathematical Modelling of Systems*, 1995.

[42] T. I. Fossen and B. A. Foss, "Sliding control of MIMO nonlinear systems," *Proceedings of the European Control Conference*, pp. 1855–1860, 1991.

[43] T. I. Fossen and S. I. Sagatun, "Adaptive control of nonlinear systems: A case study of underwater robotic systems," *Journal of Robotic Systems*, vol. 8, no. 3, pp. 393–412, 1991.

[44] T. I. Fossen and J. P. Strand, "A tutorial on nonlinear backstepping: Applications to ship control," *Modeling, identification and control*, vol. 20, no. 2, pp. 83–135, 1999.

[45] E. Fredriksen and K. Pettersen, "Global κ-exponential way-point manoeuvring of ships," *Proceedings of IEEE Conference on Decision and Control*, pp. 5360–5367, 2004.

[46] D. Galzi and Y. Shtessel, "UAV formations control using high order sliding modes," *Proceeding of the 2006 American Control Conference*, pp. 4249–4254, 2006.

[47] C. Gaskett, D. Wettergreen, and A. Zelinsky, "Reinforcement learning applied to the control of an autonomous underwater vehicle," *Proceedings of Australian Conference on Robotics and Automation*, 1999.

[48] J. M. Godhavn, "Nonlinear tracking of underactuated surface vessels," *Proceedings of the 35th IEEE Decision and Control*, vol. 1, no. 11-13, pp. 975–980, 1996.

[49] K. R. Goheen and E. R. Jefferys, "Multivariable self-tuning autopilots for autonomous and remotely operated underwater vehicles," *IEEE Journal of Oceanic Engineering*, vol. 15, no. 3, pp. 144–151, 1990.

[50] D. E. Goldberg, *Genetic Algorithms in Search, Optimization, and Machine Learning.* Boston: Addision-Wesley, 1989.

[51] G. Griffiths, *Technology and Applications of Autonomous Underwater Vehicles.* London, UK: Taylor and Francis, 2003.

[52] G. Griffiths, N. W. Millard, S. D. McPhail, P. Stevenson, J. R. Perrett, M. Pebody, and A. Webb, "Towards environmental monitoring with the autosub autonomous underwater vehicle," *IEEE Underwater Technology '98: Towards environmental monitoring with the Autosub AUV*, 1998.

[53] M. Hagan and H. Demuth, "Neural networks for control," *Invited Tutorial, 1999 American Control Conference*, pp. 1642–1656, 1999.

[54] A. J. Healey and D. Lienard, "Multivariable sliding mode control for autonomous diving and steering of unmanned underwater vehicles," *IEEE Journal of Oceanic Engineering*, vol. 18, no. 3, pp. 327–339, 1993.

[55] R. G. Hutchins and J. P. C. Roque, "Filtering and control of an autonomous underwater vehicle for both target intercept and docking," *IEEE Proceedings Conference on Control Applications*, pp. 1162–1163, 1995.

[56] Hydroid, LLC, "Remus 6000," 2006, available at http://www.hydroidinc.com/ remus6000.html.

[57] G. Indiveri, "Modelling and identification of underwater robotic system," Ph.D. dissertation, University of Genova, Italy, 1998.

[58] M. Innocenti and G. Campa, "Robust control of underwater vehicles: sliding mode vs. LMI synthesis," *Proceedings of the American Control Conference*, vol. 5, pp. 3422–3426, 1999.

[59] B. Jalving, "The NDRE-AUV flight control system," *IEEE Journal of Oceanic Engineering*, vol. 19, no. 4, pp. 497–501, 1994.

[60] B. Jalving, K. Gade, O. K. Hagen, and K. Vestgard, "A toolbox of aiding techniques for the HUGIN AUV integrated inertial navigation system," *Proceedings of Oceans*, vol. 2, pp. 1146–1153, 2003.

[61] B. Jalving and N. Storkersen, "The control system of an autonomous underwater vehicle," *Proceedings of the Third IEEE Conference on Control Applications*, vol. 2, pp. 851–856, 1994.

[62] P. Jantapremjit and P. A. Wilson, "Control and guidance for homing and docking tasks using an autonomous underwater vehicle," *The 2007 IEEE/RSJ International Conference on Intelligent Robots and Systems*, pp. 3672–3677, 2007.

[63] ——, "Optimal control and guidance for homing and docking tasks using an autonomous underwater vehicle," *The 2007 IEEE International Conference on Mechatronics and Automation*, pp. 243–248, 2007.

[64] P. Jantapremjit, P. A. Wilson, and A. J. Murphy, "A study of autonomous docking with an AUV using intelligent control," *International Conference on Underwater System Technology: Theory and Applications*, pp. 12–16, 2006.

[65] Japan Marine Science and Technology Center, "Urashima specification," 1998, available at http://www.jamstec.go.jp/jamstec-e/PR/0012/1212/Ref1.pdf.

[66] H. P. Jiang, "Lyapunov design for global tracking of underactuated ships," *Proceedings of the 40th IEEE Conference on Decision and Control*, vol. 5, pp. 4210–4215, 2001.

[67] V. Kanakakis, K. P. Valavanis, and N. C. Tsourveloudis, "Fuzzy-logic based navigation of underwater vehicles," *Journal of Intelligent and Robotic Systems*, vol. 40, pp. 45–88, 2004.

[68] N. Kato and M. Endo; "Guidance and control of unmanned, untethered submersible for rendezvous and docking with underwater station," *Proceedings on Oceans '89*, vol. 3, pp. 804–809, 1989.

[69] O. Khatib, "Real-time obstacle avoidance for robot manipulator and mobile robots," *The International Journal of Robotics Research*, pp. 90–98, 1986.

[70] J. Kim, W. K. Chung, and J. Yuh, "Dynamic analysis and two-time scale control for underwater vehicle-manipulator systems," *IEEE/RSJ International Conference on Intelligent Robots and Systems*, pp. 577–582, 2003.

[71] J. Kim, K. Kim, H. S. Choi, W. Seong, and K. Y. Lee, "Estimation of hydrodynamic coefficients for an AUV using nonlinear observers," *IEEE Journal of Oceanic Engineering*, vol. 27, pp. 830–840, 2002.

[72] K. Kim and H. S. Choi, "Navigation and control for a test bed AUV-SNUUV I," *International Symposium on Underwater Technology*, pp. 89–94, 2004.

[73] Kokusai Cable Ship Co., Ltd, "The next-generation submersible robot explores a new era in oceanographic research and survey," 2001, available at http://www.k-kcs.jp/.

[74] I. Kolmanovsky and N. H. McClamroch, "Developments in nonholonomic control problems," *IEEE Control Systems Magazine*, vol. 15, no. 6, pp. 20–36, 1995.

[75] Kongsberg Maritime, "Autonomous underwater vehicle - Hugin 3000 AUV," 2000, available at http://www.km.kongsberg.com/.

[76] ——, "Transponder applications," 2007, available at http://www.km.kongsberg.com/.

[77] M. Krstić, I. Kanellakopoulos, and P. Kokotoić, *Nonlinear and Adaptive Control Design*. New York: John Wiley and Sons Inc., 1995.

[78] S. Laghrouche, M. Smaoui, and F. Plestan, "Robust second order sliding mode controller for electropneumatic actuator," *Proceeding of the 2004 American Control Conference*, pp. 5091–5095, 2004.

[79] S. Laghrouche, M. Smaoui, F. Plestan, and X. Brun, "Higher order sliding mode control based on optimal approach of an electropneumatic actuator," *International Journal of Control*, vol. 79, no. 2, pp. 119–131, 2006.

[80] D. Lambrinos, R. Moller, T. Labhart, R. Pfeifer, and R. Wehner, "A mobile robot employing insect strategies for navigation," *Robotics and Autonomous Systems*, pp. 39–64, 2000.

[81] L. Lapierre, P. Fraisse, and P. Dauchez, "Position/force control of an underwater mobile manipulator," *Journal of Robotic Systems*, vol. 20, no. 12, pp. 707–722, 2003.

[82] L. Lapierre, D. Soetanto, and A. Pascoal, "Nonlinear path following with application to the control of autonomous underwater vehicle," *Proceeding of the 42nd IEEE Conference on Decision and Control*, 2003.

[83] ——, "Nonlinear path following control of an AUV," *Elsevier Journal of the Oceanic Engineering*, 2006.

[84] J. Latombe, *Robot Motion Planning.* Boston, MA: Kluwer Academic Publishers, 1991.

[85] S. M. LaValle, *Planning Algorithms.* [Online], 1999-2003, available at http://msl.cs.uiuc.edu/planning/.

[86] S. M. LaValle and J. J. Kuffner, "Randomized kinodynamic planning," *Proceeding of the IEEE International Conference on Robotics and Automation*, pp. 473–479, 1999.

[87] R. K. Lea, R. Allen, and S. L. Merry, "A comparative study of control techniques for an underwater flight vehicle," *International Journal of System Science*, vol. 30, no. 9, pp. 947–964, 1999.

[88] M. Lee and H. S. Choi, "A robust neural controller for underwater robot manipulators," *IEEE Transactions on Neural Networks*, vol. 11, pp. 1465–1470, 2000.

[89] E. Lefeber, K. Y. Pettersen, and H. Nijmeijer, "Tracking control of an underactuated

ship," *IEEE Transactions on Control Systems Technology*, vol. 11, no. 1, pp. 52–61, 2003.

[90] D. J. Leith and W. E. Leithead, "Survey of gain-scheduling analysis and design," *International Journal of Control*, vol. 73, no. 11, pp. 1001–1025, 2001.

[91] A. Levant, "Higher-order sliding modes, differentiation and output-feedback control," *International Journal of Control*, vol. 76, no. 76, pp. 924–941, 2003.

[92] ——, "Quasi-continuous high-order sliding-mode controllers," *IEEE transactions on automatic control*, vol. 50, no. 11, pp. 1812–1816, 2005.

[93] A. Levant and L. Alelishvili, "Universal SISO sliding-mode controllers with finite-time convergence," *IEEE Transactions on Automatic Control*, 2001.

[94] E. Liceaga-Castro and G. M. van der Molen, "Submarine H∞ depth control under wave disturbances," *IEEE Transactions on Control Systems Technology*, vol. 3, pp. 338–346, 1995.

[95] C. L. Logan, "A comparison between H-infinity/Mu-synthesis control and sliding mode control for robust control of a small autonomous vehicle," *IEEE Proceedings of Symposium on Autonomous Underwater Vehicle Technology*, pp. 399–416, 1994.

[96] F. Mazenc, K. Y. Pettersen, and H. Nijmeijer, "Global uniform asymptotic stabilization of an underactuated surface vessel," *Proceedings of the 41st IEEE Conference on Decision and Control*, vol. 1, no. 1, pp. 510–515, 2002.

[97] E. W. McGookin, D. J. Murray-Smith, and Y. Li, "Submarine sliding mode controller optimisation using genetic algorithms," *UKACC International Conference on Control*, vol. 1, pp. 424–429, 1996.

[98] E. W. McGookin, D. J. Murray-Smith, Y. Li, and T. I. Fossen, "Non-linear tanker control system parameter optimisation using genetic algorithms," *IEEE/MTS Conference Proceedings on Oceans*, vol. 1, no. 1, pp. 17–22, 1997.

[99] ——, "Ship steering control system optimization using genetic algorithms," *Control Engineering Practice*, vol. 8, no. 4, pp. 429–443, 2000.

[100] S. D. McPhail, "Autosub-1 - an auv to demonstrate autonomous data gathering in the world's oceans," *Proceeding Colloquium on Autonomous underwater Vehicles and their sub-systems - recent developments and future prospects*, 1996.

[101] S. D. McPhail and M. Pebody, "Autosub-1 a distributed approach to navigation and control of an autonomous underwater vehicle," 1997, available at http://www.soc.soton.ac.uk/OTD/asub/papers/iee97p3.html.

[102] R. Moller, "Insect visual homing strategies in a robot with analog processing," *Biological Cybernetics*, pp. 231–243, 2000.

[103] R. Moller, D. Lambrinos, R. Pfeifer, and R. Wehner, "Insect strategies of visual homing in mobile robots," *Computer Vision and Mobile Robotics Workshop CVMR'98*, pp. 37–45, 1998.

[104] Monterey Bay Aquarium Research Institute, "Mapping vehicle specifications," 2008, available at http://www.mbari.org/auv/.

[105] W. Naeem, "Model predictive control of an autonomous underwater vehicle," *Proceedings of UKACC 2002 postgraduate symposium*, pp. 19–23, 2002.

[106] W. Naeem, R. Rutton, J. Chudley, F. R. Dalgleish, and S. Tetlow, "An online genetic algorithm based model predictive control autopilot design with experimental verification," *International Journal of Control*, vol. 14, no. 78, pp. 1076–1090, 2005.

[107] W. Naeem, R. Sutton, and S. M. Ahmad, "Pure pursuit guidance and model predictive control of an autonomous underwater vehicle for cable/pipeline tracking," *Presented in the World Maritime Technology Conference*, pp. 17–20, 2003.

[108] M. S. Naika and S. N. Singh, "State-dependent Riccati equation-based robust dive plane control of AUV with control constraints," *Ocean Engineering*, vol. 34, no. 11-12, pp. 1711–1723, 2007.

[109] Y. Nakamura and S. Savant, "Nonlinear tracking control of autonomous underwater vehicles," *Proceedings of IEEE International Conference on Robotics and Automation*, pp. 12–14, 1992.

[110] National institute of marine research, "Vehicle specifications," 2008, available at http://www.ifremer.fr/.

[111] D. R. Nelson, D. B. Barber, T. W. McLain, and R. W. Beard, "Vector field path following for miniature air vehicles," *IEEE Transactions on Robotics*, vol. 23, pp. 1552–3098, 2007.

[112] K. Ngo, R. R. Mahony, and Z.-P. Jiang, "Integrator backstepping design for motion systems with velocity constraint," *5th Asian Control Conference*, vol. 1, pp. 141–146, 2004.

[113] J. Osborne and R. Rysdyk, "Waypoint guidance for small UAVs in wind," 2005, available at http://www.aa.washington.edu/research/afsl/.

[114] K. Y. Pettersen and T. I. Fossen, "Underactuated dynamic positioning of a ship experimental results," *IEEE Transactions on Control Systems Technology*, vol. 1, no. 8, pp. 856–863, 2000.

[115] K. Y. Pettersen and E. Lefeber, "Way-point tracking control of ships," *Proceedings of the 40th IEEE Conference on Decision and Control*, vol. 1, pp. 940–945, 2001.

[116] C. Pêtrès, Y. Pailhas, P. Patrón, Y. Petillot, J. Evans, and D. Lane, "Path planning for autonomous underwater vehicles," *IEEE Transactions for Autonomous Underwater Vehicles*, vol. 23, pp. 311–341, 2007.

[117] G. J. S. Rae and S. M. Smith, "A fuzzy rule based docking procedure for autonomous underwater vehicles," *Proceedings on Oceans' Mastering the Oceans Through Technology*, vol. 2, pp. 539–546, 1992.

[118] W. Ren and R. W. Beard, "Constrained nonlinear tracking control for small fixed-wing unmanned air vehicles," *American Control Conference*, pp. 4663–4668, 2004.

[119] F. Repoulias and E. Papadopoulos, "Trajectory planning and tracking control of underactuated AUVs," *IEEE International Conference on Robotics and Automation (ICRA '05)*, pp. 1622–1627, 2005.

[120] E. Rimon and D. Koditschek, "Exact robot navigation using artificial potential functions," *IEEE Transactions on Robotics and Automation*, vol. 8, pp. 501–518, 1992.

[121] C. K. Ryoo, H. S. Shin, and M. J. Tahk, "Optimal waypoint guidance synthesis," *Proceedings of 2005 IEEE Conference on Control Applications*, pp. 1349–1354, 2005.

[122] J. H. Ryu and D. S. Kwon, "Control of underwater manipulators mounted on an ROV using base force information," *Proceedings of the IEEE International Conference on Robotics and Automation*, pp. 21–26, 2001.

[123] T. Salgado-Jimenez and B. Jouvencel, "Using a high order sliding modes for diving control a torpedo autonomous underwater vehicle," *Proceedings on Oceans*, vol. 2, pp. 22–26, 2003.

[124] ——, "Using a high order sliding modes for diving control a torpedo autonomous underwater vehicle," *Proceedings on Oceans*, vol. 2, pp. 934–939, 2003.

[125] C. Samson, "Path following and time-varying feedback stabilization of a wheeled mobile robot," *Proceeding of the 2nd International Conference on Automation, Robotics and Computer Vision*, 1992.

[126] N. Sarkar and T. K. Podder, "Coordinated motion planning and control of autonomous underwater vehicle-manipulator systems subject to drag optimization," *IEEE Journal of Oceanic Engineering*, vol. 26, no. 2, pp. 228–239, 2001.

[127] I. Schjølberg and T. I. Fossen, "Modelling and control of underwater vehicle-manipulator systems," *Proceeding of Conference Marine Craft Maneuvering and Control (Southampton, U.K.)*, pp. 45–57, 1994.

[128] C. J. Schumacher, G. C. Cottrill, and H. H. Yeh, "Optimal sliding mode flight control," *AIAA guidance navigation and control conference*, vol. 1, pp. 435–443, 1999.

[129] C. Silpa-Anan, "Autonomous underwater vehicle: Vision and control," Master's thesis, The Australian National University, Canberra, Australia, 2001.

[130] C. Silvestre, A. Aguiar, P. Oliveira, and A. Pascoal, "Control of the SIRENE underwater shuttle: system design and tests at sea," *International Conference on Offshore Mechanics and Arctic Engineering*, pp. 9–16, 1998.

[131] C. Silvestre, A. Pascoal, and I. Kaminer, "On the design of gain-scheduled trajectory tracking controller," *International Journal of robust and nonlinear control*, no. 12, pp. 797–839, 2002.

[132] H. Singh, S. Lerner, K. von der Heyt, and B. A. Moran, "An intelligent dock for an autonomous ocean sampling network," *IEEE Conference Proceedings on Oceanic Engineering Society*, vol. 3, pp. 1459–1562, 1998.

[133] R. Skjetne, "The maneuvering problem," Ph.D. dissertation, Norwegian University of Science and Technology, Dept. Eng. Cybernetics, Trondheim, Norway, 2005.

[134] R. Skjetne, T. I. Fossen, and P. V. Kokotović, "Robust output maneuvering for a class of nonlinear system," *Automatica*, no. 40, pp. 373–383, 2004.

[135] J. E. Slotine and W. Li, *Applied Nonlinear Control.* New Jersey: Prentice-Hall, Inc, 1991.

[136] D. A. Smallwood and L. L. Whitcomb, "Toward model based dynamic positioning of underwater robotic vehicles," *In Proceedings of IEEE/MTS Oceans'2000*, pp. 1106–1114.

[137] S. M. Smith, G. J. S. Rae, and D. T. Anderson, "Applications of fuzzy logic to the control of an autonomous underwater vehicle," *IEEE International Conference on Fuzzy Systems*, vol. 2, pp. 1099–1106, 1993.

[138] SNAME, "Nomenclature for testing the motion of a submerged body through a fluid: Technical and research bulletin," *The Society of Naval Architects and Marine Engineers*, no. 1-5, 1950.

[139] F. Song, E. An, and S. M. Smith, "Design robust nonlinear controllers for autonomous underwater vehicles with comparison of simulated and at-sea test data," *Journal of Vibration and Control*, vol. 8, no. 2, pp. 189–217, 2002.

[140] D. T. Stansbery and J. R. Cloutier, "Position and attitude control of a spacecraft using the state-dependent Riccati equation technique," *Proceedings of the 2000 American Control Conference*, vol. 3, pp. 1867–1871, 2000.

[141] Y. C. Sun and C. C. Cheah, "Adaptive setpoint control for autonomous underwater vehicles," *Proceedings of IEEE Conference on Decision and Control*, vol. 2, pp. 1262–1267, 2003.

[142] C. S. Tan, R. Sutton, and J. Chudley, "An incremental stochastic motion planning technique for autonomous underwater vehicles," *In Proceedings Control Applications in Marine Systems (CAMS'04)*, pp. 483–488, 2004.

[143] G. J. Toussaint, T. Basar, and F. Bullo, "Tracking for nonlinear underactuated surface vessels with generalized forces," *Proceedings of the 2000 IEEE International Conference on Control Applications*, pp. 355–360, 2000.

[144] P. Tsiotras, "New control laws for the attitude stabilization of rigid bodies," *IFAC Symposium on Automatic Control in Aerospace*, pp. 12–16, 1994.

[145] K. Ushera, M. Dunbabina, P. Corkea, and P. Ridleyb, "Sensing for visual homing," *Proceedings of the 2003 Australasian Conference on Robotics and Automation*, 2003.

[146] V. I. Utkin, *Sliding Modes and Their Application in Variable Structure Systems.* Moscow: MIR Publishers, 1978.

[147] G. R. Vossoughi, A. Meghdari, and H. Borhan, "Dynamic modeling and robust control of an underwater ROV equipped with a robot manipulator arm," *Proceedings of JUSFA Symposium on Flexible Automation*, pp. 19–21, 2004.

[148] C. Vuilmet, "High order sliding mode control applied to a heavyweight torpedo," *Proceedings of 2005 IEEE Conference on Control Applications*, pp. 61–66, 2005.

[149] K. Walchko, D. Novick, and M. Nechyba, "Development of a sliding mode control system with extended kalman filter estimation for subjugator," *Florida Conference on Recent Advances in Robotics*, 2003.

[150] R. Wei, R. Mahony, and D. Austin, "A bearing-only control law for stable docking of unicycles," *IEEE/RSJ International Conference on Intelligent Robots and Systems (IROS 2003)*, pp. 27–31, 2003.

[151] J. F. Wellicome, P. A. Wilson, and X. Cheng, "Prediction of the manoeuvring forces on a slender ship using slender body theory. Part II towing tank tests using planar motion mechanism," *Ship Science Reports, University of Southampton, Southampton, UK*, p. 112, 1995.

[152] D. Wettergreen, C. Gaskett, and A. Zelinsky, "Autonomous guidance and control for an underwater robotic vehicle," *Proceedings of the International Conference on Field and Service Robotics*, 1999.

[153] K. A. White, S. M. Smith, K. Ganesan, D. Kronen, G. J. S. Rae, and R. M. Langenbach, "Performance results of a fuzzy behavioral altitude flight controller and rendezvous and docking of an autonomous underwater vehicles with fuzzy control," *Proceedings of the 1996 Symposium on Autonomous Underwater Vehicle Technology*, vol. 3, pp. 117–124, 1996.

[154] D. Whitley, "An overview of evolutionary algorithms," *Journal of Information and Software Technology*, no. 43, pp. 817–831, 2001.

[155] K. Y. Wichlund, O. J. Sordalen, and O. Egeland, "Control properties of underactuated vehicles," *Proceedings of IEEE International Conference on Robotics and Automation*, vol. 2, no. 2, pp. 2009–2014, 1995.

[156] A. Witkowska, M. Tomera, and R. Smierzchalski, "A backstepping approach to ship course control," *International Journal of Applied Mathematics and Computer Science*, vol. 17, pp. 73–86, 2007.

[157] I. Yamamoto, T. Aoki, S. Tsukioka, H. Yoshida, T. Hyakudome, T. Sawa, S. Ishibashi, T. Inada, K. Yokoyama, T: Maeda, S. Ishiguro, H. Hirayama, K. Hirokawa, A. Hashimoto, N. Hisatome, and T. Tani, "Fuel cell system of AUV 'Urashima'," *Oceans '04 MTS/IEEE Techno-Ocean*, pp. 1732–1737, 2004.

[158] D. R. Yoerger and J. E. Slotine, "Robust trajectory control of underwater vehicles," *IEEE Journal of Oceanic Engineering*, vol. 10, no. 4, pp. 462–470, 1985.

[159] G. R. Yu and H. T. Liu, "Sliding mode control of a two-degree-of-freedom helicopter via linear quadratic regulator," *IEEE International Conference on Systems, Man and Cybernetics*, vol. 4, pp. 3299–3304, 2005.

[160] J. Yuh, "Design and control of autonomous underwater robots: A survey," *Autonomous Robots*, vol. 8, pp. 7–24, 2000.

[161] J. Yuh, N. Jing, and C. Lee, "Experimental study on adaptive control of underwater robots," *Proceedings of IEEE International Conference on Robotics and Automation*, vol. 1, pp. 393–398, 1999.

[162] X. Yun and K.-C. Tan, "A wall-following method for escaping local minima in potential field based motion planning," *Proceedings of the International Conference on Advanced Robotics*, pp. 421–426, 1997.

[163] U. R. Zimmer, "The serafina project," 2005, available at http://users.rsise.anu.edu.au/serafina/.

Appendix A

Kinematic Modelling

This appendix presents the state representation of AUV kinematics, and the mathematical modelling of dynamics of the motion. The geographical reference frames that are used to describe and analyse the motion of a marine vehicle are introduced. The following parts introduce a fundamental of dynamics, reported from [39]. Two important topics are considered:

- Kinematics: It concerns the motion of an object without being concerned with the forces that cause the motion. It is possible to translate and rotate a rigid body between different frames of reference. Fundamentally kinematics is purely concerned with the geometrical aspects of motion.

- Rigid-body dynamics and mechanics: It mathematically describes the effects of external forces and moments on the motion of an object. Based on energy conservation methods or the laws of physics as derived by Newton, dynamical models can be constructed and described object's motion in space. These models play a vital rôle for simulation of motion and design of control algorithms. Fundamentally two main formulations for obtaining such dynamical

models, namely the Lagrangian formulation and the Newton-Euler formulation are widely applied in the literatures.

A.1 Notation

In this section, a common notion for an underwater vehicle is given and used throughout this report. It can be found in [39]. A summary of the notion which describes the fully coupled six degrees of freedom for an underwater vehicle is given in table A.1

Table A.1: Notation used for an underwater vehicle

DOF	Motion	Forces and Moments	Linear and Angular Velocity	Position/ Euler Angles
1	Surge	X	u	x
2	Sway	Y	v	y
3	Heave	Z	w	z
4	Roll	K	p	ϕ
5	Pitch	M	q	θ
6	Yaw	N	r	ψ

A.2 Transformation

Reference frames for modelling an AUV are defined in this section, followed by transformation formulas for vectors in different reference frames. The notation for reference frames and vectors, and transformation matrices follow those used by the communities. Figure A.1 depicts six components of different motions for an underwater vehicle.

A.2.1 Reference Frames

- **NED** : The North-East-Down coordinate system is a local reference frame defined relative to the Earth's reference ellipsoid. The frame is defined as the tangent plane that has its origin at some point on the Earth's surface, where

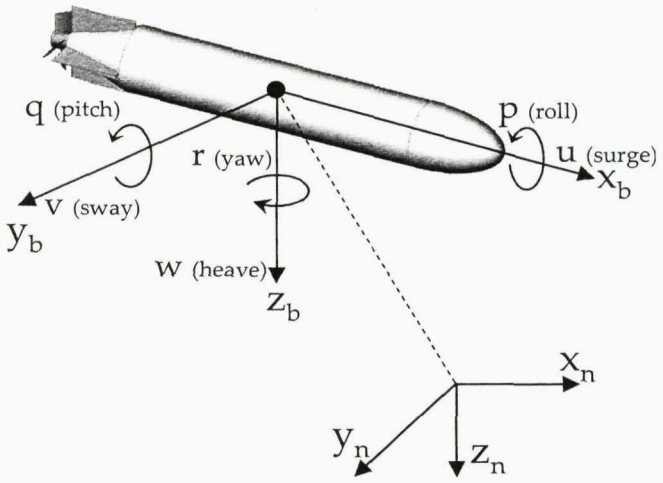

Figure A.1: Six degrees of freedom of an AUV in surge, sway, heave, roll, pitch, and yaw motion.

the x-axis pointing towards through North, the y-axis towards East and the z-axis downwards normal to the Earth's surface. The **NED** is represented with $[x_n, y_n, z_n]^\mathsf{T}$.

- **BODY** : The body-fixed reference frame is fixed to the vehicle under consideration. For a marine vehicle, the body axes are chosen to coincide with the principal axes of inertia. Thus, the x-axis is longitudinal (from stern to bow) and the y-axis transversal (from port to starboard). The z-axis points downwards, orthogonal to the plane spanned by the x- and y-axes in accordance with the convention set by the **NED** frame. The **BODY** is represented with $[x_b, y_b, z_b]^\mathsf{T}$.

A.2.2 Euler Angles

A common representation of attitude for 6-DOFs AUV is defined in term of a set of Euler angles using the z-y-x Euler angles [23]. Define ψ, θ, ϕ to be the rotation angles around the z, y and x respectively. A rotation matrix $\boldsymbol{R}_b^n \in \mathbb{R}^{3\times3}$ related to

the **BODY** and **NED** coordinate systems, is described as following,

$$\boldsymbol{R}_b^n = \boldsymbol{R}_z(\psi)\boldsymbol{R}_y(\theta)\boldsymbol{R}_x(\phi), \tag{A.1}$$

where,

$$\boldsymbol{R}_z(\psi) = \begin{bmatrix} c\psi & -s\psi & 0 \\ s\psi & c\psi & 0 \\ 0 & 0 & 1 \end{bmatrix}; \boldsymbol{R}_y(\theta) = \begin{bmatrix} c\theta & 0 & s\theta \\ 0 & 1 & 0 \\ -s\theta & 0 & c\theta \end{bmatrix}; \boldsymbol{R}_x(\phi) = \begin{bmatrix} 1 & 0 & 0 \\ 0 & c\phi & -s\phi \\ 0 & s\phi & c\phi \end{bmatrix}$$

therefore

$$\boldsymbol{R}_b^n = \begin{bmatrix} c\psi c\theta & c\psi s\theta s\phi - s\psi c\phi & c\psi c\phi s\theta + s\psi s\phi \\ s\psi c\theta & s\phi s\theta s\psi + c\psi c\phi & s\theta s\psi c\phi - c\psi s\phi \\ -s\theta & c\theta s\phi & c\theta c\phi \end{bmatrix}. \tag{A.2}$$

where $c\alpha = \cos\alpha$ and $s\alpha = \sin\alpha$, etc.

The rotation matrix has some useful properties,

- $\|\boldsymbol{R}\| = 1$,
- $\boldsymbol{R}\boldsymbol{R}^\mathsf{T} = \boldsymbol{R}^\mathsf{T}\boldsymbol{R} = \boldsymbol{I}$, which implies that $\boldsymbol{R}$ is orthogonal, thus the inverse rotation is given by, $\boldsymbol{R}^{-1} = \boldsymbol{R}^\mathsf{T}$,
- $\dot{\boldsymbol{R}} = \boldsymbol{R}\boldsymbol{S}(\omega)$, where $\boldsymbol{S}(\omega)$ is the skew-symmetrical matrix given as,

$$\boldsymbol{S}(\omega) = \begin{bmatrix} 0 & -r & q \\ r & 0 & p \\ -q & p & 0 \end{bmatrix}. \tag{A.3}$$

A.3 Kinematic Modelling

This section derives the kinematics equations of motion, and followed by the dynamic modelling of a marine vehicle. Let $\boldsymbol{\nu} \in \mathbb{R}^{6\times1}$ be the vector of the linear and angular velocity of a vehicle in the body-fixed frame and $\boldsymbol{\eta} \in \mathbb{R}^{6\times1}$ be the vector of position and attitude of a vehicle in the inertial frame,

$$\boldsymbol{\nu} = [\boldsymbol{\nu}_1, \boldsymbol{\nu}_2]^\mathsf{T} = [u, v, w, p, q, r]^\mathsf{T}, \tag{A.4}$$

$$\eta = [\eta_1, \eta_2]^\mathsf{T} = [x, y, z, \phi, \theta, \psi]^\mathsf{T}, \tag{A.5}$$

The Euler angle transformation of the vehicle between body-fixed frame and earth-fixed frame can be described as,

$$\dot{\eta} = \boldsymbol{J}(\Theta)\nu = \begin{bmatrix} \boldsymbol{R}(\Theta) & \mathbf{0} \\ \mathbf{0} & \boldsymbol{T}(\Theta) \end{bmatrix} \begin{bmatrix} \nu_1 \\ \nu_2 \end{bmatrix}, \tag{A.6}$$

for linear velocity, the transformation (equation (A.2)) is,

$$\boldsymbol{R}(\Theta) = \begin{bmatrix} c\psi c\theta & c\psi s\theta s\phi - s\psi c\phi & c\psi c\phi s\theta + s\psi s\phi \\ s\psi c\theta & s\phi s\theta s\psi + c\psi c\phi & s\theta s\psi c\phi - c\psi s\phi \\ -s\theta & c\theta s\phi & c\theta c\phi \end{bmatrix}, \tag{A.7}$$

for angular velocity, the transformation is derived,

$$\nu_2 = \begin{bmatrix} \dot{\phi} \\ 0 \\ 0 \end{bmatrix} + \boldsymbol{R}_x(\phi) \begin{bmatrix} 0 \\ \dot{\theta} \\ 1 \end{bmatrix} + \boldsymbol{R}_x(\phi)\boldsymbol{R}_y(\theta) \begin{bmatrix} 0 \\ 0 \\ \dot{\psi} \end{bmatrix} = \boldsymbol{T}^{-1}(\Theta)\dot{\eta}, \tag{A.8}$$

consequently,

$$\boldsymbol{T}(\Theta) = \begin{bmatrix} 1 & s\phi t\theta & c\phi t\theta \\ 0 & c\phi & -s\phi \\ 0 & s\phi/c\theta & c\phi/c\theta \end{bmatrix}. \tag{A.9}$$

where $c\psi = \cos\psi$ and $s\phi = \sin\phi$, $t\theta = \tan\theta$. From equation (A.9) , it is underline when $-\pi < \phi < \pi$, $-\frac{\pi}{2} < \theta < \frac{\pi}{2}$ and $0 < \psi < 2\pi$. This results in a singularity free in the system's kinematics.

Appendix B

Dynamic Modelling

The system's dynamics of an underwater vehicle are highly nonlinear, coupled and time varying which come from many parameters, such as hydrodynamic drag, damping and lift forces, Coriolis and centripetal forces, gravity and buoyancy forces and forces from thrusters. There are several dynamic models and system identifications have been proposed by various researches [39], [57], [129], [138].

B.1 Lagrange Equation

Dynamic model can be derived from the Lagrangian equation of motion of a vehicle in fluid. Consider a system with kinetic and potential energy, defined as $\mathcal{P}$ and $\mathcal{K}$, respectively. Let $\vec{q}$ be the vector of generalised coordinates and be $\vec{\mathcal{F}}$ the generalised force vector. Therefore the Lagrange's equation is basically of the from,

$$\frac{d}{dt}(\frac{\partial \mathcal{P}}{\partial \dot{\vec{q}}}) - (\frac{\partial \mathcal{P}}{\partial \vec{q}}) + (\frac{\partial \mathcal{K}}{\partial \vec{q}}) = \vec{\mathcal{F}}, \tag{B.1}$$

Consider the linear and angular velocity of a vehicle, $\boldsymbol{\nu} = [\boldsymbol{\nu}_1^\intercal, \boldsymbol{\nu}_2^\intercal]^\intercal$ thus the kinetic

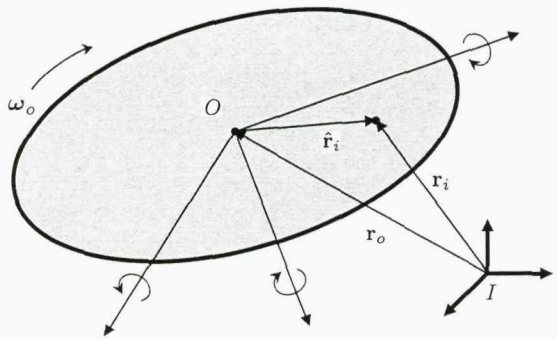

Figure B.1: A rigid body representation of an underwater vehicle [39].

energy of the vehicle is given as,

$$\mathcal{P} = \frac{1}{2}\boldsymbol{\nu}^{\top}\boldsymbol{M}\boldsymbol{\nu}, \tag{B.2}$$

The Kirchhoff's equations of motion for a vehicle can be expressed as,

$$\frac{d}{dt}(\frac{\partial \mathcal{P}}{\partial \boldsymbol{\nu}_1}) + \boldsymbol{\nu}_2 \times \frac{\partial \mathcal{P}}{\partial \boldsymbol{\nu}_1} = \boldsymbol{\tau}_1,$$

$$\frac{d}{dt}(\frac{\partial \mathcal{T}}{\partial \boldsymbol{\nu}_2}) + \boldsymbol{\nu}_2 \times \frac{\partial \mathcal{T}}{\partial \boldsymbol{\nu}_2} + \boldsymbol{\nu}_1 \times \frac{\partial \mathcal{P}}{\partial \boldsymbol{\nu}_1} = \boldsymbol{\tau}_2,$$

In general, the equation of motion of the vehicle in the body-fixed reference frame is written in a compact form as,

$$\boldsymbol{M}\dot{\boldsymbol{\nu}} + \boldsymbol{C}(\boldsymbol{\nu})\boldsymbol{\nu} + \boldsymbol{D}(\boldsymbol{\nu})\boldsymbol{\nu} + \boldsymbol{g}(\boldsymbol{\eta}) = \boldsymbol{\tau}. \tag{B.3}$$

where $\boldsymbol{M} \in \mathbb{R}^{6\times6}$ is an inertia matrix, $\boldsymbol{C}(\boldsymbol{\nu})) \in \mathbb{R}^{6\times6}$ is a matrix of Coriolis and centripetal terms, $\boldsymbol{D}(\boldsymbol{\nu}) \in \mathbb{R}^{6\times6}$ is a hydrodynamic damping and lift matrix, $\boldsymbol{g}(\boldsymbol{\eta}) \in \mathbb{R}^{6\times1}$ is a gravitational and buoyancy force and moment vectors of a vehicle, $\boldsymbol{\tau} \in \mathbb{R}^{6\times1}$ is an external force and moment input. The motion of a 6-DOFs underwater vehicle with respect to the body-fixed frame (see figure B.1) can be derived from the Newtonian formulation [39], [41],

$$m(\dot{\boldsymbol{\nu}}_1 + \boldsymbol{\nu}_2 \times \boldsymbol{\nu}_1 + \dot{\boldsymbol{\nu}}_2 \times \hat{\mathbf{r}}_i + \boldsymbol{\nu}_2 \times (\boldsymbol{\nu}_2 \times \hat{\mathbf{r}}_i)) = \boldsymbol{\tau}_1,$$

$$\boldsymbol{I}_o\dot{\boldsymbol{\nu}}_2 + \boldsymbol{\nu}_2 \times \boldsymbol{I}_o\boldsymbol{\nu}_2 + m\hat{\mathbf{r}}_i \times (\dot{\boldsymbol{\nu}}_1 + \boldsymbol{\nu}_2 \times \boldsymbol{\nu}_1) = \boldsymbol{\tau}_2,$$

where $\hat{\mathbf{r}}_i = [x, y, z]$ is the centroid and the rigid body inertia matrix $\boldsymbol{I}_o$ corresponding to the body-fixed coordinate frame with origin O, that is,

$$\boldsymbol{I}_o = \begin{bmatrix} I_{xx} & -I_{xy} & -I_{xz} \\ -I_{yx} & I_{yy} & -I_{yz} \\ -I_{zx} & -I_{zy} & I_{zz} \end{bmatrix}$$

for the rigid body, the equation of motion of the vehicle can be written as,

$$\boldsymbol{M}_{RB}\dot{\boldsymbol{\nu}} + \boldsymbol{C}_{RB}(\boldsymbol{\nu})\boldsymbol{\nu} = \boldsymbol{\tau}_{RB}. \tag{B.4}$$

From equation (B.4), the rigid body inertia matrix $\mathbf{M}_{RB}\dot{\boldsymbol{\nu}}$ can be written as,

$$\boldsymbol{M}_{RB}\boldsymbol{\nu} = \begin{bmatrix} m\dot{\boldsymbol{\nu}}_1 + m\dot{\boldsymbol{\nu}}_2 \times \hat{\mathbf{r}}_i \\ \boldsymbol{I}_o\dot{\boldsymbol{\nu}}_2 + m\hat{\mathbf{r}}_i \times \dot{\boldsymbol{\nu}}_1 \end{bmatrix}, \tag{B.5}$$

this yields,

$$\boldsymbol{M}_{RB} = \begin{bmatrix} m & 0 & 0 & 0 & -mz_g & -my_g \\ 0 & m & 0 & -mz_g & 0 & mx_g \\ 0 & 0 & m & my_g & -mx_g & 0 \\ 0 & -mz_g & -my_g & I_{xx} & -I_{xy} & -I_{xz} \\ mz_g & 0 & -mx_g & -I_{xy} & I_{yy} & -I_{yz} \\ -my_g & mx_g & 0 & -I_{xz} & -I_{yz} & I_{zz} \end{bmatrix} \equiv \begin{bmatrix} m\boldsymbol{I}_{3\times 3} & -m\boldsymbol{S}(\hat{\mathbf{r}}_i) \\ m\boldsymbol{S}(\hat{\mathbf{r}}_i) & \boldsymbol{I}_o \end{bmatrix}, \tag{B.6}$$

and an operator $\boldsymbol{S}(\cdot)$ is skew-symmetric matrix defined in equation A.3. Referred to [1] and [39], the important property of the M-matrix is,

$$\boldsymbol{M} = \boldsymbol{M}^{\mathsf{T}} > 0; \qquad \dot{\boldsymbol{M}} = 0. \tag{B.7}$$

Thus, the Coriolis and centripetal matrix, $\boldsymbol{C}_{RB}(\boldsymbol{\nu})\boldsymbol{\nu}$ in equation (B.4) can be expressed such that $\boldsymbol{C}(\boldsymbol{\nu}) = -\boldsymbol{C}^{\mathsf{T}}(\boldsymbol{\nu})$ as,

$$\boldsymbol{C}_{RB}(\boldsymbol{\nu})\boldsymbol{\nu} = \begin{bmatrix} m\boldsymbol{\nu}_2 \times \boldsymbol{\nu}_1 + m\boldsymbol{\nu}_2 \times (\boldsymbol{\nu}_2 \times \hat{\mathbf{r}}_i) \\ \boldsymbol{\nu}_2 \times \boldsymbol{I}_o\boldsymbol{\nu}_2 + m\hat{\mathbf{r}}_i \times (\boldsymbol{\nu}_2 \times \boldsymbol{\nu}_1) \end{bmatrix}, \tag{B.8}$$

this yields,

$$
\begin{aligned}
\boldsymbol{C}_{RB}(\boldsymbol{\nu}) &= \begin{bmatrix}
0 & 0 & 0 \\
0 & 0 & 0 \\
0 & 0 & 0 \\
m(y_g q + z_g r) & m(z_g q - w) & -m(x_g r + v) \\
-m(z_g q - w) & -m(z_g r + x_g p) & m(y_g r - u) \\
-m(z_g p - v) & m(z_g q + u) & -m(x_g r + y_g q)
\end{bmatrix} \\
&\quad \begin{bmatrix}
m(y_g q + z_g r) & -m(z_g q - w) & m(x_g r + v) \\
-m(y_g p - w) & m(z_g r + x_g p) & -m(y_g r - u) \\
-m(z_g p - v) & -m(z_g q + u) & m(x_g r + y_g q) \\
0 & -I_{yz} q + I_{xz} p + I_{zz} r & I_{yz} r + I_{xy} p - I_{yy} q \\
I_{yz} q + I_{xz} p - I_{zz} r & 0 & -I_{xz} r - I_{xy} q + I_{xx} q \\
-I_{yz} r - I_{xy} p - I_{yy} q & I_{xz} r + I_{xy} q - I_{xx} q & 0
\end{bmatrix} \\
&\equiv \begin{bmatrix}
\mathbf{0}_{3\times 3} & \boldsymbol{C}_{11}(\boldsymbol{\nu}) \\
-\boldsymbol{C}_{12}^{\mathsf{T}}(\boldsymbol{\nu}) & \boldsymbol{C}_{22}(\boldsymbol{\nu})
\end{bmatrix}.
\end{aligned}
\tag{B.9}
$$

B.2 Hydrodynamics

This section presents the forces and moments applied to the vehicle which is caused by hydrodynamic effects. It consists of two components, added mass and hydrodynamic damping.

B.2.1 Added Mass Term

When moving in the fluid, a vehicle experiences a pressure field. This phenomenon is captured by the added mass term. Suppose the fluid is considered as ideal, a conservation of the total kinetic energy of the fluid-vehicle body is applied. Added mass can be separated into rigid body-like added mass and Coriolis-like added mass.

The inertia matrix of the vehicle $\boldsymbol{M}$ consists of a rigid body mass and inertia $\boldsymbol{M}_{RB}$ and hydrodynamic added mass $\boldsymbol{M}_A$, such that,

$$\boldsymbol{M} = \boldsymbol{M}_{RB} + \boldsymbol{M}_A, \tag{B.10}$$

where the rigid body-like hydrodynamic added mass coefficient is defined as,

$$\boldsymbol{M}_A = -\begin{bmatrix} X_{\dot{u}} & X_{\dot{v}} & X_{\dot{w}} & X_{\dot{p}} & X_{\dot{q}} & X_{\dot{r}} \\ Y_{\dot{u}} & Y_{\dot{v}} & Y_{\dot{w}} & Y_{\dot{p}} & Y_{\dot{q}} & Y_{\dot{r}} \\ Z_{\dot{u}} & Z_{\dot{v}} & Z_{\dot{w}} & Z_{\dot{p}} & Z_{\dot{q}} & Z_{\dot{r}} \\ K_{\dot{u}} & K_{\dot{v}} & K_{\dot{w}} & K_{\dot{p}} & K_{\dot{q}} & K_{\dot{r}} \\ M_{\dot{u}} & M_{\dot{v}} & M_{\dot{w}} & M_{\dot{p}} & M_{\dot{q}} & M_{\dot{r}} \\ N_{\dot{u}} & N_{\dot{v}} & N_{\dot{w}} & N_{\dot{p}} & N_{\dot{q}} & N_{\dot{r}} \end{bmatrix} \equiv \begin{bmatrix} \boldsymbol{A}_{11} & \boldsymbol{A}_{12} \\ \boldsymbol{A}_{21} & \boldsymbol{A}_{22} \end{bmatrix}. \tag{B.11}$$

The expression in equation (B.11) is defined by Society of Naval Architects and Marine Engineer (SNAME), for example the hydrodynamic added mass force Y_A along the y-axis due to the acceleration, $\dot{u}$ in the x direction is expressed as $Y_A = Y_{\dot{u}}\dot{u}$, where $Y_{\dot{u}} = \frac{\partial Y}{\partial \dot{u}}$.

The term $\boldsymbol{C}(\boldsymbol{\nu})$ is a matrix describing the centrifugal and coriolis forces and moments acting on the vehicle. $\boldsymbol{C}(\boldsymbol{\nu})$ consists of a rigid body Coriolis and centripetal matrix $\boldsymbol{C}_{RB}(\boldsymbol{\nu})$ induced from $\boldsymbol{M}_{RB}(\boldsymbol{\nu})$ and hydrodynamic added mass which gives a Coriolis-like matrix $\boldsymbol{C}_A(\boldsymbol{\nu})$ induced from $\boldsymbol{M}_A(\boldsymbol{\nu})$,

$$\boldsymbol{C}(\boldsymbol{\nu}) = \boldsymbol{C}_{RB}(\boldsymbol{\nu}) + \boldsymbol{C}_A(\boldsymbol{\nu}), \tag{B.12}$$

according to [39], the hydrodynamic added mass which gives a Coriolis-like matrix,

$$\begin{aligned} \boldsymbol{C}_A(\boldsymbol{\nu}) &= \begin{bmatrix} \boldsymbol{0}_{3\times 3} & -\boldsymbol{S}(\boldsymbol{A}_{11}\boldsymbol{\nu}_1) + \boldsymbol{A}_{12}\boldsymbol{\nu}_2) \\ -\boldsymbol{S}(\boldsymbol{A}_{11}\boldsymbol{\nu}_1 + \boldsymbol{A}_{12}\boldsymbol{\nu}_2) & -\boldsymbol{S}(\boldsymbol{A}_{21}\boldsymbol{\nu}_1) + \boldsymbol{A}_{22}\boldsymbol{\nu}_2) \end{bmatrix}, \\ &= \begin{bmatrix} 0 & 0 & 0 & 0 & -a_3 & a_2 \\ 0 & 0 & 0 & a_3 & 0 & -a_1 \\ 0 & 0 & 0 & -a_2 & a_1 & 0 \\ 0 & -a_3 & a_2 & 0 & -b_3 & b_3 \\ a_3 & 0 & -a_1 & b_3 & 0 & -b_1 \\ -a_2 & a_1 & 0 & -b_2 & b_1 & 0 \end{bmatrix}, \end{aligned} \tag{B.13}$$

where,

$$\begin{aligned} a_1 &= X_{\dot{u}}\dot{u} + X_{\dot{v}}\dot{v} + X_{\dot{w}}\dot{w} + X_{\dot{p}}\dot{p} + X_{\dot{q}}\dot{q} + X_{\dot{r}}\dot{r}, \\ a_2 &= Y_{\dot{u}}\dot{u} + Y_{\dot{v}}\dot{v} + Y_{\dot{w}}\dot{w} + Y_{\dot{p}}\dot{p} + Y_{\dot{q}}\dot{q} + Y_{\dot{r}}\dot{r}, \\ a_3 &= Z_{\dot{u}}\dot{u} + Z_{\dot{v}}\dot{v} + Z_{\dot{w}}\dot{w} + Z_{\dot{p}}\dot{p} + Z_{\dot{q}}\dot{q} + Z_{\dot{r}}\dot{r}, \\ b_1 &= K_{\dot{u}}\dot{u} + K_{\dot{v}}\dot{v} + K_{\dot{w}}\dot{w} + K_{\dot{p}}\dot{p} + K_{\dot{q}}\dot{q} + K_{\dot{r}}\dot{r}, \\ b_2 &= M_{\dot{u}}\dot{u} + M_{\dot{v}}\dot{v} + M_{\dot{w}}\dot{w} + M_{\dot{p}}\dot{p} + M_{\dot{q}}\dot{q} + M_{\dot{r}}\dot{r}, \\ b_3 &= N_{\dot{u}}\dot{u} + N_{\dot{v}}\dot{v} + N_{\dot{w}}\dot{w} + N_{\dot{p}}\dot{p} + N_{\dot{q}}\dot{q} + N_{\dot{r}}\dot{r}. \end{aligned}$$

B.2.2 Hydrodynamic Damping Term

The term $\boldsymbol{D}(\boldsymbol{\nu})$ is a collection of other hydrodynamic forces and moments which is a quadratic lift plus drag. It can be written as,

$$\boldsymbol{D}(\boldsymbol{\nu}) = \begin{bmatrix} X_u + X_{u|u|}|u| & 0 & 0 & 0 & 0 & 0 \\ 0 & Y_v + Y_{v|v|}|v| & 0 & 0 & 0 & 0 \\ 0 & 0 & Z_w + Z_{w|w|}|w| & 0 & 0 & 0 \\ 0 & 0 & 0 & K_p + K_{p|p|}|p| & 0 & 0 \\ 0 & 0 & 0 & 0 & M_q + M_{q|q|}|q| & 0 \\ 0 & 0 & 0 & 0 & 0 & N_r + N_{r|r|}|r| \end{bmatrix}, \tag{B.14}$$

$$\equiv -\operatorname{diag}\{X_u, Y_u, Z_u, K_p, M_q, N_r\} - \operatorname{diag}\{X_{u|u|}|u|, Y_{v|v|}|v|, Z_{w|w|}|w|, K_{p|p|}|p|, M_{q|q|}|q|, N_{r|r|}|r|\}. \tag{B.15}$$

B.3 Restoring Forces and Moments

Apart from the hydrodynamics, a vehicle will be affected by gravity and buoyancy forces. The gravitational force f_g is induced by the weight of the vehicle $W = mg$. The buoyancy force f_b is induced by the buoyancy $B = \rho g V$ where ρ is the fluid density g is the earth gravity and V is the vehicle volume. The gravitational and buoyancy forces of the vehicle in the body-fixed coordinate system is,

$$\begin{aligned} \boldsymbol{g}(\boldsymbol{\eta}) &= \begin{bmatrix} f_b + f_g \\ r_b \times f_b + r_g \times f_g \end{bmatrix}, \\ &= \begin{bmatrix} (W-B)\sin\theta \\ -(W-B)\cos\theta\sin\phi \\ -(W-B)\cos\theta\cos\phi \\ -(y_gW - y_bB)\cos\theta\cos\phi + (z_gW - z_bB)\cos\theta\cos\phi \\ (z_gW - z_bB)\sin\theta + (x_gW - x_bB)cos\theta\cos\phi \\ -(x_gW - x_bB)\cos\theta\sin\phi + (y_gW - y_bB)\sin\theta \end{bmatrix}, \\ &\equiv \begin{bmatrix} G_X & G_Y & G_Z & G_K & G_M & G_N \end{bmatrix}^{\mathsf{T}}. \end{aligned} \tag{B.16}$$

B.4 Vehicle Rigid-Body Dynamics

By combining the equations for the vehicle rigid-body dynamics with the equations for the forces and moments on the vehicle, a general nonlinear equations of motion for an AUV in six degrees of freedom is expressed as,

- Surge (Translation along the vehicle's x-axis)

$$m[\dot{u} - vr + wq - x_g(q^2 + r^2) + y_g(pq - \dot{r}) + z_g(pr + \dot{q})] = \sum X$$

- Sway (Translation along the vehicle's y-axis)

$$m[\dot{v} - wp + ur - y_g(r^2 + p^2) + z_g(qr - \dot{p}) + x_g(qp + \dot{r})] = \sum Y$$

- Heave (Translation along the vehicle's z-axis)

$$m[\dot{w} - uq + vp - z_g(p^2 + q^2) + x_g(rp - \dot{q}) + y_g(rq + \dot{p})] = \sum Z$$

- Roll (Rotation about the vehicle's x-axis)

$$\begin{aligned} I_{xx}\dot{p} + (I_{zz} - I_{yy})qr - (\dot{r} + pq)I_{xz} + (r^2 - q^2)I_{yz} + (pr - \dot{q})I_{xy} & \\ +m[y_g(\dot{w} - uq + vp) - z_g(\dot{v} - wp + ur)] &= \sum K \end{aligned}$$

- Pitch (Rotation about the vehicle's y-axis)

$$\begin{aligned} I_{yy}\dot{q} + (I_{xx} - I_{zz})rp - (\dot{p} + qr)I_{xy} + (p^2 - r^2)I_{xz} + (qp - \dot{r})I_{yz} & \\ +m[z_g(\dot{u} - vr + wq) - x_g(\dot{w} - uq + vp)] &= \sum M \end{aligned}$$

- Yaw (Rotation about the vehicle's z-axis)

$$\begin{aligned} I_{zz}\dot{r} + (I_{yy} - I_{xx})pq - (\dot{q} + rp)I_{yz} + (q^2 - p^2)I_{xy} + (rq - \dot{p})I_{xz} & \\ +m[x_g(\dot{v} - wp + ur) - y_g(\dot{u} - vr + wq)] &= \sum N \end{aligned}$$

The sum of forces and moments on the vehicle can be expressed as,

$$\begin{aligned} \sum X &= G_X + X_{u|u|}u|u| + X_{\dot{u}}\dot{u} + X_{wq}wq + X_{qq}qq + X_{vr}vr + X_{rr}rr + X_{prop} \\ \sum Y &= G_Y + Y_{v|v|}v|v| + Y_{r|r|}r|r| + Y_{\dot{v}}\dot{v} + Y_{\dot{r}}\dot{r} + Y_{ur}ur + Y_{wp}wp + Y_{pq}pq \\ &\quad + Y_{uv}uv + Y_{uu}u_0^2\delta_r \\ \sum Z &= G_Z + Z_{w|w|}w|w| + Z_{q|q|}q|q| + Z_{\dot{w}}\dot{w} + Z_{\dot{q}}\dot{q} + Z_{uq}uq + Z_{vp}vp + Z_{rp}rp \\ &\quad + Z_{uw}uw + Z_{uu}u_0^2\delta_s \\ \sum K &= G_K + K_{p|p|}p|p| + K_{\dot{p}}\dot{p} + K_{prop} \\ \sum M &= G_M + M_{w|w|}w|w| + M_{q|q|}q|q| + M_{\dot{w}}\dot{w} + M_{\dot{q}}\dot{q} + M_{uq}uq + M_{vp}vp \\ &\quad + M_{rp}rp + M_{uw}uw + M_{uu}u_0^2\delta_s \\ \sum N &= G_N + N_{v|v|}v|v| + N_{r|r|}r|r| + N_{\dot{v}}\dot{v} + N_{\dot{r}}\dot{r} + N_{ur}ur + N_{wp}wp + N_{pq}pq \\ &\quad + N_{uv}uv + N_{uu}u_0^2\delta_r \end{aligned}$$

Appendix C

Mathematical Preliminaries

This appendix briefly provides mathematical tools using in this thesis. The references are collected from various references [39], [133], [135].

C.1 Stability

Consider the semiautonomous system,

$$\dot{x} = f(t, x) \tag{C.1}$$

where $f : \mathbb{R}^n \times \mathbb{R}_{\geq 0} \to \mathbb{R}^n$ is locally Lipschitz in t and continuous in x (f depends explicitly on time). Locally Lipschitz is said that for each point $x \in D \in \mathbb{R}^n$ at a fixed time t, there exists a neighborhood $D_0 \in D$ such that,

$$\|f(t, x) - f(t, y)\| \leq L\|x - y\|, \quad \forall x, y \in D_0$$

where L is called the Lipschitz constant on D_0.

Definition C.1. *The point $x_e \in \mathbb{R}^n$ is the equilibrium point for (C.1) if*

$$f(t, x_e) = 0, \quad \forall t \geq 0.$$

Definition C.2. *A continuous function* $\alpha : \mathbb{R}_{\geq 0} \rightarrow \mathbb{R}_{\geq 0}$ *belongs to class* $\mathcal{K}$ *if it strictly increasing and* $\alpha(0) = 0$. *It belongs to class* $\mathcal{K}_\infty$ *if it is belong to class* $\mathcal{K}$ *and in addition* $\lim_{r\rightarrow\infty} \alpha(r) = \infty$.

Definition C.3. *A continuous function* $\beta : \mathbb{R}_{\geq 0} \times \mathbb{R}_{\geq 0} \rightarrow \mathbb{R}_{\geq 0}$ *belongs to class* $\mathcal{KL}$ *if, for each fixed* s, *the function* $\beta(r, s)$ *belongs to class* $\mathcal{K}$ *with respect to* r *and, for each fixed* r, *the function* $\beta(r, s)$ *is decreasing with respect to* s *and* $\beta(r, s) \rightarrow 0$ *as* $s \rightarrow 0$.

Now we can consider the following definitions regarding the stability:

Definition C.4. *The equilibrium point* $x = 0$ *of (C.1) is,*

- *uniformly stable, if there exists a class function* $\alpha(\cdot)$, *such that,*

$$\|x(t)\| \leq \alpha(\|x(t_0)\|), \quad \forall t \geq t_0 \tag{C.2}$$

- *uniformly globally stable, if (C.2) is satisfied with* $\alpha \in \mathcal{K}$ *for any initial state* $x(t_0)$.

- *uniformly globally attractive, if for each* $r, \sigma > 0$, *there exist* $T > 0$ *such that,*

$$\|x(t_0)\| < r \|x(t)\| \leq \sigma, \quad \forall t \geq t_0 + T \tag{C.3}$$

- *uniformly globally asymptotically stable, if it is uniformly globally stable and uniformly globally attractive.*

Theorem C.1. (*Lyapunov's Global Stability Theorem) If a scalar function* $V(\sigma)$ *of a variable* σ *has continuous first order derivative and satisfies the following conditions:*

- $V(\sigma)$ *is positive definite,*

- $\dot{V}(\sigma)$ *is negative definite,*

- $V(\sigma) \rightarrow \infty \quad as \quad \| \sigma \| \rightarrow \infty$,

then the equilibrium at the origin of $V(\sigma)$ *is uniformly globally asymptotically stable.*

C.2 Eigenvector

The characteristic equation of the system matrix $\boldsymbol{A}$ is given as,

$$\boldsymbol{A}v = \lambda v$$

where λ are scalar values called the eigenvalues, and v are the corresponding eigenvectors. To solve for the eigenvalues of a matrix, it can be written as,

$$(\boldsymbol{A} - \lambda \boldsymbol{I})v = 0$$

where $\boldsymbol{I}$ is the identity matrix. A matrix equation of this form can only be solved if the determinant of the matrix is nonzero that is, if,

$$|\boldsymbol{A} - \lambda \boldsymbol{I}| = 0$$

Consider a right eigenvector corresponding to the eigenvalue λ. If $\lambda_1, \lambda_2, \ldots, \lambda_n$ are the eigenvalues and $v_1, v_2, \ldots, v_n$ are the corresponding right eigenvectors, then it can see that the set of right eigenvectors form a basis of a vector space. If this vector space is of dimension n, then we can construct the $n \times n$ diagonal matrix whose columns are the components of the right eigenvectors.

C.3 Pole Placement

Consider the state space,

$$\begin{aligned} \dot{\boldsymbol{x}} &= \boldsymbol{A}\boldsymbol{x} + \boldsymbol{B}\boldsymbol{u} \\ \boldsymbol{y} &= \boldsymbol{C}\boldsymbol{x} + \boldsymbol{D}\boldsymbol{u} \end{aligned}$$

The pole placement method is to determine the control matrix $\boldsymbol{K}$. Hence, a feedback law must satisfy the characteristic polynomial $Q(s) = |s\boldsymbol{I} - (\boldsymbol{A} - \boldsymbol{B}\boldsymbol{K})|$.

Example

This work used PLACE function in MATLAB® which return a state-feedback matrix $\boldsymbol{K}$ such that the eigenvalues of $\boldsymbol{A} - \boldsymbol{B}\boldsymbol{K}$ are those specified in given poles.

Appendix D

Underwater Vehicle Model

This appendix contains the parameters of the ARIES (Acoustic Radio Interactive Exploratory Server), an autonomous underwater vehicle (shown in figure D.1) at Naval Postgraduate School, Monterey, California, USA demonstrating for sample cases of simulations in this thesis. The material is collected from Healey and Lienard [54].

Table D.1: ARIES Underwater vehicle parameters

$W = 53.4$ kN	$B = 53.4$ kN	$L = 5.3$ m	$I_{xx} = 13587$ Nms^2
$I_{xy} = -13.58$ Nms^2	$I_{yz} = -13.58$ Nms^2	$I_{zx} = -13.58$ Nms^2	$I_{yy} = 13587$ Nms^2
$I_{xx} = 2038$ Nms^2	$x_g = 0.0$	$y_g = 0.0$	$z_g = 6.1$ cm
$x_b = 0.0$	$y_b = 0.0$	$z_b = 0.0$	$g = 9.81$ m/s^2
$\rho = 1000$ kg/m^3	$m = 5454.54$ kg		
$X_{pp} = 7.0e-3$	$X_{qq} = -1.5e-2$	$X_{rr} = 4.0e-3$	$X_{pr} = 7.5e-4$
$X_{\dot{u}} = -7.6e-3$	$X_{wq} = -2.0e-1$	$X_{vp} = -3.0e-3$	$X_{vr} = 2.0e-2$
$X_{q\delta s} = 2.5e-2$	$X_{q\delta b/2} = -1.3e-3$	$X_{r\delta r} = -1.0e-3$	$X_{vv} = 5.3e-2$
$X_{ww} = 1.7e-1$	$X_{v\delta r} = 1.7e-3$	$X_{w\delta s} = 4.6e-2$	$X_{w\delta b/2} = 0.5e-2$
$X_{\delta s\delta s} = -1.0e-2$	$X_{\delta b\delta b/2} = -4.0e-3$	$X_{\delta r\delta r} = -1.0e-2$	$X_{q\delta sn} = 2.0e-3$
$X_{w\delta sn} = 3.5e-3$	$X_{\delta s\delta sn} = -1.6e-3$		
$Y_{\dot{p}} = 1.2e-4$	$Y_{\dot{r}} = 1.2e-3$	$Y_{pq} = 4.0e-3$	$Y_{qr} = -6.5e-3$
$Y_{\dot{v}} = -5.5e-2$	$Y_p = 3.0e-3$	$Y_r = 3.0e-2$	$Y_{vq} = 2.4e-2$
$Y_{wp} = 2.3e-1$	$Y_{wr} = -1.9e-2$	$Y_v = -1.0e-1$	$Y_{vw} = 6.8e-2$
$Y_{\delta r} = 2.7e-2$			

Table D.2: ARIES Underwater vehicle parameters (continued)

$Z_{\dot{q}} = -6.8e-3$	$Z_{pp} = 1.3e-4$	$Z_{pr} = 6.7e-3$	$Z_{rr} = -7.4e-3$
$Z_{\dot{w}} = -2.4e-1$	$Z_q = -1.4e-1$	$Z_{vp} = -4.8e-2$	$Z_{vr} = 4.5e-2$
$Z_w = -3.0e-1$	$Z_{vv} = -6.8e-2$	$Z_{\delta s} = -7.3e-2$	$Z_{\delta b/2} = -1.3e-2$
$Z_{qn} = -2.9e-3$	$Z_{wn} = -5.1e-3$	$Z_{\delta sn} = -1.0e-2$	
$K_{\dot{p}} = -1.0e-3$	$K_{\dot{r}} = -3.4e-5$	$K_{pq} = -6.9e-5$	$K_{qr} = 1.7e-2$
$K_{\dot{v}} = 1.2e-4$	$K_p = -1.1e-2$	$K_r = -8.4e-4$	$K_{vq} = -5.1e-3$
$K_{wp} = -1.3e-4$	$K_{wr} = 1.4e-2$	$K_v = 3.1e-3$	$K_{vw} = -1.9e-1$
$K_{\delta b/2} = 0$	$K_{pn} = -5.7e-4$	$K_{prop} = 0$	
$M_{\dot{q}} = -1.7e-2$	$M_{pp} = 5.3e-5$	$M_{pr} = 5.0e-3$	$M_{rr} = 2.9e-3$
$M_{\dot{w}} = -6.8e-3$	$M_{uq} = -6.8e-2$	$M_{vp} = 1.2e-3$	$M_{vr} = 1.7e-2$
$M_{uw} = 1.0e-1$	$M_{vv} = -2.6e-2$	$M_{\delta s} = -4.1e-2$	$M_{\delta b/2} = 3.5e-3$
$M_{qn} = -1.6e-3$	$M_{wn} = -2.9e-3$	$M_{\delta sn} = -5.2e-3$	
$N\dot{p} = -3.4e-5$	$N_{\dot{r}} = -3.4e-3$	$N_{pq} = -2.1e-2$	$N_{qr} = 2.7e-3$
$N_{\dot{v}} = 1.2e-3$	$N_p = -8.4e-4$	$N_r = -1.6e-2$	$N_{vq} = -1.0e-2$
$N_{wp} = -1.7e-2$	$N_{wr} = 7.4e-3$	$N_v = -7.4e-3$	$N_{vw} = -2.7e-2$
$N_{\delta r} = -1.3e-2$	$N_{prop} = 0.0$		

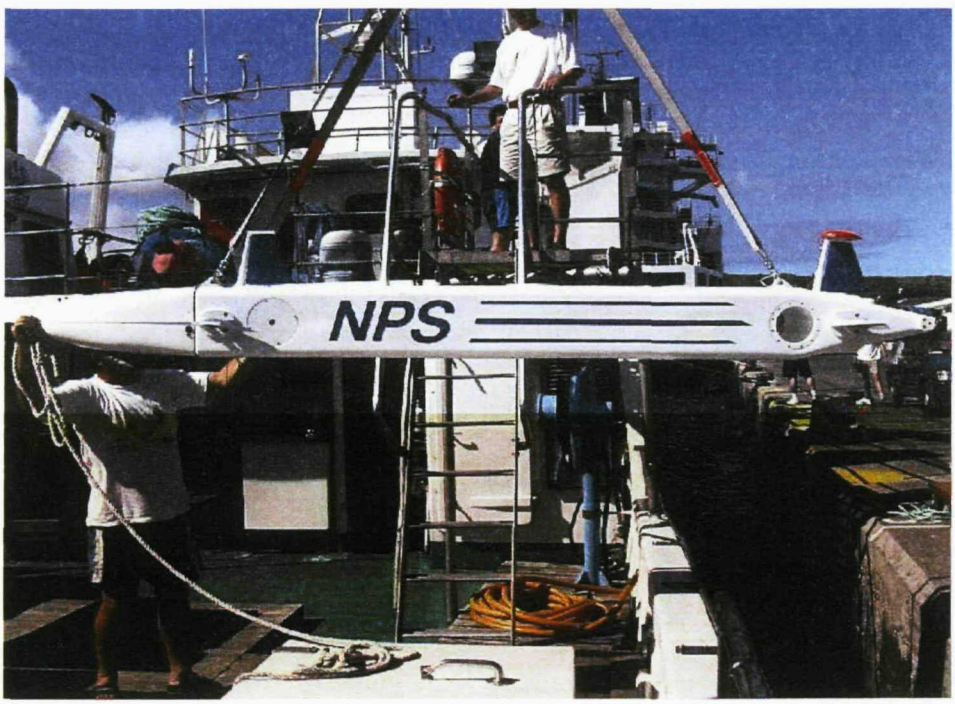

Figure D.1: Illustration of the ARIES AUV.

Appendix E

Comparative Results of Controller Design

This appendix contains the comparison of the heading and depth using a high-order sliding mode and a combination of high-order sliding mode with a use of state-dependent Riccati equation technique (see chapter 3).

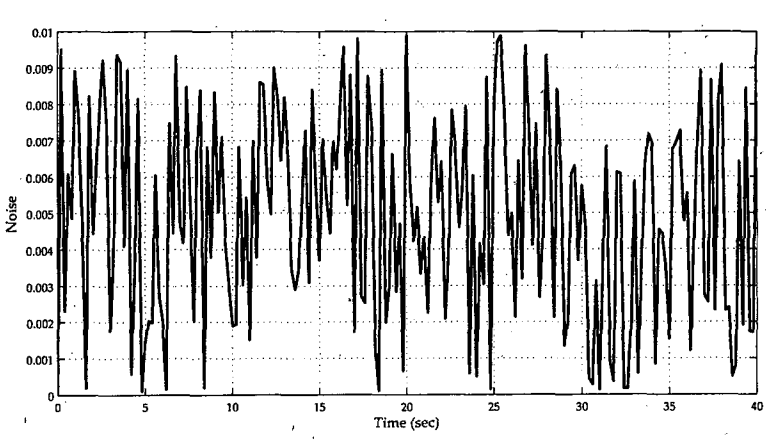

Figure E.1: Noise model using a function 0.01*rand(1).

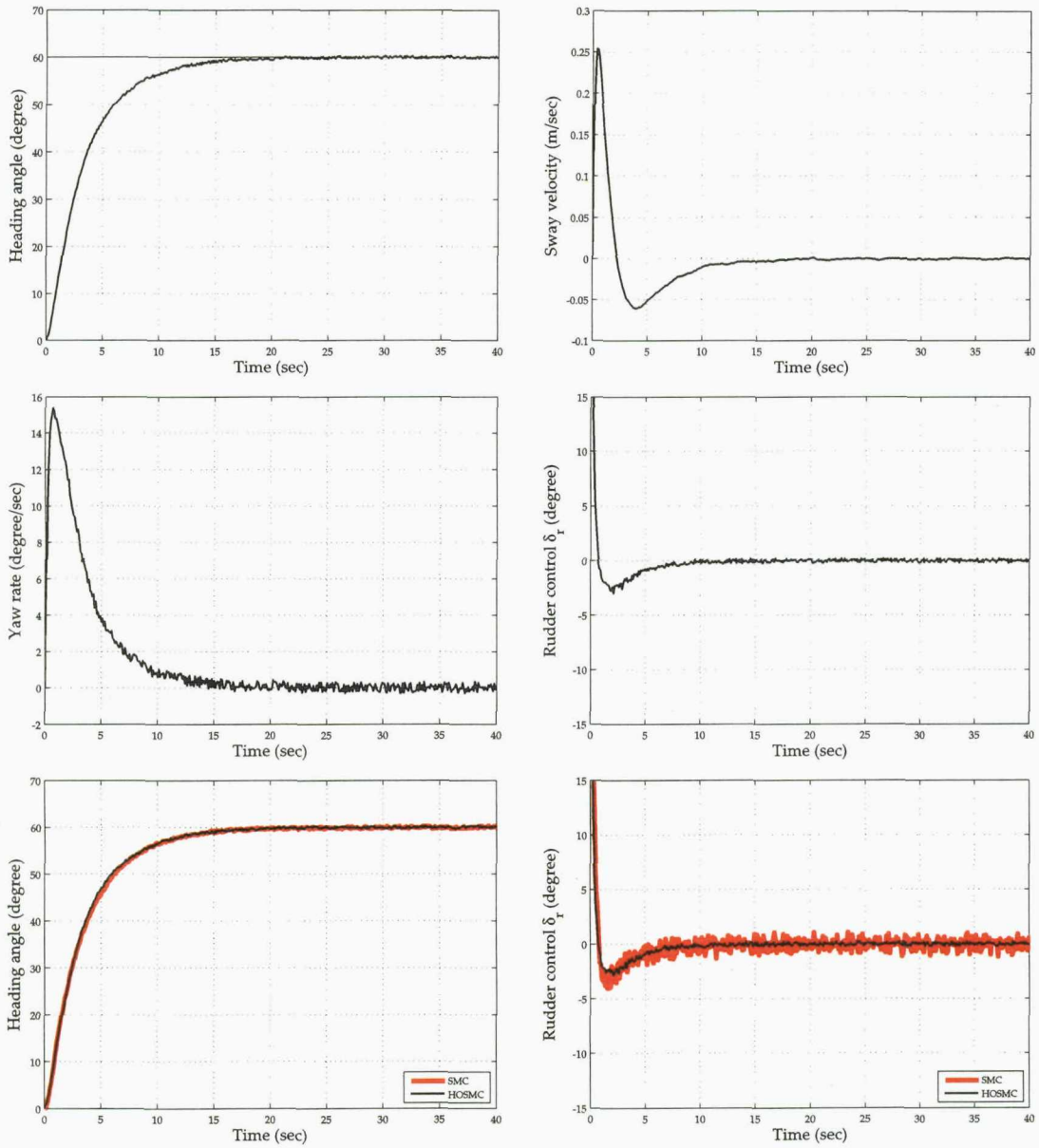

Figure E.2: Comparisons of heading control using SMC and HOSMC techniques with disturbance.

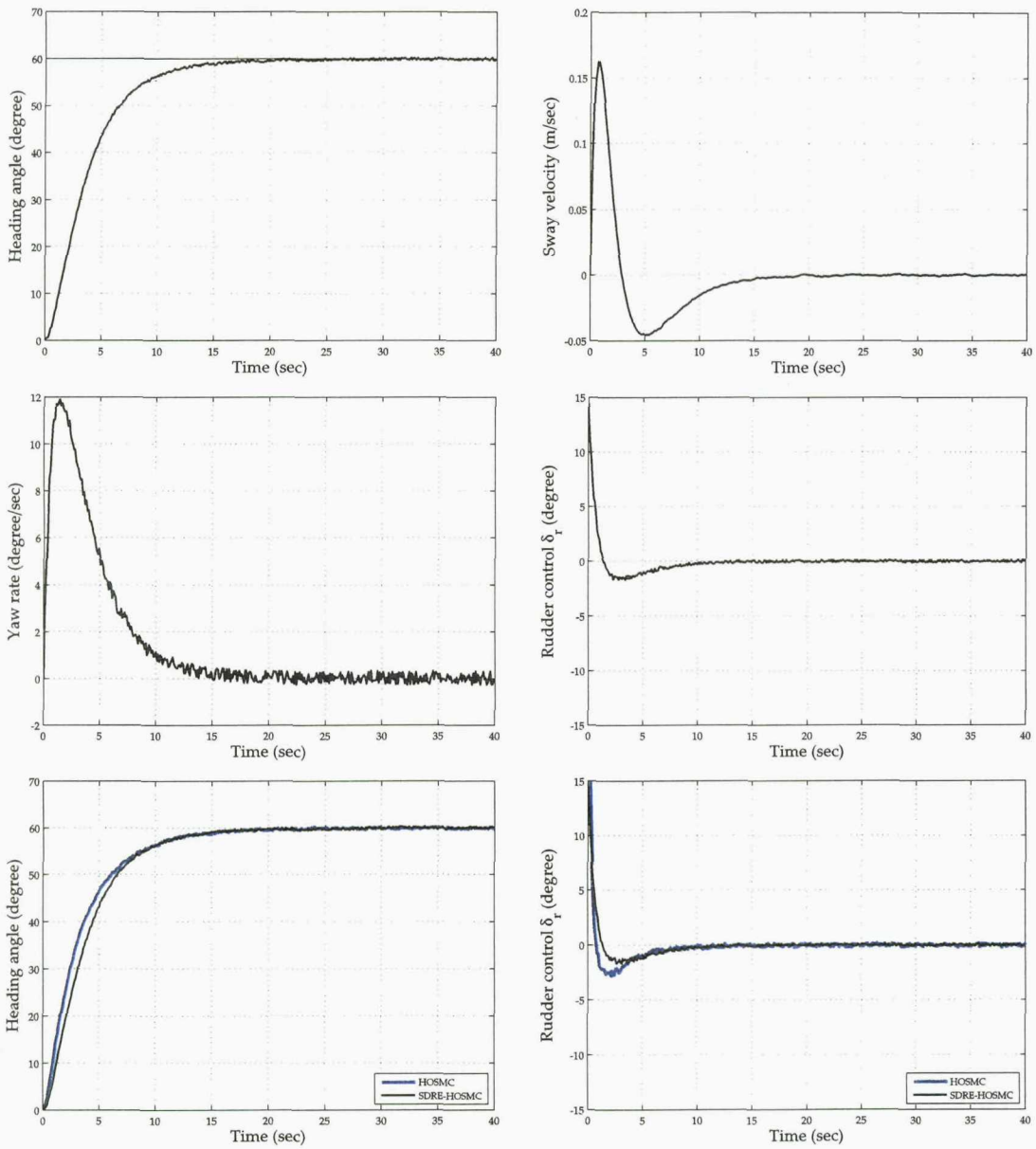

Figure E.3: Comparisons of heading control using HOSMC and SDRE-HOSMC techniques with disturbance.

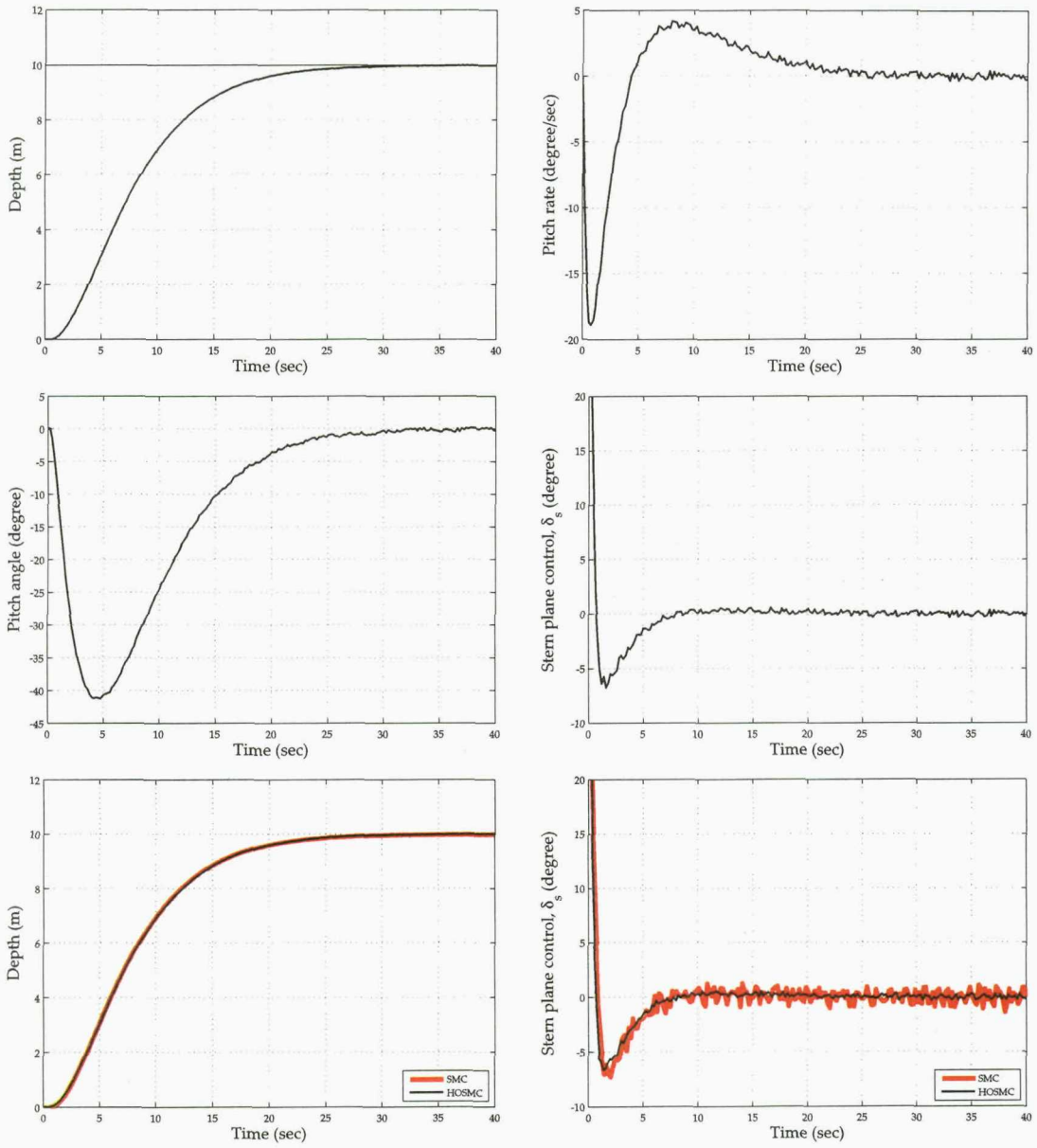

Figure E.4: Comparisons of depth control using SMC and HOSMC techniques with disturbance.

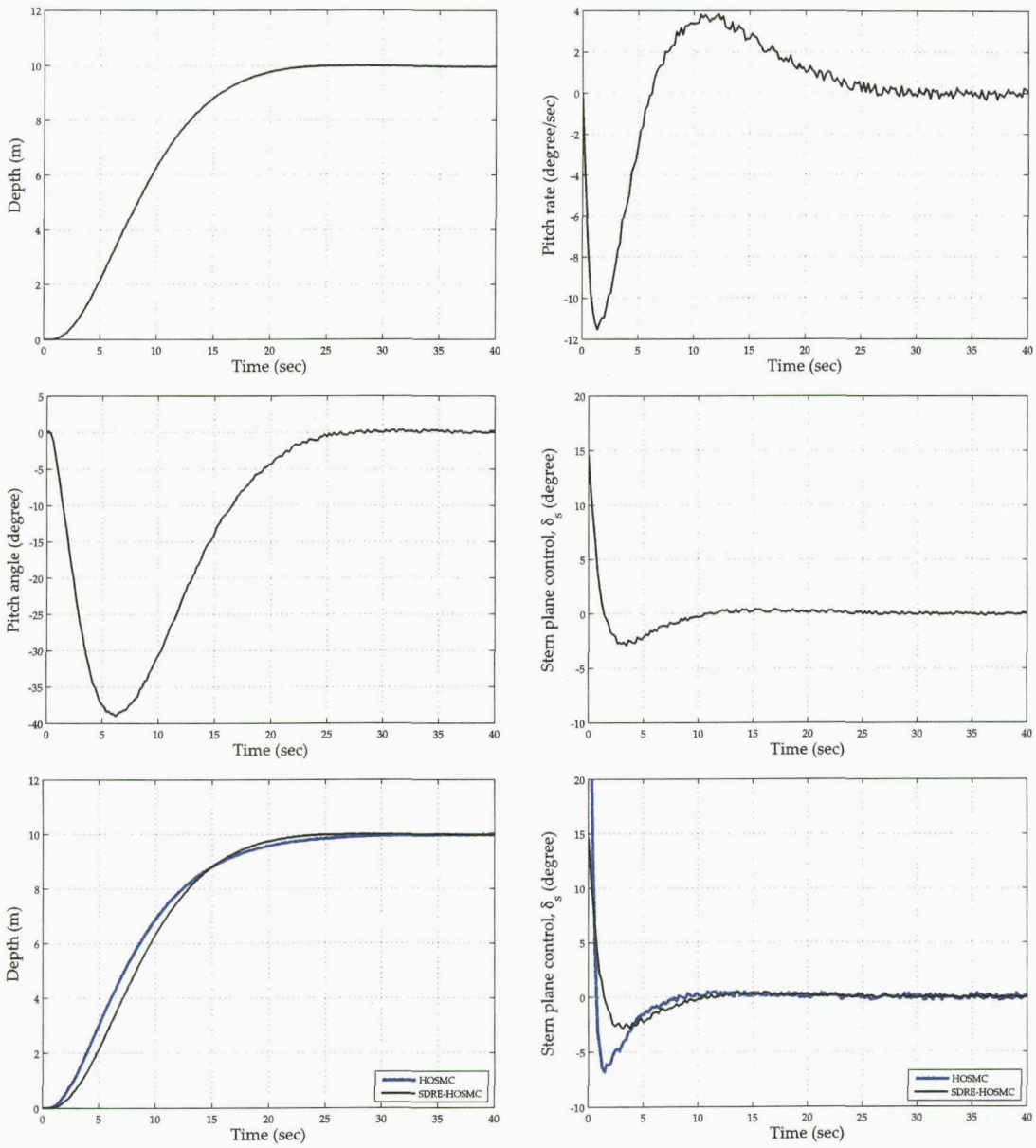

Figure E.5: Comparison of depth control using HOSMC and SDRE techniques with disturbance.